Labrador Sea Water exported through Flemish Pass: Hydrographic trends and transport variability inducing processes

Linn Sanguineti

Universität Bremen, 2017

Labrador Sea Water exported through Flemish Pass: Hydrographic trends and transport variability inducing processes

Vom Fachbereich für Physik und Elektrotechnik der
Universität Bremen genehmigte Dissertation
zur Erlangung des akademischen Grades
Doktor der Naturwissenschaften (Dr. rer. nat.)

von

Dipl. Phys. Linn Sanguineti
aus Bremen

1. Gutachterin: Dr. Dagmar Kieke
2. Gutachter: Prof. Dr. Torsten Kanzow

Eingereicht am: 18.04.2017
Tag des Promotionskolloquiums: 06.07.2017

Abstract

This study investigates the deep water flow through Flemish Pass, a passage (sill depth 1200 m) located at the western subpolar margin, constrained by the Grand Banks and the underwater plateau Flemish Cap. In addition to the Deep Western Boundary Current (DWBC) pathway offshore of Flemish Cap, Flemish Pass represents another southward transport pathway for two modes of Labrador Sea Water (LSW), a main component of the climate modulating Atlantic Meridional Overturning Circulation (AMOC). This pathway avoids potential stirring regions southeast of Flemish Cap and deflection into the interior North Atlantic. Hydrographic time series from ship-based measurements show a significant warming of 0.3°C/decade and a salinification of 0.03/decade of the Upper LSW in Flemish Pass between 1993 and 2013. Almost identical trends were found for the evolution in the Labrador Sea and in the DWBC east of Flemish Cap. This indicates that the long-term hydrographic variability of Upper LSW in Flemish Pass as well as in the DWBC at 47°N is dominated by changes in the Labrador Sea, which are advected southward. By using numerical model time series of hydrographic anomalies starting in 1960, the observed trends in Flemish Pass were identified as part of a multidecadal cycle.

Ship-based velocity measurements between 2009 and 2013 at 47°N in Flemish Pass and in the DWBC east of Flemish Cap revealed a considerable southward transport of Upper LSW through Flemish Pass (15–27%). About 98% of the denser Deep LSW were carried around Flemish Cap as Flemish Pass is too shallow for considerable transport of Deep LSW. Mooring based transport time series revealed an average southward LSW transport of -1.9 ± 0.5 Sv (-1.4 ± 0.5 Sv) and a range of -3.5 Sv to 0.7 Sv (-5 Sv to 3 Sv) in Flemish Pass for the period 2012 - 2013 (2013 - 2014). The highest transports as well as transport reversals occurred during the winter periods. Seasonal effects on the LSW density layer and the flow field had only a minor influence on the LSW transports and were negligible in the range of the transport uncertainty. The dominant LSW transport variability was observed

on intra-seasonal time scales of 20 - 50 days and related to baroclinic topographic Rossby waves trapped at the western slope of Flemish Pass. Further results indicated that fast coastal trapped waves also influence the transport variability of LSW in Flemish Pass and create coherent oscillations with upstream transports in the DWBC at 53°N in winter periods.

Zusammenfassung

Die vorliegende Arbeit untersucht den Tiefenwasserfluss durch die Flämische Passage, eines 1200 m tiefen Kanals am westlichen subpolaren Rand, der durch die Grand Banks und ein Unterwasserplateau (Flämische Kappe) begrenzt wird. Neben dem tiefen westlichen Randstrom (DWBC) küstenabgewand von der Flämischen Kappe ist die Flämische Passage ein weiterer Transportpfad nach Süden für zwei Moden von Labradorseewasser (LSW), einer Hauptkomponente der klimamodulierenden atlantischen meridionalen Umwälzzirkulation (AMOC). Dieser Transportpfad vermeidet potentiell turbulente Regionen südöstlich der Flämischen Kappe, wo LSW in den inneren Nordatlantik abgelenkt wird. Hydrographische Zeitreihen basierend auf Schiffsmessungen in der Flämischen Passage zeigen eine signifikante Erwärmung von 0.3°C/Dekade und zunehmende Salzgehalte von 0.03/Dekade im oberen LSW zwischen 1993 und 2013. Beinahe identische Trends wurden in der Labradorsee und im DWBC östlich der Flämischen Kappe beobachtet. Dies gibt zu erkennen, dass die langzeitige hydrographische Variabilität von oberem LSW in der Flämischen Passage sowie im DWBC bei 47°N von Veränderungen in der Labradorsee dominiert werden, die mit der Strömung nach Süden transportiert werden. Durch den Vergleich mit Zeitreihen hydrographischer Anomalien beginnend im Jahr 1960 aus einem numerischen Ozeanmodell konnte gezeigt werden, dass die beobachteten Trends in der Flämischen Passage Teil eines multidekadischen Zyklus sind.

Schiffbasierte Strömungsgeschwindigkeitsmessungen zwischen 2009 und 2013 bei 47°N in der Flämischen Passage und im DWBC östlich der Flämischen Kappe zeigten einen erheblichen Anteil am südwärtigen Transport von oberem LSW durch die Flämische Passage (15–27%). Ungefähr 98% vom tiefen LSW wurden mit dem DWBC östlich der Flämischen Kappe transportiert, da die Flämische Passage zu flach ist für einen größeren Transport von tiefem LSW. Verankerungsbasierte Transportzeitreihen ergaben einen durchschnittlichen südwärtigen LSW Transport von -1.9 ± 0.5 Sv (-1.4 ± 0.5 Sv) und eine Spannweite von -3.5 Sv bis 0.7 Sv (-5 Sv

bis 3 Sv) für die Periode 2012 - 2013 (2013 - 2014). Die stärksten südwärtigen Transporte sowie auch Transportumkehrungen traten während der Winterperioden auf. Saisonale Effekte auf die LSW Dichteschicht und das Strömungsfeld hatten einen geringen Einfluss auf die LSW Transporte und warem im Rahmen der Transportunsicherheit vernachlässigbar. Die domiante Variabilität im LSW Transport wurde auf intra-saisonalen Zeitskalen von 20 - 50 Tagen beobachtet, und mit baroklinen, topographischen Rossbywellen in Verbindung gebracht. Weitere Ergebnisse deuteten darauf hin, dass außerdem schnelle, sich am Kontinentalhang ausbreitende Küstenwellen die Transportvariabilität in der Flämischen Passage beeinflussen, und dadurch kohärente Oszillationen mit stromaufwärtigen Transporten im DWBC bei 53°N in Winterperioden auslösen.

Contents

List of Tables

List of Figures

1 The Flemish Pass - a key region for Labrador Sea Water export?

Labrador Sea Water (LSW) is one of the main water masses of the deep southward return flow of the climate-modulating Atlantic meridional overturning circulation (AMOC). It is important to investigate and monitor changes in the formation, hydrographic properties and export rates of LSW as many model studies have revealed links between changes in the strength of the AMOC and long-term variations in LSW formation in times of global climate change [e.g., *Getzlaff et al.* (2005), *Marsh et al.* (2005), *Böning et al.* (2006), *Medhaug et al.* (2012)]. After formation by wintertime convection in the central Labrador Sea [e.g. *Lazier* (1973), *Lazier et al.* (2002)], LSW is exported out of its formation region along different pathways (Figure 1a). The fastest export pathway carrying the youngest and least diluted LSW [*Rhein et al.* (2015)] is southward along the Canadian continental shelf, where LSW is an integral part of the Deep Western Boundary Current (DWBC) [e.g. *Talley and McCartney* (1982), *Stramma et al.* (2004), *Kieke et al.* (2007), *Kieke et al.* (2009)]. Within the DWBC it flows below and offshore of the southbound shallow Labrador Current (LC), which transports a mixture of cold and fresh near-surface waters from Hudson Strait at 60°N to the Tail of the Grand Banks at 43°N along the continental slope. These waters have their origin in Baffin Bay and the West Greenland Current [*Lazier and Wright* (1993)]. Other LSW pathways follow eastward directions, one into the Irminger Sea and another one towards the Mid-Atlantic Ridge and the eastern subpolar North Atlantic [*Talley and McCartney* (1982), *Sy et al.* (1997), *Koltermann et al.* (1999), *Rhein et al.* (2002), *Yashayaev* (2007), *Kieke et al.* (2009)]. At about 49°N/47°W (Figure 1a), the underwater plateau Flemish Cap splits the DWBC into two branches: one branch carrying LSW through Flemish Pass, a shallow channel located to the west of Flemish Cap having a sill depth of 1200 m (hereafter called the Flemish Pass branch), and a second branch located on the eastern side of Flemish Cap (called the

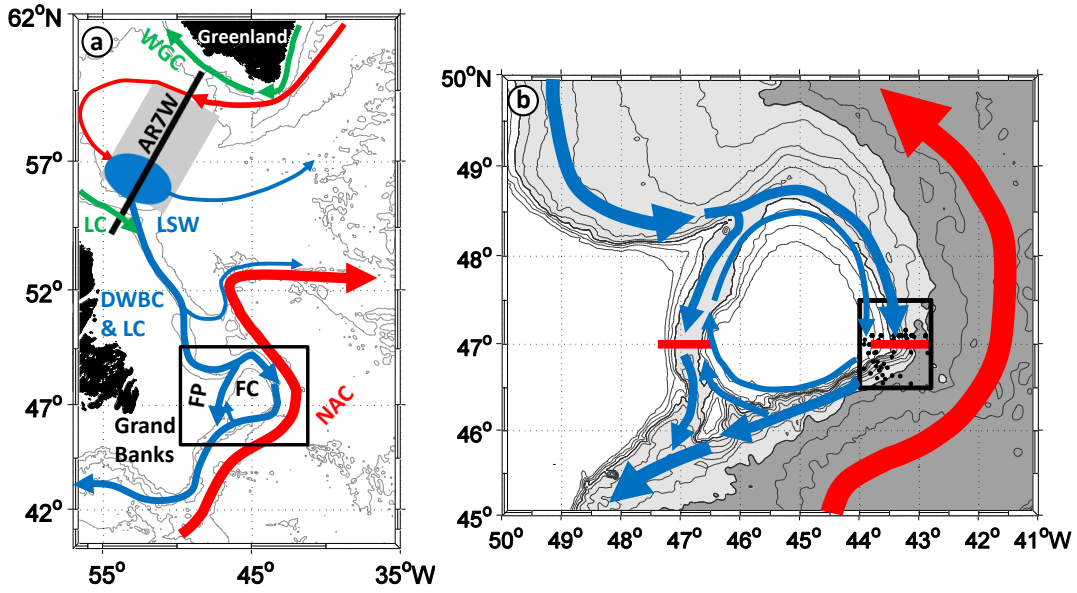

Figure 1.1: (a) Idealized Labrador Sea Water (LSW) circulation (blue) and upper ocean circulation features (red, green) in the western subpolar North Atlantic. FP: Flemish Pass, FC: Flemish Cap, NAC: North Atlantic Current, WGC: West Greenland Current, LC: Labrador Current, DWBC: Deep Western Boundary Current. The LSW formation area is shown as blue ellipse. The black line marks the standard hydrographic section AR7W occupied annually in the Labrador Sea, and the grey shaded box indicates limits of Argo float measurements, which were confined within the 3250 m isobath and a 150 km distance range from the AR7W line following *Yashayaev and Loder* (2009). The part of the map limited by the black box is magnified in Figure 1b. (b) Topographic setting of the 1200 m deep Flemish Pass. Bathymetry from the ETOPO2 database [*National Geophysical Data Center* (2006)] is indicated by gray lines; the depth interval is 200 m between 400 - 1200 m, and 500 m below 1500 m depth. Water depths between 1000 and 3500 m are shaded in light grey to indicate the deep Flemish Pass and the slope part of the DWBC, greater depths are shaded dark. The idealized LSW and LC circulation and the anticyclonic gyre around FC according to *Gil et al.* (2004) are displayed in blue, the NAC path in red. Red lines indicate CTD/LADCP repeat sections at 47°N in both current branches. The black box marks the limits of Argo float measurements in the DWBC branch, and black dots indicate available CTD profiles additional to the 47°N section.

DWBC branch), [*Bower et al.* (2009), *Rhein et al.* (2011), *Mertens et al.* (2014)]. Both branches presumably merge again south of Flemish Cap [*Bower et al.* (2009), Figure 1b]. Offshore of the DWBC branch at Flemish Cap, the strongly meandering North Atlantic Current (NAC) is in close vicinity, and some LSW is deflected into the interior ocean by cross-frontal interactions [*Dutkiewicz et al.* (2001), *Kieke et al.* (2009)]. In an experiment with 59 acoustically tracked isobaric RAFOS floats released in the DWBC, *Bower et al.* (2009) and *Bower et al.* (2011) studied LSW spreading pathways for 32 floats ballasted for 700 m and 27 floats ballasted for 1500 m. In total, 70% of floats left the DWBC at the southeastern corner of the Flemish Cap, which highlights this region as a primary location for LSW to leave the DWBC and to be entrained into the interior North Atlantic. In contrast, 10 out of the 32 shallow floats passed through the Flemish Pass. These floats were about four times more likely to be exported to the subtropics than floats that went around Flemish Cap. Therefore, the Flemish Pass is considered to protect LSW from being diverted into the interior Newfoundland Basin by meanders of the NAC [*Bower et al.* (2011)].

Apart from the mentioned floats studies, the importance of Flemish Pass for the southward transport of LSW and its contribution to the AMOC has yet not been studied in detail using observations. Mooring based estimates of the southward transport through the Flemish Pass either exclude the deep water component or are limited in the record duration. *Petrie and Buckley* (1996) for instance calculated a transport of -3.7 ± 1.2 Sv ($1\,\mathrm{Sv} = 10^6\,\mathrm{m^3\,s^{-1}}$) for the upper 350 m of the water column from moored current meters deployed for a period of 3 months in 1985 - 1986. In combination with additional archived current meter data, an estimate for the total volume transport (surface to bottom, addressed as the total transport of the Labrador Current) through the Flemish Pass of -6.3 to -9.8 Sv was derived [*Petrie and Buckley* (1996), *Ross* (1980), *Greenberg and Petrie* (1988)]. No estimate for a particular LSW transport was provided. From a 2009 survey at 47°N combining hydrographic observations with velocity measurements from Lowered Acoustic Doppler Current Profilers (LADCP), *Rhein et al.* (2011) showed LSW flowing through Flemish Pass, but they did not provide transport estimates. The important contribution of the Flemish Pass branch to the southward transport of upper LSW was confirmed in the model study of *Varotsou et al.* (2015), who focused on interannual transport variability. Knowledge about the processes driving the flow variability in Flemish Pass are limited. *Varotsou et al.* (2015) linked the

interannual transport variability of upper LSW to changes of the atmospheric forcing and to changes of the NAC's position based on model data. On intra-seasonal time scales, the model study of *Varotsou* (2016) documented high variance in the Flemish Pass transports for periods of less than 25 days and linked it to coastal trapped waves. Other model studies found a non-negligible contribution of wind forcing to the transport in Flemish Pass [e.g. *Han* (2005), *Han et al.* (2008)]. *Han* (2005) for instance attributed one fourth of the Flemish Pass transports to wind forcing. Observations of the current variability in the Flemish Pass region are documented in a study of *Layton* (2016), who investigated the current variability based on mooring data from the northern entrance of Flemish Pass at about 48°30′W and from the upper water column of the western slope of Flemish Pass at 47°N. *Layton* (2016) found high intra-seasonal variability on a three week time scale at all three moorings and related that to the influence of topographic Rossby waves. Topographic Rossby waves were previously observed by several studies up- and downstream of Flemish Pass [e.g. *Johns and Watts* (1986) *Pickart and Watts* (1990), *Mertens et al.* (2014), *Fischer et al.* (2015)].

The present study was performed in the frame of the project "Transports and variability-driving mechanisms in Flemish Pass at the western boundary of the subpolar North Atlantic (FLEPVAR)". FLEPVAR was a cooperative project, investigating the Flemish Pass based on observational data on one side, and based on numerical model data on the other side. The observational part of this project was carried out at the Institute of Environmental Physics (IUP) at the University of Bremen, and the results are presented in the present study. The modeling part of this project took place at the Institute of Oceanography (IFM/CEN) at University of Hamburg.

The present study aims to extend the knowledge about the LSW flowing through Flemish Pass by answering the following research questions:

1. Is the Flemish Pass a southward export pathway for LSW from the Labrador Sea?

2. What is the magnitude of transports and its associated variability for LSW passing through Flemish Pass? What is the amplitude of the seasonal cycle?

3. Which processes drive the transport variability of LSW?

To answer research question 1, the characteristics of flow and hydrography in Flemish Pass inferred from ship measurements are presented in chapter 3 in comparison to the DWBC branch, which so far had the scientific focus as the major propagation pathway [e.g. *Fischer and Schott* (2002), *Rhein et al.* (2011), *Mertens et al.* (2014), *Rhein et al.* (2015)]. Furthermore, the interannual hydrographic variability of LSW flowing through Flemish Pass in 1993 - 2013 is investigated based on shipboard CTD measurements, and put into a context with the variability observed in the LSW source region, the central Labrador Sea in chapter 4. In the central Labrador Sea, hydrographic properties and densities of the newly formed LSW varied strongly with time due to the changing intensity of oceanic convection and associated surface forcing [e.g. *Lazier et al.* (2002), *Yashayaev and Loder* (2009), *Kieke and Yashayaev* (2015), *Yashayaev et al.* (2015)], which resulted in the formation of two different modes of LSW [e.g., *Stramma et al.* (2004), *Kieke et al.* (2006), and *Kieke et al.* (2007)]. In the early 1990s, high convection activity in the Labrador Sea produced the cold dense LSW mode that is here addressed as Deep Labrador Sea Water (DLSW). Since the mid-1990s, the convection activity in the Labrador Sea has not been as strong and persistent as over the first pentad of that decade, resulting in the lighter Upper Labrador Sea Water (ULSW) to become the dominant product of water mass formation in the Labrador Sea [e.g. *Lazier et al.* (2002), *Azetsu-Scott et al.* (2003), *Stramma et al.* (2004), *Kieke et al.* (2006), *Yashayaev* (2007), *Kieke and Yashayaev* (2015)]. Following *Stramma et al.* (2004), ULSW and DLSW is defined here in the potential density ranges σ_θ = 27.68 - 27.74 kg m^{-3} and σ_θ = 27.74 - 27.80 kg m^{-3}, respectively. The LSW hydrographic variability in Flemish Pass is additionally analyzed on decadal time scales by using monthly data from an eddy resolving ocean model, run at 8 km resolution for the period 1960 - 2009 in support of the observations.

After the long term hydrographic variability is discussed in the first part of this study, the second part focuses on the short term variability of the LSW transports in Flemish Pass and the processes driving the variability. In chapter 5, research question 2 is examined based on time series data of a mooring array located in the deep water of Flemish Pass at 47°N. The LSW transports inferred from the mooring data are compared to estimates from ship based current velocity measurements. Furthermore, seasonal effects of the LSW transports from variations in the thickness of the LSW density layer as well as from variations in the flow field are studied. Characteristic time scales of variability of the LSW transports

are identified in a spectral analysis. Chapter 5 is completed by a mooring estimate of a top to bottom transport through Flemish Pass, which was calculated based on additional upper water column velocity data from a shallow mooring from Bedford Institute of Oceanography (BIO). The data was kindly provided for this study [B. Greenan, pers. communication]. In chapter 6 and chapter 7, research question 3 of this study is investigated. Both chapters address local and remote processes that potentially drive the transport variability of LSW in Flemish Pass. In chapter 6, a potential influence of the recirculation around Flemish Cap on the southward LSW transport is investigated based on the available mooring data. Furthermore, baroclinic Rossby waves are examined as a driving mechanism for the LSW variability, as these waves were previously observed in the Flemish Pass region [*Layton* (2016), *Mertens et al.* (2014)], as well as up- and downstream of Flemish Pass[e.g. *Johns and Watts* (1986) *Pickart and Watts* (1990), *Fischer et al.* (2015)]. In chapter 7, a remote connection with upstream processes is analyzed. In addition, the local atmospheric forcing as well as fast coastal trapped waves (CTWs) propagating along the continental shelf are studied, which have been identified in model studies as important processes influencing the LSW transport variability in Flemish Pass [e.g. *Han* (2005), *Han et al.* (2008), *Varotsou* (2016)] The following chapter 2 provides an overview of the data used in this study.

2 Data and Methods

2.1 Velocity observations

2.1.1 Acoustic Doppler Current Profilers - Principles of Operation

An Acoustic Doppler Current Profiler (ADCP) is an instrument to determine current velocity through the Doppler effect. An acoustic signal is transmitted by the instrument at a specified frequency, which is partly reflected back by sound scatterers like plankton or other small particles passively floating in the water and having on average the same horizontal velocity [Broadband Primer (2006)]. The reflected sound signal is subject to a Doppler shift due to the motion of the particles. This frequency shift is detected by the ADCP and used to calculate the velocity of the current that carries the passive floaters.
An important feature of an ADCP is its ability to measure velocity profiles similar to a string of current meters, as the travel time of the reflected acoustic signal can be assigned to different depth bins [Broadband Primer (2006)]. The length of the profile depends on the frequency of the device and on the abundance of scattering particles in the water. The difference between the ADCP profile and a profile from a string of current meters is that the ADCP measures the average velocity over the range of each depth bin while the current meters measure only at one discrete point in space. Due to instrument motion during the measuring process, the velocity raw data needs further processing to get absolute current velocities. The processing of the data is usually dependent on the application of the ADCP. There are three different application types of ADCPs:

- **Lowered ADCP (LADCP):**
  For the application as LADCP, the ADCP is attached to a carousel water sampler with a battery pack as an autonomous energy source. It is lowered

from the ocean surface to near the ocean bottom and then brought back to the surface (down- and up-cast), meanwhile it sends out acoustic pulses continuously and records a "time series" of short profiles [e.g. *Visbeck* (2002)]. The movements of the LADCP during the down- and up-cast are contained in the raw velocity data and need to be removed to obtain the real current velocity. Due to this, the LADCP records its pitch, roll and heading. After retrieving the data from the ADCP, the short profiles are processed to obtain one full depth profile of absolute horizontal velocity.

- **Vessel mounted ADCP (VmADCP):**
  For the application as VmADCP, an ADCP is permanently mounted on a ship, e.g. in the ship's hull or sea chest, and continuously records velocity data in the upper water column [Broadband Primer (2006)]. Processing of the raw VmADCP data is necessary to avoid heading errors, which can be induced by misalignment of the instrument transducer. Heading errors have a large impact on the measured velocity data. A heading error of 1° introduces a sideways velocity error of almost $10\,\mathrm{cm\,s^{-1}}$ when a ship steams at $5\,\mathrm{m\,s^{-1}}$ [Broadband Primer (2006)]. Therefore, the transducer orientation must be known. It is determined during data post processing in a water-track calibration.

- **Moored ADCP:**
  For the application as moored ADCP, the ADCP is deployed on a mooring in the study area to record continuous measurements of current velocity in a specified depth range over a period of several months up to a year. Moored ADCPs often have a pressure sensor to measure the instrument depth and monitor the mooring motion [Broadband Primer (2006)]. Severe mooring motion during recording of the data may require post processing of the data.

The following sections give detailed information about the current velocity data conducted through ship based as well as mooring based measurements in Flemish Pass, which were used in this study.

Table 2.1: Cruises, date, instrument type and number of velocity profiles conducted in the Flemish Pass along 47°N. Measurements of the VmADCPs OS 75 and OS 38 provided larger numbers of profiles than the LADCP measurements, as about 1 velocity profile per minute was recorded (see text in section 2.1.3 for explanation). Research vessel abbreviations are: M - Meteor, MSM - Maria S. Merian. For cruises in which multiple Flemish Pass sections were measured, brackets in column one indicate the section number.

Cruise	Date	Instrument type	Profiles
M59/2	Aug 2003	OS 75	44
MSM5/1	Apr 2007	OS 75	86
MSM12/3	Jul 2009	OS 75	142
MSM12/3	Jul 2009	LADCP	7
M82/2	Aug 2010	OS 38	199
M82/2	Aug 2010	LADCP	7
M85/1 (1)	Jul 2011	OS 75/OS 38	253
M85/1 (2)	Jul 2011	OS 75/OS 38	218
M85/1 (2)	Jul 2011	LADCP	7
MSM21/2 (1)	Jul 2012	OS 75/OS 38	197
MSM21/2 (2)	Jul 2012	OS 75/OS 38	211
MSM21/2 (2)	Jul 2012	LADCP	10
MSM27	Apr 2013	OS 75/OS 38	213
MSM27	Apr 2013	LADCP	10
MSM28	Jun 2013	OS 75/OS 38	178
MSM38 (1)	May 2014	OS 75/OS 38	205
MSM38 (2)	May 2014	OS 75/OS 38	203
MSM38 (2)	May 2014	LADCP	11

2.1.2 Shipboard LADCP measurements

Shipboard LADCP measurements were conducted in Flemish Pass during six cruises between 2009 - 2014 (see Table 2.1). The current velocity measurements were recorded using two 300 kHz LADCPs of type Teledyne-RD Instruments Workhorse Monitor, operated in a synchronized master-slave configuration, in which the downward looking master device triggers the upward looking slave device. Both instruments were set to a ping rate of 1 Hz and a 10 m depth cell size during all cruises. The vertical resolution of 10 m yielded an accuracy of $2\,\mathrm{cm\,s^{-1}}$ for the individual velocity estimates [e.g. *Walter and Mertens* (2013)]. The range of each instrument in the study region was typically about 150 m. Most of the velocity raw data was processed by applying an inverse method incorporating bottom track velocities as described by *Visbeck* (2002), with the exception of one profile each during the cruises M82/2 (profile 7), M85/1 (profile 60), and MSM27 (profile 7), which were processed using a shear method following *Fischer and Visbeck*

(1993). In a nutshell, the separation of the horizontal current velocities from the instruments motion with the shear method is based on the following assumption: Oceanic currents may change over the range of the ADCP measurements (vertical velocity shear), while the instrument velocity has no vertical shear in an individual profile [*Fischer and Visbeck* (1993)]. The instrument velocity therefore can be eliminated by vertical differentiation of the velocity raw data, which provides shear profiles. By vertical integration of the shear profiles, relative velocity profiles are derived, which can be corrected for the ship drift using GPS ship positioning to get absolute velocities. In the inverse method of *Visbeck* (2002), the data processing is based on a set of linear equations, which are solved using standard least squares methods. This approach is advantageous to the shear method, as it easily includes additional constraints such as bottom-referenced velocities, which are measured when the ocean bottom is in the range of the LADCP, and which essentially are the instrument motions.

To determine the scale of an appropriate horizontal resolution of the LADCP measurements, the Rossby radius of deformation R was determined for the Flemish Pass area, which is defined as $R = \frac{N \cdot D}{\pi \cdot f_0}$ [*Gill* (1982)]. Here, N is the Brunt-Väisälä frequency, D is the water depth, and, f_0 is the Coriolis parameter. The Brunt-Väisälä frequency was calculated from hydrographic measurements in Flemish Pass (see section 2.2), and the water depth of Flemish Pass is 1200 m. The resulting Rossby radius for the study region was 11 km. In this regard, the current field was well resolved in each individual LADCP section, as all individual LADCP surveys delivered 7 - 10 velocity profiles between 47°24'W to 46°24'W, which resulted in a typical spatial resolution of the current field of 8 - 11 km. LADCP measurements in the DWBC at 47°N conducted during the same cruises were used for a comparison of the southward volume transports in Flemish Pass and the DWBC (see section 3.2). The individual LADCP sections in the DWBC between 43°40'W and 41°W were resolved with 9 - 11 profiles resulting in station distances increasing from about 4 km at the slope of Flemish Cap towards 40 km further offshore. As the instrument settings were the same during all cruises, the data quality is assumed to be comparable for all measured LADCP profiles.

The dominant current direction in the DWBC at 47°N given by the topography is meridional [*Mertens et al.* (2014)], so no rotation of the coordinate system was applied. The main current direction in Flemish Pass is investigated in section 3.1. Each individual LADCP section of Flemish Pass and the DWBC was interpolated

onto an equidistant grid of $1/20° \times 10\,\mathrm{m}$ in order to calculate comparable transport estimates.

All LADCP profiles have been detided using the TPXO7.2 tidal model [*Egbert and Erofeeva* (2002)] following *Mertens et al.* (2014), who investigated deep water transports in the DWBC east of Flemish Cap for the period 2003 - 2011. Predictions of the tides at the times and locations of all LADCP profiles of the Flemish Pass and the DWBC sections were extracted from the tidal model. The results for the Flemish Pass region were compared to tides estimated from a moored single point current meter, which was deployed at 1070 m in the central Flemish Pass at 47°N for 10 months as part of a pilot mooring of the FLEPVAR project in 2011 - 2012, and from two moored ADCPs of the FLEPVAR project, located in the western and central Flemish Pass in 2012 - 2013 (see section 2.1.4, table 2.2). Significant tidal components were identified from the mooring records following procedures given by *Leffler and Jay* (2009) and *Pawlowicz et al.* (2002), the dominating tides were K1 (lunar diurnal), O1 (lunar diurnal), and M2 (principal lunar semidiurnal). The observational tidal amplitudes revealed reasonable agreement with the results of the tidal model, on average the amplitudes differed by about 1 cm or less, and there was no phase difference between the model and the observations. The model prediction of the tidal amplitudes mostly ranged between $\pm 2\,\mathrm{cm\,s^{-1}}$ for both the Flemish Pass and the DWBC section, which was only exceeded in the Flemish Pass sections in 2011 and 2012 ($\pm 4\,\mathrm{cm\,s^{-1}}$). In the DWBC, the maximum tidal amplitude was located slightly inshore of 43°W and decreased further offshore, which agrees with the results of *Mertens et al.* (2014) based on earlier data. The effect of the subtracted tides on the calculated volume transports (section 3.2.2) was rather small for the DWBC section, for the ULSW layer it was generally less than 0.2 Sv or 3%. The impact on the Flemish Pass ULSW transports was higher; it ranged between 0.04 - 0.4 Sv or 4 - 32%.

2.1.3 VmADCP measurements

VmADCP sections in the Flemish Pass were conducted in the years 2003, 2007, and 2009 - 2014 (see Table 5.3) using a 75 kHz and a 38 kHz Ocean Surveyor (OS) from Teledyne-RD Instruments. Both instruments were configured to collect narrow bandwidth water-profile data. Typically, one profile per minute was

measured, with the exception of cruise M59/2 (one profile in 5 minutes) and the cruises MSM5/1 and MSM12/3 (one profile in 2 minutes). To achieve maximum range, the data of the 38 kHz OS were collected in 32 m bins, which resulted in a range of 900 - 1000 m in the study area. The bin depth of the 75 kHz OS was set to 8 m to get a high vertical resolution of the upper water column, which resulted in a range of about 700 m.
Echoes of the acoustic signal at the water surface or at the bottom topography induce artifacts in the post processed data. Therefore, the first two velocity bins were excluded, and artifacts in close proximity to the Flemish Pass topography were removed manually. Furthermore, data with "percent good" parameter less than 30% were discarded. The percent good quality control parameter indicates what fraction of the pings passed the various error thresholds of the instrument. The accuracy of the velocity measurements of both OS instruments is $\pm 1.0\% \pm 0.5\,\mathrm{cm\,s^{-1}}$ according to the manufacturer [Broadband Primer (2006)]. All VmADCP sections were detided as described in section 2.1.2. In order to calculate transports comparable to the LADCP estimates, the VmADCP sections were interpolated onto the same grid of $1/20^{\circ} \times 10$ m. Furthermore, data from the 75 and the 38 kHz OS instruments were merged to create one section.

2.1.4 Mooring based measurements of current velocity and hydrography

Continuous mooring based measurements of current velocity and hydrography were conducted in the deep water of Flemish Pass during three deployment periods in 2011 - 2012, 2012 - 2013, and 2013 - 2014.

- **2011 - 2012**
  Prior to the FLEPVAR project, a pilot mooring array was deployed in Flemish Pass by the IFM/CEN from August 2011 to May 2012. The array was composed of two moorings (Figure 2.1a), one was deployed in the western Flemish Pass (FP 01-11) on the slope of the Grand Banks at an approximate water depth of 1001 m, and the other one in the center of Flemish Pass at 1253 m depth (FP 02-11). The western slope mooring consisted of an ADCP placed in a 45"buoyancy float at the top of the mooring. The ADCP was of type Teledyne-RD Instruments Long Ranger operating at 75 kHz, and

measured the horizontal current velocity over a range of 600 m. An additional temperature/conductivity recorder (MicroCAT) from Sea-Bird Electronics (type SBE37) was attached right below the ADCP to record point measurements of near bottom temperature and salinity, which was followed by an added element of buoyancy (Nautilus) and an acoustic releaser of type IXSEA/OCEANO AR 861 B1S, which disconnects the mooring from the anchor when the mooring period is terminated (Figure 2.1b). Unfortunately, the western slope mooring could not be recovered. In the central Flemish Pass, a mooring consisting of two MicroCATs SBE37 and two Aanderaa Rotor Current Meters 8 (RCM8) was deployed, recording near bottom point measurements of temperature, salinity and horizontal current velocity. Detailed information about the moorings (location, instrument depths, deployment duration, etc.) is displayed in table 2.2.

- **2012 - 2013**
  Between July 2012 and May 2013, two Long Ranger ADCP moorings with an additional MicroCAT designed as shown in Figure 2.1b were deployed in Flemish Pass as part of the FLEPVAR project (table 2.2), one on the western slope (BM25/1) at a water depth of 1009 m, and one in the center (BM26/1) at a depth of 1170 m. At BM25/1, horizontal current velocity measurements in a depth range of 370 - 915 m and near bottom (at 946 m, converted from pressure data) point measurements of temperature and conductivity were recorded. At BM26/1, current velocities in a range of 536 - 1080 m and temperature and conductivity at 1114 m depth were measured.

- **2013 - 2014**
  In 2013 - 2014, only one Long Ranger ADCP mooring with a MicroCAT (Figure 2.1b) from the FLEPVAR project was redeployed in Flemish Pass on the western slope position (BM25/2, table 2.2) at a water depth of 1014 m. Horizontal current velocity measurements in a depth range of 364 - 908 m, and point measurements of temperature and salinity at 940 m were recorded. Unfortunately, this mooring could not be recovered in May 2014 and was thought to be lost. However, the ADCP in the buoyancy float washed on shore and was found in August 2015 on the Island of Madeira in the Eastern Atlantic. The instrument was still intact and the data could be fully retrieved. The ADCP had measured on its location from June 2013 until end of April 2014, which was about one month prior to the recovery cruise.

In addition to the FLEPVAR mooring, the BIO (Canada) deployed a Long Ranger ADCP mooring located slightly northwest from the BM25/2 position, which measured the current velocity in the upper water column between the surface and 370 m depth during July 2013 to July 2014. The data was kindly made available for this study [B. Greenan (BIO), pers. communication].

All moored instruments were kept in close proximity to the bottom (within 30 m) to keep them out of reach of icebergs passing through Flemish Pass at spring times and to prevent potential damage from fishery activities. Due to the close proximity to the bottom, there was barely any vertical displacement of the instruments by currents. The maximum displacement measured by the western slope ADCPs at BM25/1 and BM25/2 was 4 m, and just 2 m were measured at BM26/1 in the center.

All ADCPs as well as the RCMs performed hourly measurements, while the MicroCATs recorded the temperature and conductivity every ten minutes. All in-

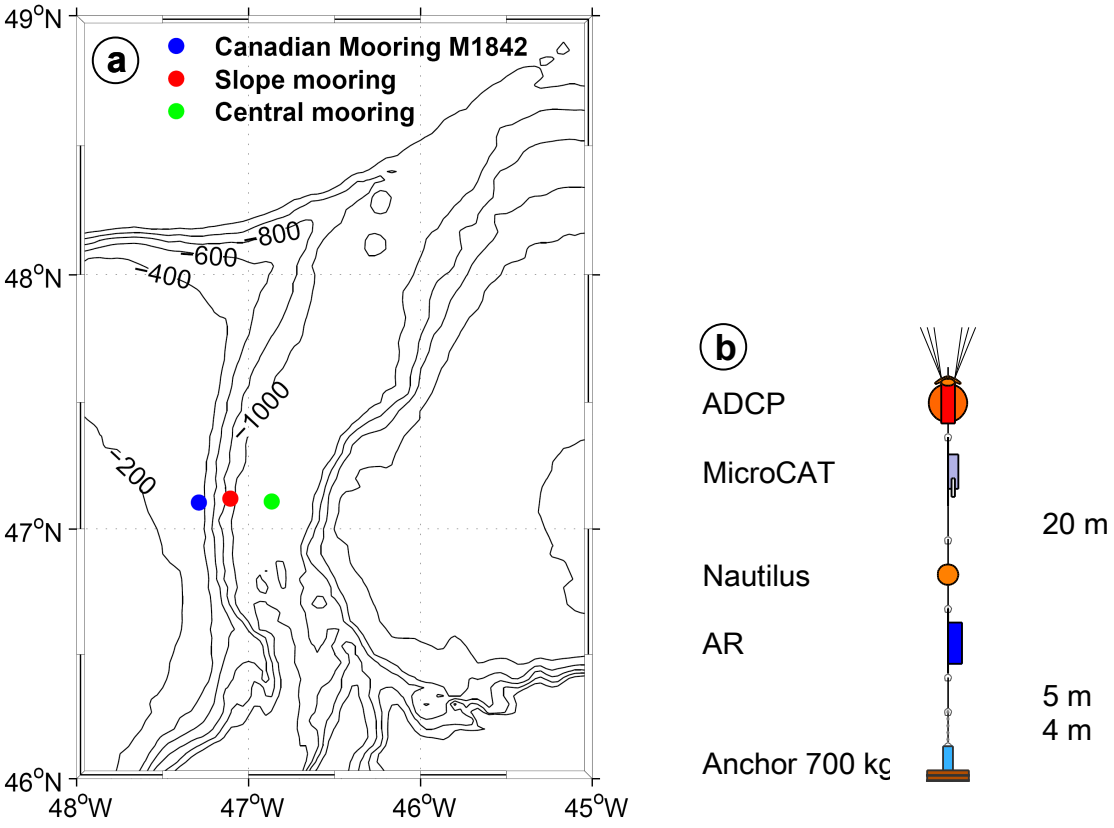

Figure 2.1: General location of the Flemish Pass moorings (a), and design of the Long Ranger ADCP moorings (b). AR: Acoustic releaser.

struments provided good quality data throughout the duration of measurements. Concerning the ADCPs of the FLEPVAR project, the percent good parameter of the data was generally higher than 85%, which indicates good quality data. The FLEPVAR ADCPs were used with a depth cell size of 16 m and 21 pings per ensemble following *Mertens et al.* (2014), resulting in a standard deviation of velocity measurements of $1.65\,\mathrm{cm\,s^{-1}}$. The Canadian ADCP M1842 was set to a depth cell size of 8 m, and 120 pings per ensemble, which resulted in a standard deviation of velocity measurements of $1.33\,\mathrm{cm\,s^{-1}}$. A quality control of the M1842 data revealed high error velocity and low percent good values in the uppermost 60 m of the record. There, the data quality is most likely reduced due to echoes of the acoustic signal at the surface. A visual control of the velocity profile data confirmed that the measurements within the upper 60 m had to be excluded. Below 60 m, the data had a good quality however.
All ADCP data of the two depth bins closest to the instruments were excluded from further analysis to prevent effects of instrument ringing induced by the acoustic pulse. The magnetic declination of the ADCP and RCM compasses was corrected. All velocity data was detided by applying a 40-h low pass fiter, and daily averages were calculated, following *Fischer et al.* (2015).
To improve the accuracy of the MicroCATS, a calibration cast was performed before each deployment. In the calibration cast, the MicroCATS were lowered together with the CTD probe, and then paused at different depths during the up-cast for five minutes to allow for water exchange as the MicroCATS were not equipped with a water pump. The MicroCAT and CTD data measured during these stops were compared to derive the average deviation of the MicroCATs from the CTD measurements, which was then corrected. The offsets of both instruments did not exceed $-0.002\,^{\circ}\mathrm{C}$ and $-0.009\,\mathrm{mS\,cm^{-1}}$. The initial accuracy of the MicroCATs is $0.002\,^{\circ}\mathrm{C}$ for temperature and $0.003\,\mathrm{mS\,cm^{-1}}$ for conductivity according to the manufacturer (Sea-Bid Electronics).

2.2 Hydrographic ship based and Argo float measurements

The hydrographic properties in Flemish Pass between 1993 and 2013 were investigated based on repeated ship sections delivering Conductivity-Temperature-

Table 2.2: Flemish Pass mooring records between 2011 and 2014.

Mooring	Position & water depth	Instrument type	Instrument pressure level (dbar)	Sampling Interval (min)	Start and End Date	Accuracy	Remarks
FP 01-11	47°06,02'N	MicroCAT	1068, 1148	10	07.08.2011	0.002° C,	
	46°51,56'W				- 13.05.2012	0.003 mS cm^{-1}	
(Center)	1160 m	RCM8	1069, 1149	60		±1.5%	
FP 02-11	47°05,99'N	ADCP	947	60	07.08.2011	1.65 cm s^{-1}	Mooring lost
(Slope)	47°06,18'W	MicroCAT	948	10		0.002° C,	
	1001 m					0.003 mS cm^{-1}	
BM25/1	47°07,13'N	ADCP	955	60	09.07.2012	1.65 cm s^{-1}	
(Slope)	47°06,20'W	MicroCAT	956	10	- 20.04.2013	0.002° C,	Conductivity sensor failure after
	1009 m					0.003 mS cm^{-1}	28.03.2013
BM26/1	47°05,94'N	ADCP	1125	60	09.07.2012	1.65 cm s^{-1}	
(Center)	46°51,58'W	MicroCAT	1126	10	- 23.04.2013	0.002° C,	
	1170 m					0.003 mS cm^{-1}	
BM25/2	47°07,11'N	ADCP	949	60	03.06.2013	1.65 cm s^{-1}	Record aborted after 28.04.2014
(Slope)	47°06,38'W	MicroCAT	950	10	- 28.04.2014	0.002° C,	MicroCAT lost
	1014 m					0.003 mS cm^{-1}	
M1842	47°05,76'N	ADCP	404	60	02.07.2013	1.65 cm s^{-1}	
(Slope)	47°16,88'W				- 08.07.2014		
	408 m						

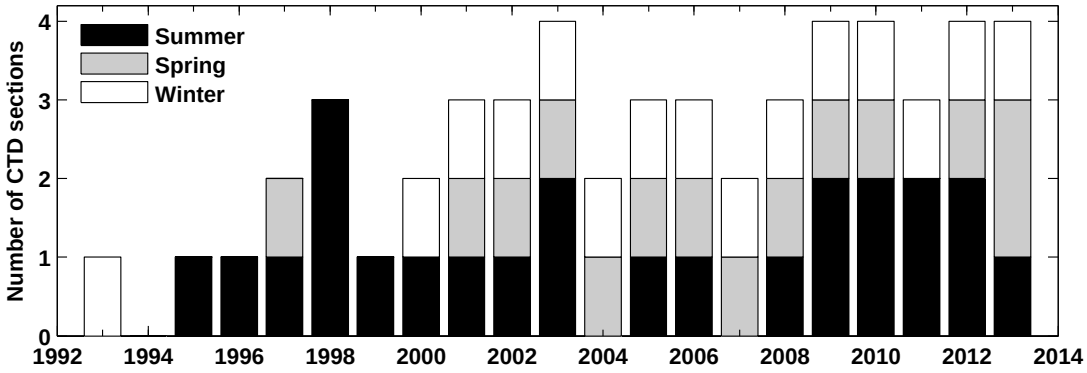

Figure 2.2: Time distribution of CTD sections measured in the Flemish Pass along 47°N during 1993 - 2013.

Depth (CTD) data along 47°N (Figure 1.1b). The cruises were conducted in the framework of several national German and Canadian projects as well as national contributions to international projects and provide Flemish Pass measurements in spring (April/May), summer (July/August) and winter (November/December) up to four times per year (Table 2.3). Since 2001, these three seasons were regularly covered by measurements, with notable exceptions in the years 2004, 2007, and 2011 (Figure 2.2). The data coverage along the 47°N section between 47°24'W - 46°24'W was usually 6 - 10 profiles with a typical spatial resolution of about 6 km over the western slope and 11 - 14 km in the center and east. Six sections consisted of only 4 - 5 hydrographic profiles. Of these, in five sections the overall spatial resolution was kept, but the sections lacked measurements over the eastern slope (cruises TL39356 in 2001, HU03038 in 2003, and TL39601 in 2005, see Table 2.3), in the center (cruise PA21014 in 1997), or over the western slope (in one out of two section realizations during cruise V172 in 1998). In one case (cruise HU93039, 1993) the station distances along the entire section were increased to 18 km. The CTD measurements conducted in the framework of German projects were recorded with a Sea-Bird Electronics (SBE) 9plus underwater unit, which was calibrated in conductivity to a salinometer standardized with IAPSO standard seawater batches. After calibration and data processing, the accuracy of the 1 dbar binned CTD data was 0.001°C for temperature and 0.002 for salinity [e.g. *Mertens et al.* (2014)]. The Canadian Atlantic Zone Monitoring Program (AZMP) provided the major part of the hydrographic measurements in Flemish Pass. The data was also measured with a SBE-9plus CTD, and calibrated to a salinometer

up until 2006. The calibrations always showed that the conductivity sensors were within specifications, and no offsets were applied to the data. After 2006, calibrations of the Canadian sensors were regularly carried out by the manufacturer of the CTD. Additionally, redundant conductivity sensors were operated which always showed values for salinity within 0.002 [E. Colbourne, Northwest Atlantic Fisheries Center (NWAFC), pers. communication]. Therefore, the individual errors of the measurements of both the German and Canadian projects are assumed to have a similar range. Salinities are reported on the practical salinity scale (PSS-78).
To compare the evolution of hydrographic properties in the Flemish Pass, in the DWBC branch off Flemish Cap and in the central Labrador Sea between 1993 and 2013, time series of hydrographic properties were calculated for the ULSW and DLSW layers for all three regions. The time series of the central Labrador Sea were provided to this study by I. Yashayaev (BIO, Canada). The time series were derived from ship-based CTD measurements along the AR7W line (see Figure 1.1a) collected during 1993 - 2013 as part of the World Ocean Circulation Experiment (WOCE), Climate Variability and Predictability (CLIVAR), and the Atlantic Zone Off-Shelf Monitoring Program (AZOMP). Since 2002, measurements from the international Argo float program complement this data set with temperature and salinity profiles of the upper 2000 m of the water column. The assumed accuracy of the Argo float profiles is ± 0.002°C for temperature, ± 2.4 dbar for pressure, and ± 0.01 for salinity [B. Klein, Federal Maritime and Hydrographic Agency (BSH), Germany, pers. communication]. The Argo float measurements used here were confined to the central Labrador Sea within the 3250 m isobath and a 150 km distance range from the AR7W line following *Yashayaev and Loder* (2009).
The time series of hydrographic properties in the DWBC branch east of Flemish Cap at 47°N were inferred from annual CTD sections conducted between 1993 and 2013. Respective data was collected in the framework of the same projects mentioned for Flemish Pass except of AZMP (see Table 2.3), as this program does not fully resolve the section and the water masses investigated here in depth and space. Argo float measurements confined by a box at 44°W - 42°54'W and 46°30'N - 47°30'N (see Figure 1.1b) and available since 2002 were also included in the time series to increase the temporal resolution. Argo data were collected and made freely available by the International Argo Program and the national programs that contribute to it (http://www.argo.ucsd.edu, http://argo.jcommops.org). B. Klein (BSH, Germany) kindly provided additional quality control on a subset of

the Argo data that were downloaded from the Coriolis data repository on 25 June 2014. From this data set, the data of the study region was extracted. As both real time and delayed mode Argo float data were used, an initial quality control of the data was performed following *Wong et al.* (2015). Only data with a quality flag 1 was selected for further analysis, and spike and gradient checks were performed. An additional visual control of the data confirmed good data quality.

Table 2.3: Cruises, date, number of CTD profiles and related projects of measurements conducted in the Flemish Pass along 47°N. Research vessel abbreviations are: HU - Hudson, M - Meteor, MSM - Maria S. Merian, PA - Parizeau, TL - Teleost, V - Valdivia, WT - Wilfred Templeman. Project abbreviations: WOCE - World Ocean Circulation Experiment; CLIVAR - Climate and Ocean: Variability, Predictability and Change; AZMP - Atlantic Zone Monitoring Program [*Therriault et al.* (1998)]; SFB 460 - Sonderforschungsbereich 460; Nordatlantik - Cooperative Research Program North Atlantic; FLEPVAR - Transports and variability-driving mechanisms in Flemish Pass at the western boundary of the subpolar North Atlantic; NAFO - Northwest Atlantic Fisheries Organization, RACE - Regional Atlantic Circulation and Global Change.

Cruise Identifier	Date	No. of profiles	Project
HU93039	December 1993	4	WOCE
PA21011	July 1995	6	NAFO sampling programs
PA21013	July 1996	6	NAFO sampling programs
PA21014	May 1997	5	NAFO sampling programs
PA21015	July 1997	6	NAFO sampling programs
TL39068	July 1998	6	NAFO sampling programs
V172	July 1998	5	SFB 460
V172	July 1998	7	SFB 460
TL39080	July 1999	6	AZMP
TL39305	July 2000	6	AZMP
HU20004	November 2000	6	AZMP
TL39352	April 2001	6	AZMP
TL39356	July 2001	4	AZMP
HU20390	November 2001	6	AZMP
TL39403	April 2002	6	AZMP
TL39408	July 2002	6	AZMP
HU20449	November 2002	6	AZMP
TL39462	April 2003	6	AZMP

Cruise Identifier	Date	No. of profiles	Project
HU03038	July 2003	5	CLIVAR
TL39466	July 2003	6	AZMP
HU20507	November 2003	6	AZMP
TL39524	April 2004	6	AZMP
HU20586	November 2004	7	AZMP
TL39601	May 2005	4	AZMP
WT10624	July 2005	6	AZMP
HU20656	November 2005	6	AZMP
TL39670	April 2006	6	AZMP
W10675	July 2006	6	AZMP
HU20731	December 2006	6	AZMP
TL39741	April 2007	6	AZMP
HU20754	November 2007	6	AZMP
TL39807	April 2008	6	AZMP
TL39811	July 2008	6	AZMP
HU20865	December 2008	6	AZMP
TL39886	April 2009	6	AZMP
TL39890	July 2009	6	AZMP
MSM12/3	August 2009	7	Nordatlantik
HU20929	December 2009	6	AZMP
TL39971	April 2010	6	AZMP
TL39973	July 2010	6	AZMP
M82/2	August 2010	7	Nordatlantik
HU20983	December 2010	6	AZMP
TL39093	July 2011	6	AZMP
M85/1	August 2011	7	Nordatlantik
HU20111	November 2011	6	AZMP
TL39101	April 2012	6	AZMP
TL39104	July 2012	6	AZMP
MSM21/2	July 2012	10	Nordatlantik
HU20112	November 2012	6	AZMP
TL39114	April 2013	6	AZMP
MSM27	April 2013	10	FLEPVAR
TL39117	July 2013	6	AZMP
HU20113	November 2013	6	AZMP
MSM38	May 2014	11	RACE

2.3 Hydrography in a numerical model

The temporal evolution of hydrographic properties in the ULSW observed in the Flemish Pass was furthermore compared to a model time series. The model data was derived from a high resolution version of the MIT/gcm [*Marshall et al.* (1997)], which is run and processed at the Institute of Oceanography (IfM/CEN), Hamburg, Germany. There, the coupled ocean - sea ice model is configured for the Atlantic north of 33°S including the Nordic Seas and the Arctic Ocean in the period 1960 - 2009 [*Serra et al.* (2010)] and provides monthly output. The spatial resolution in the study area is 8 km horizontally with 50 vertical depth levels varying from 10 m in the upper ocean to 550 m in the deep ocean. The model is forced with atmospheric fluxes computed using the atmospheric state from the NCEP RA1 reanalysis [*Kalnay et al.* (1996)]. A separate study analyzing ULSW transport variability in the vicinity of Flemish Cap in the model run is presented by *Varotsou et al.* (2015). There, detailed model validation is given, and processes modulating ULSW variability over a period of 50 years are discussed. For the present purpose, model data provided by N. Serra and E. Varotsou (both IFM/CEN) was used to compare the general hydrographic and velocity structure in Flemish Pass for those periods when observations and model data overlap. Following *Varotsou et al.* (2015), the definitions of the model boundaries defining ULSW and DLSW are identical to those applied to the observations and given above. To validate the multidecadal representation of ULSW hydrographic properties in the model, model time series of ULSW temperature and salinity anomalies from the central Labrador Sea were compared to observations from this region, which date back to the late 1940s (see Figure 2.3). To take differences in the hydrographic properties of the model and the observations into account, which are described in more detail in section 3.3.1, temperature and salinity anomalies relative to the mean of the period 1994 - 2009 (the overlapping time frame of model data and observations in the Flemish Pass area) were used for the validation. The multidecadal variability of the model agrees with the observed temperature and salinity evolution. Therefore, hydrographic anomaly time series of the model were further utilized to put variations found in the hydrographic properties in Flemish Pass into a multidecadal context.

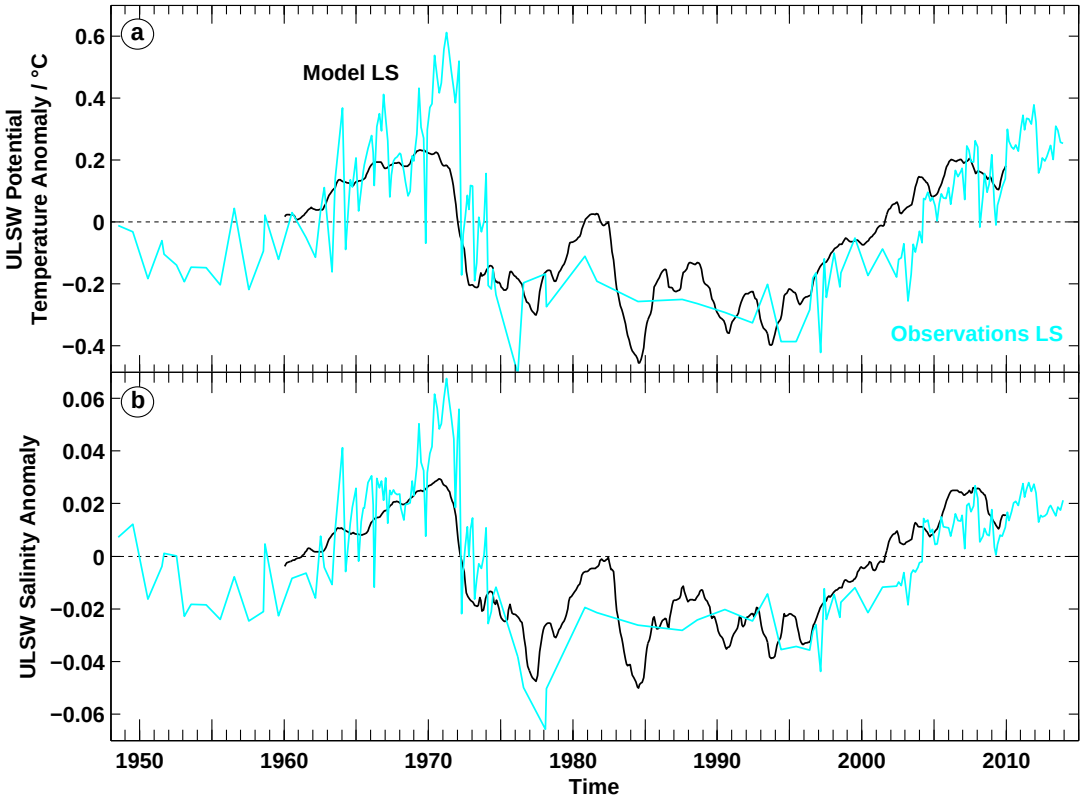

Figure 2.3: Time series of ULSW hydrographic anomalies in the central Labrador Sea based on hydrographic measurements (cyan, seasonal cycle removed) and derived from the MIT/gcm model (black, 15 months low pass filtered). (a) Median potential temperature anomaly (°C) and (b) median salinity anomaly relative to the mean of the period 1994 - 2009 (as in Figure 4.7). Note that the temporal resolution of observed data is much coarser in the late 1970s and 1980s than in the previous and the following decades.

3 Characteristics of flow and hydrography in the Flemish Pass area

In this chapter, the main characteristics of the flow and hydrography in Flemish Pass are investigated and compared to the DWBC at 47°N using ship based LADCP and CTD measurements. Furthermore, LADCP based estimates of the LSW transport through Flemish Pass and in the DWBC are determined to assess the contribution of the Flemish Pass branch to the total southward LSW transport across 47°N. The results shown in the present and the following chapter were published in *Schneider et al.* (2015).

3.1 Principal component analysis of the flow in Flemish Pass

At 47°N, the Flemish Pass topography is nearly in meridional direction. To estimate the main orientation of flow through Flemish Pass, a principal component analysis was performed using the moored ADCP data of 2012 - 2013. In this period, two moorings were deployed in Flemish Pass. By principal component analysis, the principal axes are found along which the variance in the observed velocity fluctuations $u' = u - \bar{u}$, $v' = v - \bar{v}$ is maximized; here u and v are the respective zonal and meridional velocity components and $\bar{u}$, $\bar{v}$ the respective means. According to *Emery and Thomson* (2001), the orientations of the two principal axes differ by 90° and are defined by the principal angle θ_p, which is determined

by:

$$\theta_p = \frac{1}{2}\tan^{-1}\left[\frac{2\overline{u'v'}}{\overline{u'^2} - \overline{v'^2}}\right] \tag{3.1}$$

with $-\pi/2 \leq \theta_p \leq \pi/2$. The principal variances λ_1 and λ_2 give the variance of the flow along the major axis and minor axis, respectively. They are defined by:

$$\left\{ \begin{array}{c} \lambda_1 \\ \lambda_2 \end{array} \right\} = \frac{1}{2}\left\{ \left(\overline{u'^2} + \overline{v'^2}\right) \pm \left[\left(\overline{u'^2} - \overline{v'^2}\right)^2 + 4\left(\overline{u'v'}\right)^2\right]^{1/2} \right\} \tag{3.2}$$

The orientation of the major principal axis determined from the data of each depth bin of the moored ADCP BM25/1, exemplary shown in three different pressure levels in Figure 3.1, deviate slightly from meridional direction by 3° to 8° depending on the depth of the measurements, with the largest deviation at the deepest level and the smallest deviation in the shallowest level. Furthermore, they appear to be parallel to the local isobaths of the western slope of Flemish Pass. The minor principal axes are much smaller than the major ones, showing that there is only little cross-shore variability at this location. In the central Flemish Pass at the location of ADCP mooring BM26/1, the major axes are shorter and the minor axes are longer than at BM25/1, indicating that there is less long-shore and a bit more cross-shore variability than at the western slope (Figure 3.1). The major axis of the depth bins deviate by 9° to 19° from meridional direction with the deviation increasing with depth.
Additionally, the orientation of the mean current velocity axis during each time series was calculated and compared to the orientation of the principal axes. The mean current axes at BM25/1 and BM26/1 deviated from meridional direction by 9 to 11° and 25 to 28°, respectively. For both moorings, the orientation of the mean current axis therefore agreed within a few degrees with the principal angles. The best agreement was found for the near bottom levels of both moorings (depths exceeding 750 m at BM25/1 and 920 m at BM26/1).
As both the major axes and the mean current direction at both mooring locations deviate from the meridional direction due to the topographic setting, it was neces-

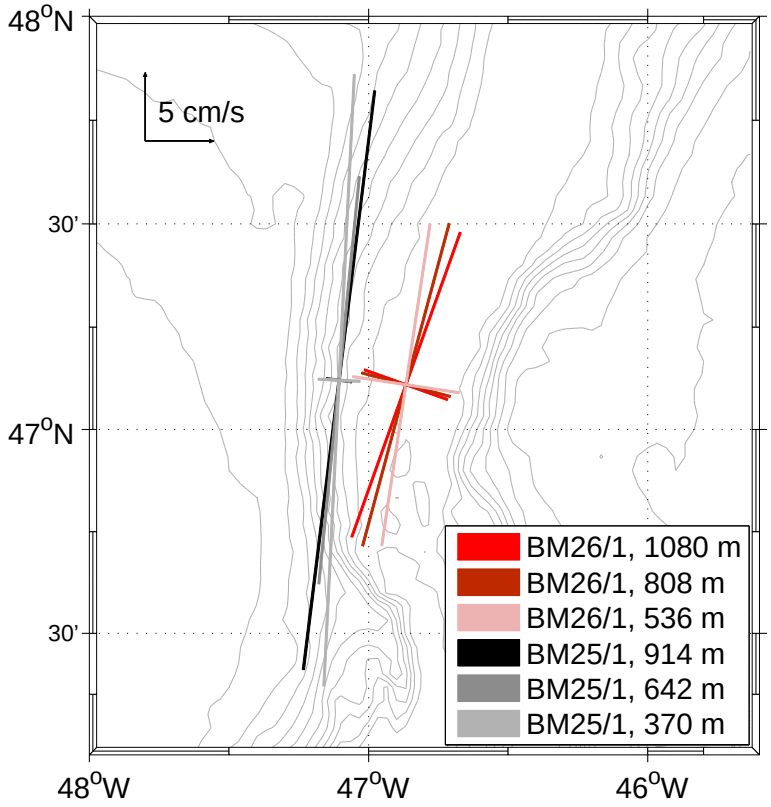

Figure 3.1: Principal axes for daily averaged velocity components u and v measured by the two Flemish Pass ADCP moorings in 2012 - 2013, each in three different depth levels.

sary to consider, if a rotation of the coordinate system around the principal axes was needed. Therefore, transport estimates were calculated both for an unrotated coordinate system, and for a rotation of 3° and 19°, which are the minimum and maximum principal angles determined in the principal component analysis. The mean transports for the minimum and maximum rotation only differed by 0.04 - 0.14 Sv (2 - 7 %) from the transport estimate without rotation. As the effect of the rotation of the coordinate system on the transports is small, no rotation of the coordinate system was applied to the velocity data in the following.

3.2 General flow structure of the LSW branches

3.2.1 Flemish Pass compared to the DWBC, 2009 - 2013

The average meridional velocity distribution in Flemish Pass, 2009 - 2013 (Figure 3.2a), divides into an area of southward flow dominating the western and central pass, and a smaller area of northward flow further east located over the slope of Flemish Cap. The southward core of the shallow Labrador Current indicated by velocities exceeding $-30\,\mathrm{cm\,s^{-1}}$ is the characteristic feature in the upper part of the water column (p <200 dbar) above the western slope of Flemish Pass (Figure 3a). In the ULSW and DLSW layers, the average southward velocities are -5 to $-10\,\mathrm{cm\,s^{-1}}$ and exceed $-10\,\mathrm{cm\,s^{-1}}$ at the western slope between 800 - 1100 dbar (Figure 3a). As indicated by the isopycnals, the ULSW layer was completely captured in the average section; it was the dominant LSW mode in Flemish Pass over the considered years. The denser DLSW formed the bottom layer and was confined in its vertical extent as the Flemish Pass represents a natural barrier for deeper and denser flow (see also Figure 3.3). The southward transport through Flemish Pass is limited in the east by the northward flow, which results from a topographically generated anticyclonic gyre around Flemish Cap, previously described by e.g. *Kudlo et al.* (1984), *Colbourne and Foote* (2000), and *Gil et al.* (2004). The mean southward transport of ULSW through Flemish Pass calculated from the average velocity section for the period 2009 - 2013 is -1.2 ± 0.1 Sv with the uncertainty denoting the standard error of the mean. The mean southward DLSW transport of -0.1 ± 0.03 Sv is relatively small, as just a fraction of the DLSW layer is shallow enough to be carried through Flemish Pass.

The meridional velocity section within the DWBC branch averaged over the same period (Figure 3.2b) revealed two distinct velocity cores of the DWBC, a slope and a rise core, which were previously observed and discussed by *Mertens et al.* (2014) for a different set of sections. In the mean of 2009 - 2013, the slope core with average southward velocities up to $-30\,\mathrm{cm\,s^{-1}}$ was located at the eastern slope of Flemish Cap and comprised almost the entire water column. The second core, located offshore at the continental rise between 42°48'W - 41°30'W, was bottom-intensified and had velocities exceeding $10\,\mathrm{cm\,s^{-1}}$ close to the seafloor. East of the DWBC was the northward flowing NAC. As the rise part of the DWBC transports mainly deep water components to the south that are denser than LSW, the focus here was on the slope part and the mean southward ULSW transport

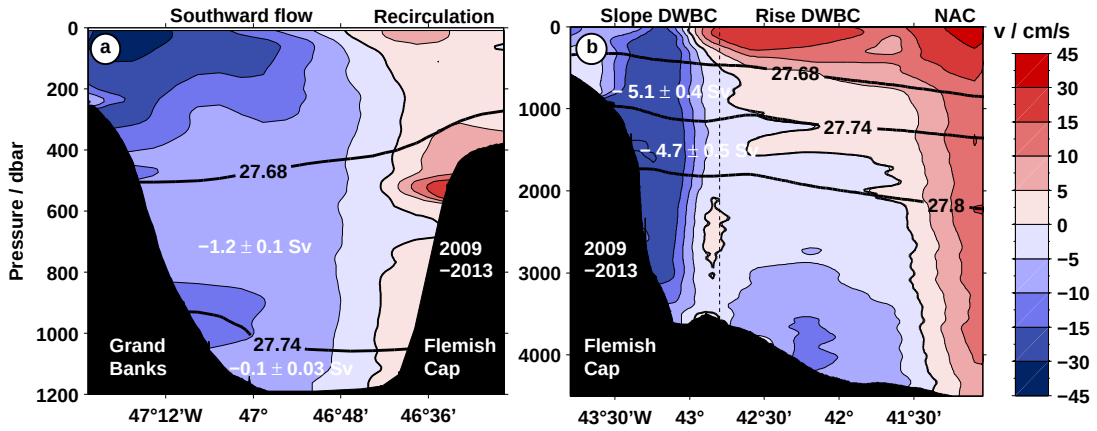

Figure 3.2: Meridional velocity distribution ($\mathrm{cm\,s^{-1}}$) averaged for the period 2009 - 2013 and derived from LADCP data of (a) the Flemish Pass, and (b) the DWBC, both at 47°N. Black lines indicate σ_θ-isopycnals ($\mathrm{kg\,m^{-3}}$) as water mass boundaries of ULSW and DLSW. Respective transports for the ULSW and DLSW layers with standard mean error margins are given in white numbers. The dashed line in (b) indicates the limit between the slope and rise part of the DWBC following *Mertens et al.* (2014). Note the different vertical scales in the two subfigures.

of 2009 - 2013 between 44°W - 42°48'W was calculated following *Mertens et al.* (2014), who inferred deep water transports for $\sigma_\theta > 27.68\,\mathrm{kg\,m^{-3}}$ in the DWBC at 47°N. The resulting mean southward transport of ULSW is $-5.1 \pm 0.4\,\mathrm{Sv}$, and the corresponding mean southward transport of DLSW is $-4.7 \pm 0.5\,\mathrm{Sv}$. Considering the southward ULSW transport of $-6.3\,\mathrm{Sv}$ across 47°N (Flemish Pass branch and slope part of the DWBC), 19 % of this ULSW transport is through the Flemish Pass. Concerning the DLSW, only 2 % of the southward transport follows the Flemish Pass branch, while the major part is carried within the DWBC branch around Flemish Cap.

3.2.2 Individual velocity sections and transports in Flemish Pass and the DWBC in 2009 - 2013

The individual snapshots of the meridional current velocity observed in 2009 - 2013 (Figure 3.3b - f) yield insight into the variability of the strength and lateral extent of the recirculation area, which limits the southward transports through

the Flemish Pass in the east. In the ULSW layer, the zero velocity contour separating southward and northward flow was nearly vertical at about 46°42' W in the year 2009 and tilted towards the Flemish Cap between 46°44'W - 46°39' W in 2010. In 2011, its location changed with depth from 46°36'W between 300 and 600 dbar to about 46°48'W below 800 dbar. In 2012 and 2013, it was variable with depth between 46°44'W - 46°39'W. Within the northward flow, velocities were mostly $<10\,\mathrm{cm\,s^{-1}}$ except in 2009, when the maximum northward flow exceeded velocities of $20\,\mathrm{cm\,s^{-1}}$. *Kudlo et al.* (1984) found a predominately anticyclonic gyre circulation around Flemish Cap, which occasionally breaks down influenced by atmospheric forcing such as storm activity. *Colbourne and Foote* (2000) noted that this circulation feature is particularly common over the summer months when wind-forcing due to passing storms is reduced. Frequent breakdown of this circulation into flows meandering across the Flemish Cap may occur, which impacts the residence time of waters on the cap [*Colbourne and Foote* (2000)]. The Flemish Pass velocity sections conducted in 2009, 2010, and 2012 (Figure 3.3b, c and e) were all measured in the summer month July or August, and they all show a pronounced northward flow around Flemish Cap. The sections measured 2011 (Figure 3.3d) and especially in 2013, which was conducted in April (Figure 3.3f) exhibit weaker northward flow, and the recirculation was interrupted within the upper 400 m of the water column, confirming the observations of *Kudlo et al.* (1984) and *Colbourne and Foote* (2000).

The southward ULSW transports calculated from all individual LADCP section snapshots serve to describe the transport variability of the Flemish Pass and the DWBC branch (Table 3.1). ULSW estimates from the individual sections crossing Flemish Pass ranged between -1.0 and -1.5 Sv, which ranks on the lower end of the mooring based transports as will be further discussed in chapter 5.3.2. In the slope part of the DWBC branch the southward ULSW transports varied between -3.9 and -6.3 Sv. The contribution of the Flemish Pass branch to the total southward ULSW transport across the two 47°N segments ranged between 15 - 27 %. The DLSW transport is small in the Flemish Pass and reached only up to 2 % compared to the slope part of the DWBC.

August 2009 is the only velocity field of the numerical model having a direct overlap in time with the observations. For this reason it is included here (Figure 3.3a) and compared to the individual velocity snapshots (Figure 3.3b - f). The model section exhibits similar structures, but also some expected differences to the ob-

Table 3.1: Southward volume transports [Sv] for the ULSW layer derived from detided shipboard LADCP measurements conducted at 47°N in Flemish Pass and in the slope part of the DWBC (West of 42°48'W).

	Southward ULSW transports (Sv)	
Date	Flemish Pass	Slope DWBC
August 2009	-1.1	-5.1
August 2010	-1.4	-3.9
July 2011	-1.1	-6.3
July 2012	-1.0	-4.7
April (June*) 2013	-1.5	-6.3*

servations, because monthly model output is compared to an individual LADCP snapshot. Overall, the model velocity field in Flemish Pass shows a dominant southward flow, which is intensified towards the centre. In the observations, the velocity field is intensified towards the western boundary of the Flemish Pass. Velocity maxima exceeding $-20\,\mathrm{cm\,s^{-1}}$ in the upper 200 dbar pressure range indicate the core of the model's representation of the Labrador Current. The southward ULSW transport calculated from the model velocity field is -1.4 Sv, which is slightly higher than the transport of -1.1 Sv observed in August 2009, but similar to the observed estimate of August 2010. The northward recirculation is also visible in the model section on the western slope of Flemish Cap. In contrast to the observations it has a much smaller lateral extent and does not extent into the ULSW layer. Different from the observations, LSW transport through Flemish Pass in the model is limited to the ULSW layer in August 2009, any DLSW is absent. *Varotsou et al.* (2015) investigated the model meridional velocity section average over the period 1960 - 2009. Over this period, the model reproduces the average flow structure observed in the Flemish Pass between 2009 - 2013. The contribution of the model Flemish Pass branch to the average southward ULSW transport across 47°N in 1960-2009 is 20%. This agrees well with the observations (19% on average in 2009 - 2013).

3.3 The Flemish Pass hydrography

3.3.1 Average water mass structure in Flemish Pass, 1995 - 1998 vs. 2009 - 2013

The average structure of hydrographic properties and representation of water masses in Flemish Pass shown in Figure 3.4b, c, e, f is derived from CTD sections measured in summers during two time frames. The first time frame 1995 - 1998 represents the period just following the high convection activity in the Labrador Sea observed in the early 1990s [*Lazier et al.* (2002)], while the second time frame 2009 - 2013 covers the recent period of variable and less intense convection [*Kieke and Yashayaev* (2015)]. In the upper 200 dbar range of the water column, the average distributions of potential temperature θ and salinity reveal similar patterns in both periods. The upper layer with salinities below 34.6 is generally fresher than the deeper waters (Figure 5e, f). Another common feature on the western side of Flemish Pass is the core of the cold Labrador Current centered at about 100 dbar with temperatures well below 2°C (Figure 3.4b, c). Since the focus here is on the LSW layers, further details of the upper layer are not discussed here and not highlighted in the figure, which has a color scale optimized for the LSW layers. At pressures exceeding 200 dbar, temperature maxima (exceeding 3.35°C in 1995 - 1998 and 4.1°C in 2009 - 2013) are located over the western Flemish Cap and extend into the ULSW layer in both periods. The ULSW layer in the western and central Flemish Pass had temperatures that were colder by more than 0.1°C (up to 0.35°C at the bottom of the ULSW layer in the second period) compared to the east above Flemish Cap in both periods. The salinities in the eastern Flemish Pass were elevated throughout the entire ULSW layer (exceeding 34.84 in 1995 - 1998 and 34.9 in 2009 - 2013) in both periods (Figure 3.4e, f), while the central and western Flemish Pass was fresher by 0.01 - 0.03. The local temperature and salinity maxima in the eastern Flemish Pass most likely result from the anticyclonic gyre around Flemish Cap, [e.g. *Kudlo et al.* (1984), *Colbourne and Foote* (2000), and *Gil et al.* (2004)]. The water within this gyre possibly interacted with the warm and salty NAC east or south of Flemish Cap before recirculating northwards into the Flemish Pass (Figure 1.1a); a process, which will be further addressed in section 3.3.2.

The major differences between the property distributions in the LSW layers of

both periods are that the water was significantly warmer and more saline in 2009 - 2013 with a much deeper location of the $\sigma_\theta = 27.74\,\mathrm{kg\,m^{-3}}$ isopycnal than observed in 1995 - 1998. Due to the deepening of the $\sigma_\theta = 27.74\,\mathrm{kg\,m^{-3}}$ isopycnal, the layer thickness of the ULSW more than doubled. Thus, the overall presence of LSW in the Flemish Pass was dominated by its lighter component (ULSW) in 2009 - 2013. Only a small fraction of DLSW, which was the dominant LSW mode in the first period, could pass through Flemish Pass in the second period.
Furthermore, model output of the period 1995 - 1998 (Figure 3.4a, d) was compared with the respective observations (Figure 3.4b, e) as the model run ends in 2009. The model hydrography differs from the observations (mind the different colorbars in Figure 3.4a, d, and Figure 3.4b, e), with the temperatures and salinities of the ULSW layer being about 1°C and 0.15 higher. Only the lighter ULSW is present in the model average section in Flemish Pass and no DLSW (also seen in Figure 3.3a). DLSW was found in Flemish Pass in the model only in seven months of the considered period (June - November 1995, and August 1996).

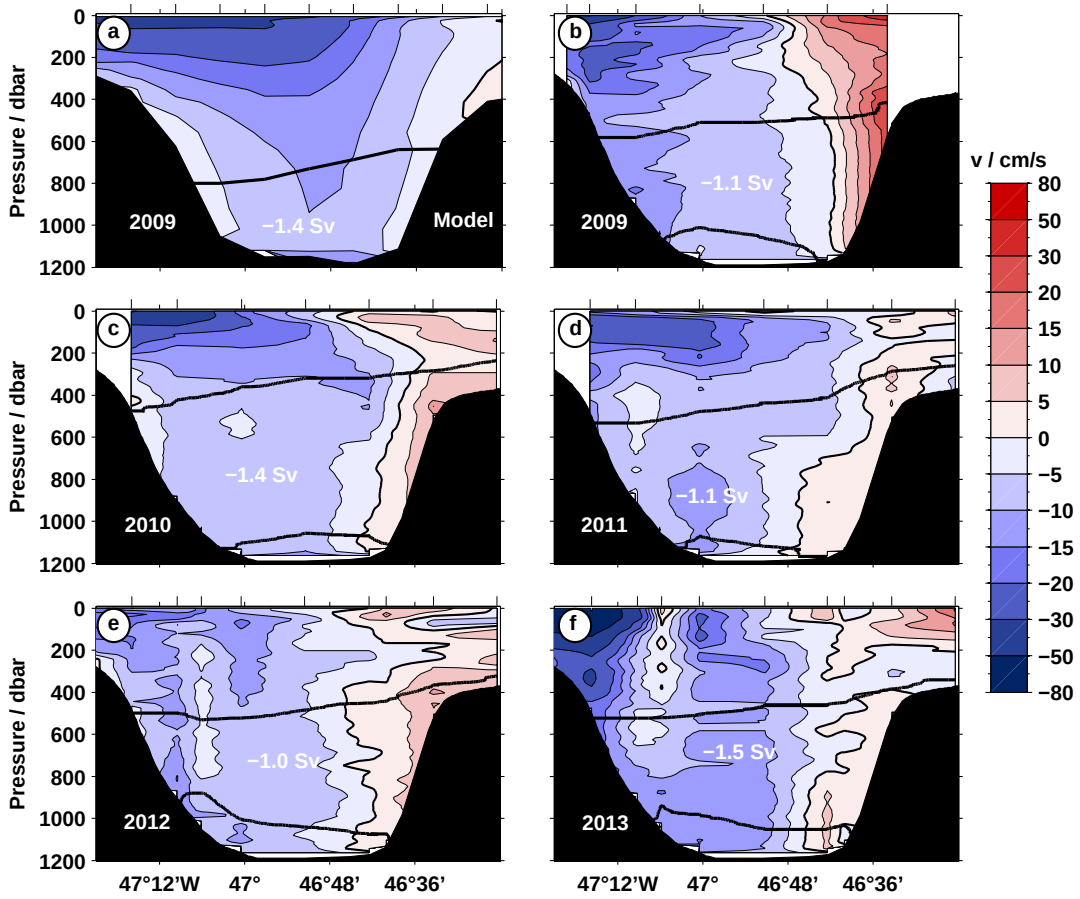

Figure 3.3: Meridional velocity ($\mathrm{cm\,s^{-1}}$) in the Flemish Pass along 47°N from (a) the MIT/gcm model output, mean of August 2009, (b) - (f) individual LADCP sections carried out on five cruises between 2009 and 2013. σ_θ-isopycnals ($\mathrm{kg\,m^{-3}}$) defining ULSW are given as black lines. In (a), only the upper ULSW isopycnal is captured in the section. Profiles are indicated by ticks at the top of each plot.

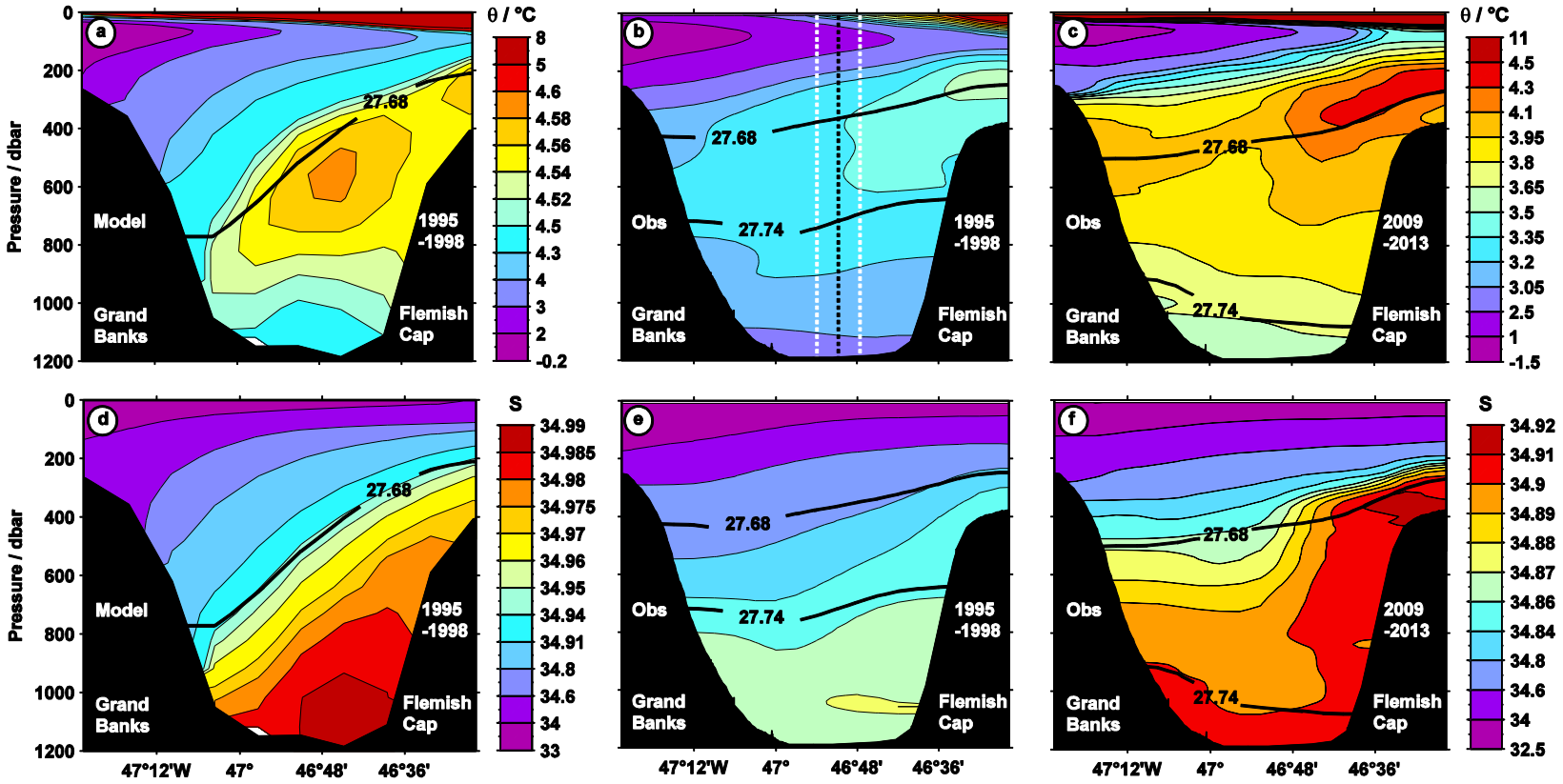

Figure 3.4: Average property distributions of two time periods in the Flemish Pass at 47°. Top row: Mean potential temperature θ (°C) of (a, b) 1995 - 1998 from the MIT/gcm model and observations, respectively, and (c) from observations in 2009 - 2013. Bottom row: As in top row, but for salinity. Note different color bars for the model (a, d) and the observations. Black lines indicate σ_θ-isopycnals (kg m^{-3}) as water mass boundaries of ULSW. Dashed lines in (b) indicate the mean (black) and standard deviation (white) of the location of the deepest measured profile per section used for constructing Figure 4.3c.

However, the general hydrographic structures represented in the model sections are similar to the observations. In the upper 200 dbar range, the cold Labrador Current with core temperatures <2°C is visible (Figure 3.4a). The upper ULSW isopycnal has a slope from east to west across the Flemish Pass as a result of the model's salinity stratification, which has higher salinities over the slope of Flemish Cap. The slope of the ULSW isopycnal is steeper than in the observations indicating that the model is more baroclinic. In the ULSW layer, maxima of model temperatures are located further in the centre of Flemish Pass than in the observations, but they extend to the slope of Flemish Cap, while the model salinities have a maximum at the bottom. This points to model ULSW being generally more saline compared to the observations. To summarize, the Flemish Pass observations revealed remarkable property changes in the deeper water layers between the periods 1995 - 1998 and 2009 - 2013. These changes are further studied in the section 4.1. The focus is on the LSW, which is transported southwards through the Flemish Pass, but the evolution in the northward recirculation, which also exhibits warming and salinification between the two time periods, will be analyzed as well. The characteristic hydrographic structures in the Flemish Pass are reproduced by the model, even though the salinities and temperatures are higher than in the observations.

3.3.2 Average hydrographic properties of LSW in Flemish Pass in comparison to the DWBC at 47°N

The average hydrographic property distributions derived from CTD sections occupied in summers 2009 - 2013 reveal very similar temperature and salinity signatures of ULSW in the western and central Flemish Pass (Figure 3.5a, c, as in Figure 3.4c, f with different color scale) and in the slope part of the DWBC at 47°N (Figure 3.5b, d). The fraction of DLSW flowing through the Flemish Pass also agrees well with the upper part of DLSW in the slope DWBC. The hydrography in the slope part of the DWBC at 47°N is not affected by exchange with the warm and saline NAC as both are separated by a pronounced front that hinders strong mixing and diversion between the two. The rise part of the DWBC, however, is warmer and saltier than the slope part by more than 0.1°C and 0.01, respectively, due to interactions with the NAC, which was also observed by *Mertens et al.* (2014). These elevated tem-

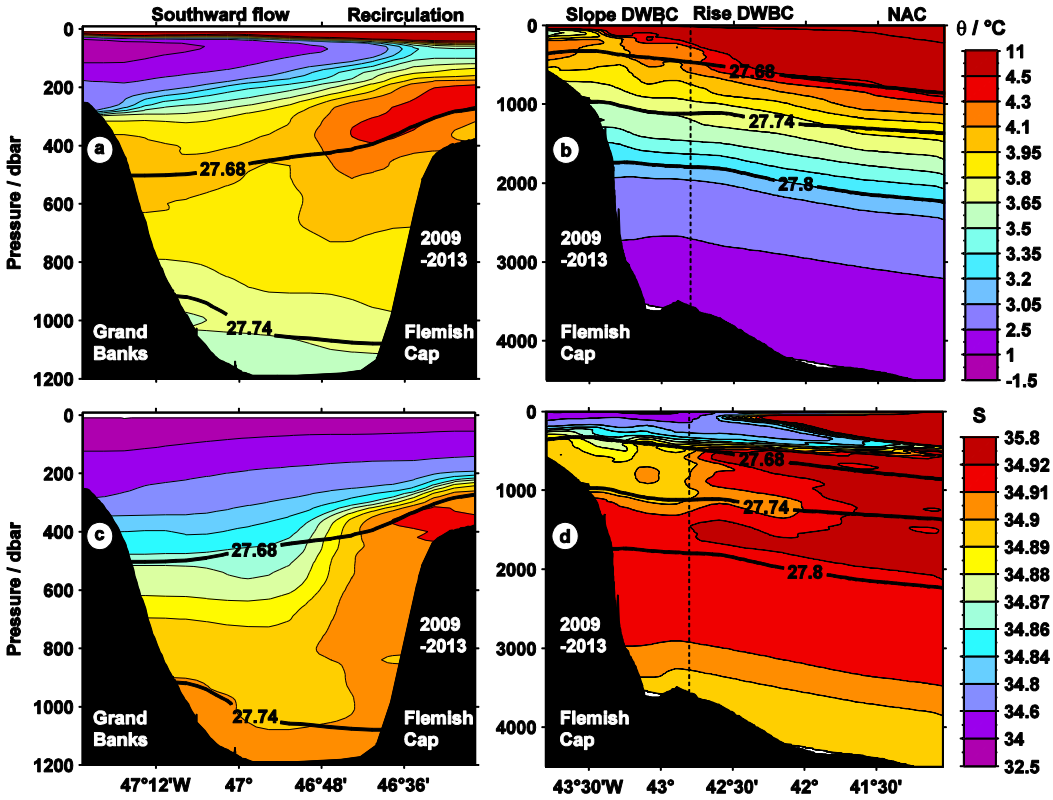

Figure 3.5: Average property distributions in the Flemish Pass (a, c; same as in Figure 5 c, f but with different colorscale) and in the DWBC at 47°N (b, d). Top row: Mean potential temperature θ (°C), bottom row: as in top row, but for salinity. Black lines indicate σ_θ-isopycnals (kg m^{-3}) as water mass boundaries of ULSW.

peratures and salinities are very similar to the temperature and salinity maxima in the northward recirculation area of the Flemish Pass. This indicates that warm and salty NAC water might be mixed into the slope part of the DWBC south of 47°N on the way around the Flemish Cap, before part of it recirculates northward into the Flemish Pass [*Colbourne and Foote* (2000)]. This is in agreement with *Cerviño et al.* (1999), who found a water mass on the southwestern Flemish Cap at a depth of 200 to 300 m with hydrographic properties similar to the NAC in July 1996, which they referred to as Slope Water originating south of Flemish Cap by mixing of the NAC and the Labrador Current [*Hayes et al.* (1977)]. *Keeley* (1982) furthermore identified the western Flemish Cap as a region of mixed water types of warm and salty NAC water and cold and fresh Labrador Current water.

This process of mixing of water masses of different properties and origin creates a density gradient across Flemish Pass.

4 Hydrographic variability of LSW transported through Flemish Pass during 1993 - 2013

Chapter 3 revealed remarkable changes in the Flemish Pass hydrography between the late 1990s and recent years. In this chapter, the hydrographic variability of LSW flowing through Flemish Pass between 1993 and 2013 is investigated. In order to do this, CTD based time series of hydrographic properties were derived. Furthermore, research question 1 of this study "Is the Flemish Pass a southward export pathway for LSW from the Labrador Sea?" is addressed by comparing the long-term hydrographic variability of the Flemish Pass with the hydrographic variability of the LSW source region, the central Labrador Sea, and the DWBC at 47°N, which is so far recognized as the main southward export route of LSW [e.g. *Talley and McCartney* (1982)].

4.1 Long term variability of the LSW hydrographic properties

To investigate the long-term variability within the southward flow in Flemish Pass, the analysis was confined to the central Flemish Pass west of 46°48'W and includes only profiles with a maximum pressure exceeding 1000 dbar (area shown in Figure 3.4b). By this, a better distinction between the ULSW and DLSW layers was facilitated, vertical variations in the depth of their interface and the interface of ULSW with the shallower waters were minimized, and the influence of the warm and salty recirculation was avoided. By comparison with time series of ULSW restricted to the western slope of Flemish Pass west of 47°W (DLSW

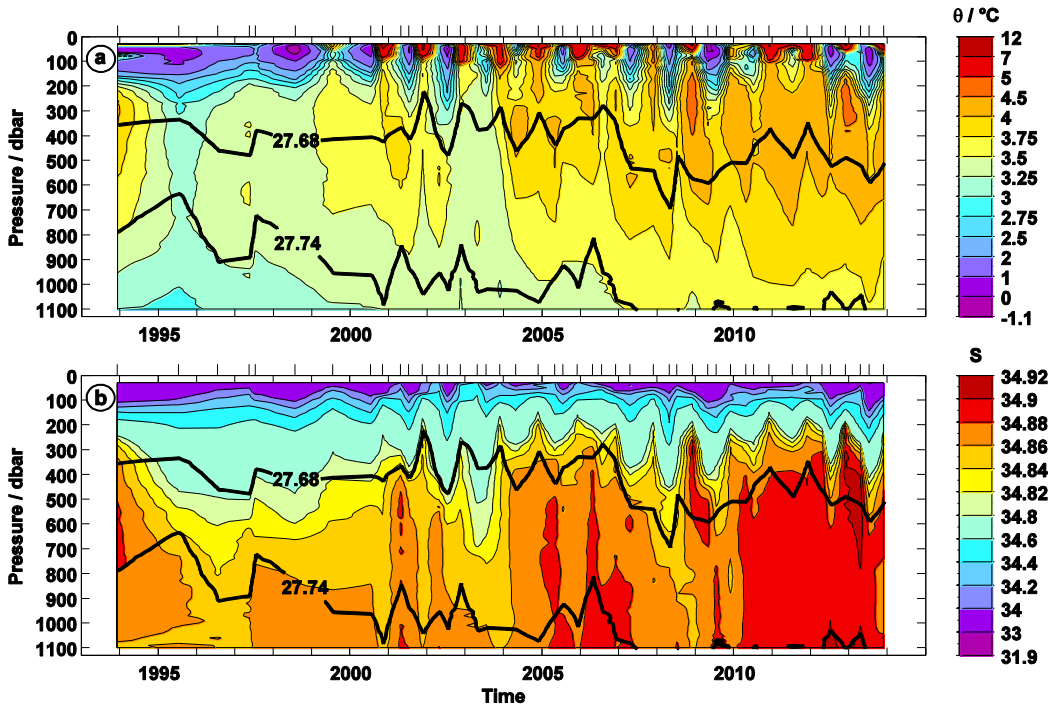

Figure 4.1: Hydrographic evolution in the water column of Flemish Pass during 1993-2013, (a) potential temperature θ (°C); (b) salinity. Ticks at the top of each subplot highlight available data. σ_θ-isopycnals (kg m^{-3}) defining ULSW are given as black lines.

is not fully resolved over the slope), a high significant correlation of R = 0.96 was found. Therefore, the limitation of the analysis to the central Flemish Pass was considered sufficient to represent the variability of hydrographic properties within the southward flow. The long-term variability of ULSW in the northward recirculation east of 46°48'W was analyzed separately (see below).

Water masses mostly mix along isopycnals, and isopycnal averaging avoids artifacts in average water properties [*Lozier et al.* (1995)]. Consequently, the respective profiles were interpolated on σ_θ-surfaces (grid spacing 0.002 kg m^{-3}), and isopycnal averaging was used to generate one mean profile for each section, which was then recalculated to a pressure grid. When multiple section measurements in the time span of a month were available (due to two cruises following closely after each other), the mean profiles of those were averaged as well to generate resulting time series of temperature and salinity in the water column of Flemish Pass in 1993 - 2013, which are presented in Figure 4.1. Before 2001, the temporal

resolution of the time series is yearly, thus not resolving seasonal variability; afterwards averaged profiles are mostly available for each of the three survey seasons - spring, summer and winter. In the upper water column seasonal changes, seen after 2001 (Figure 4.1a), dominate: Seasonal cooling to temperatures below 3°C penetrates to approximately 300 dbar, and warming to temperatures higher than 5°C is limited to the upper 100 dbar. A seasonal influence on the ULSW layer is visible from the variability of the depth of the ULSW isopycnals. Apart from that, the deeper layers exhibit strong interannual changes. In 1995, both density layers showed the lowest temperatures of less than 3.25°C (Figure 4.1a) and salinities <34.86 (Figure 4.1b), and the $\sigma_\theta = 27.74\,\mathrm{kg\,m^{-3}}$ isopycnal used as the upper boundary of the DLSW layer in Flemish Pass rose to the pressure level of 630 dbar. During the subsequent years, the $\sigma_\theta = 27.74\,\mathrm{kg\,m^{-3}}$ isopycnal deepened, reducing the fraction of DLSW and enhancing the presence of ULSW. Since 1999, the ULSW and the water located above showed a general warming. Between 2004 - 2013, this warming extended deeper into the water column and became stronger, reaching temperatures of 3.5 - 4.5°C in the ULSW layer. At the same time, the salinities within the whole ULSW layer increased to values between 34.86 - 34.92 (Figure 4.1b). This warming and salinification was interrupted in 2003 - 2004. The respective ULSW temperature and salinity minimum was also observed in the DWBC south of Flemish Pass at about 43°N by *Kieke et al.* (2009) (their Figure 3) from hydrographic data measured along the WOCE line A2/AR19. The DLSW layer in Figure 4.1 showed a remarkable increase in potential temperature and in salinity from 3°C to 3.75°C and 34.84 to 34.92, respectively, over the whole period 1993 to 2013. Meanwhile, its layer thickness decreased until only a small fraction of DLSW passed through Flemish Pass at the end of the period.

The long-term evolution of the median LSW density layer properties in the southward flow part of Flemish Pass as well as in the northward recirculation east of 46°48'W (compare Figure 3.4) was further investigated with a trend analysis using the data shown in Figure 4.1. The median was chosen over the mean value of the layer to avoid the influence of small-scale structures such as eddies or lenses [e.g. *Azetsu-Scott et al.* (2003)] and was calculated for the temperature and salinity of the ULSW and DLSW layers. The maximum layer thickness of ULSW and DLSW was estimated from the deepest profile of each Flemish Pass section. The range of the location of the deepest profile and its mean position is indicated in Figure 3.4b. To avoid a seasonal bias of the trends as the majority of the measure-

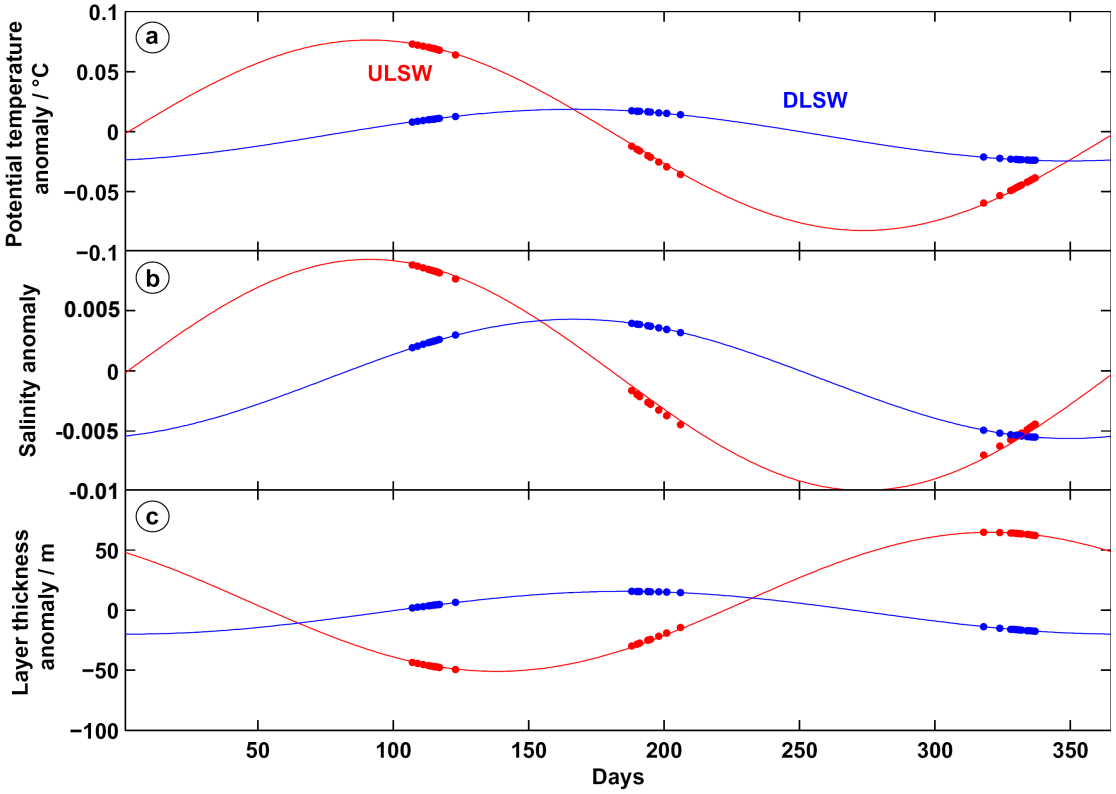

Figure 4.2: Harmonic analysis of the median density layer properties in Flemish Pass in 1993 - 2013. (a) Potential temperature anomaly (°C), (b) salinity anomaly, (c) layer thickness anomaly (m). The median properties of ULSW (red) and DLSW (blue) are shown by circles, harmonic fits of the seasonal cycle are indicated by lines.

ments were recorded in summer, the seasonal cycle of both LSW modes observed in the Flemish Pass was estimated from a harmonic analysis (see Figure 4.2) and then removed from the time series of median hydrographic properties of the ULSW layer prior to calculating the trends. Amplitudes of about 0.08°C and 0.01 were found for the seasonal cycle of the ULSW potential temperature and salinity, and about 0.02°C and 0.005 respectively for DLSW, so the seasonal influence was almost an order of magnitude smaller on the DLSW than on the ULSW. Furthermore, there is a phase shift of 2.5 month between the seasonal cycles of ULSW and DLSW. The fitted seasonal cycle maxima of temperature and salinity occur in early April for ULSW and in the middle of June for DLSW, respective minima occur in early October (ULSW) and in December (DLSW). Concerning layer thickness, the seasonal cycle amplitude is about 50 m for ULSW and about

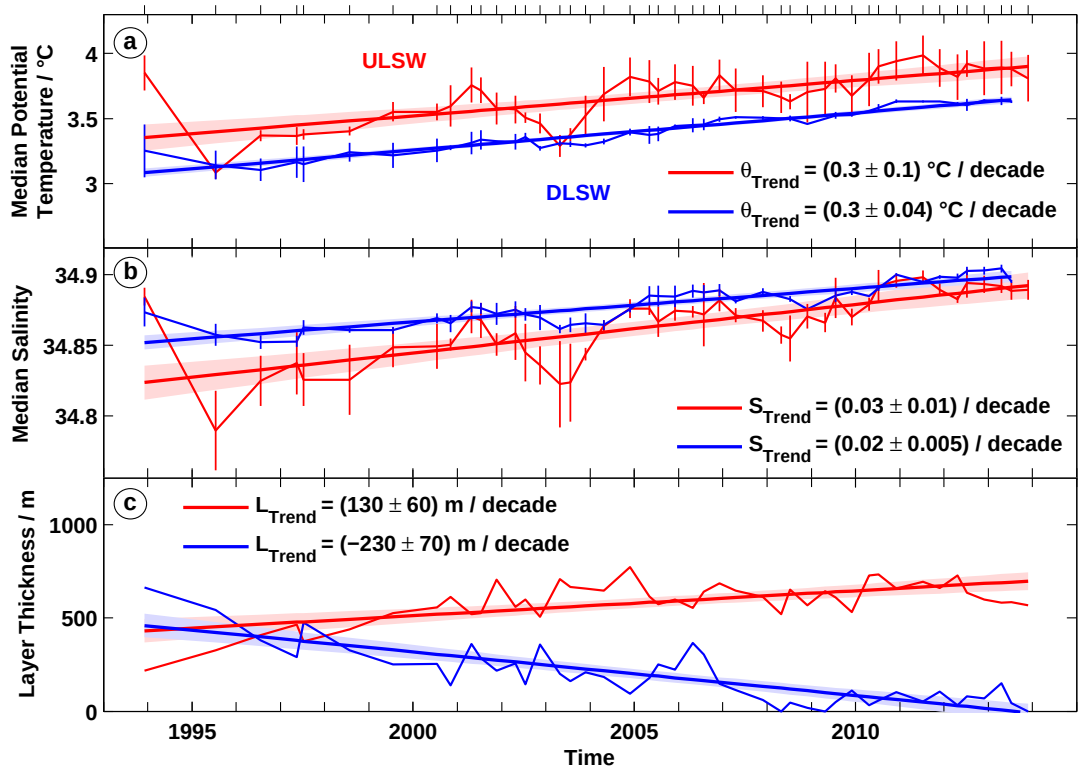

Figure 4.3: Time series of LSW properties in Flemish Pass from 1993 - 2013. (a) Median potential temperature θ (°C) and (b) median salinity S of the ULSW and DLSW layers, standard deviations are shown as vertical bars; (c) evolution of the layer thickness L (m) estimated from the deepest profile per Flemish Pass section; ticks at the top of the figure indicate available data; 95% confidence limits of the trend lines are shaded in red (ULSW) and blue (DLSW). The seasonal cycle was removed from the data as described in section 4.1.

20 m for DLSW. The minimum and maximum of the layer thickness seasonal cycle occur in the end of April and in the end of October respectively for ULSW, and in June and December for DLSW. The seasonal cycles of the ULSW and DLSW layer thickness are opposed to each other, DLSW is almost at its maximum layer thickness when ULSW is at its minimum, and vice versa.

A two sided t-test (95% significance level) was used to verify the significance of the trends seen in the evolution of the LSW properties and to examine a correlation between the ULSW and DLSW. The standard error margins of the trends are based on the 95% confidence bounds.

The deseasoned time series of ULSW and DLSW density layer properties are shown in Figure 4.3. Both LSW modes show the same significant warming

trend of 0.3°C/decade with a standard error of ± 0.1°C/decade for ULSW and ± 0.04°C/decade for DLSW (Figure 4.3a). The detrended time series of temperature for ULSW and DLSW are furthermore significantly correlated with R = 0.66. The median salinity of both LSW modes increased significantly as well. The salinity increases of (0.03 ± 0.01)/decade in the ULSW layer and of (0.02 ± 0.005)/decade in the DLSW layer (Figure 4.3b) are not different from each other at the 95% confidence level. The detrended salinity evolution of ULSW and DLSW is significantly correlated by R = 0.65. DLSW, which was the dominant LSW mode with a greater layer thickness at the beginning of the time series, exhibited a decrease in layer thickness of about (−230 ± 70)m/decade (Figure 4.3c). The ULSW layer was thickening by (130 ± 60)m/decade, since 1998 it was the dominant LSW mode in the Flemish Pass. A significant negative correlation of R = -0.70 was found for the detrended evolution of the layer thickness of both LSW modes.

A trend analysis was also performed for time series of median potential temperature and salinity of ULSW in the recirculation east of 46°48'W (DLSW is not fully resolved over the slope). The seasonal cycle was removed from the data as previously described. The time series of ULSW in the recirculation showed the same trends of warming and salinification ((0.3 ± 0.1)°C/decade and (0.03 ± 0.01)/decade, respectively) as the southward flowing ULSW. The time series of temperatures and salinities of ULSW in the recirculation and in the southward flow of Flemish Pass were furthermore significantly correlated by R = 0.53 and R = 0.63, respectively. This correlation is lower than the above mentioned correlation between the ULSW time series from the western slope of Flemish Pass west of 47°W and the center (R = 0.96 for both temperature and salinity), showing that the hydrographic variability of ULSW in the recirculation is also influenced by other factors which are presumably interactions with warm and salty NAC water south of the Flemish Cap (see chapter 3.3.2). In the long term, however, ULSW in the recirculation is subject to the same hydrographic change as the southward flowing ULSW.

4.2 Long term variability in Flemish Pass in relation to variability in the central Labrador Sea and in the DWBC at 47°N

The comparison of the long term hydrographic variability in Flemish Pass, in the Labrador Sea and in the DWBC is focused on the evolution of ULSW. The evolution of the DLSW layer in the Flemish Pass is not directly comparable with the other two regions, as the sill depth of the Flemish Pass restricts the DLSW flow to the upper part of the layer. Figure 9 shows the hydrographic evolution of ULSW in the southward flow part of Flemish Pass in comparison to ULSW from the central Labrador Sea and from the slope part of the DWBC east of Flemish Cap (Figure 1.1a) in 1993 - 2013. As previously described for Flemish Pass, a seasonal correction was also applied to the ULSW time series of the central Labrador See and the DWBC. The time resolution of the measurements within the three regions is very different. For the Labrador Sea time series (provided by I. Yashayaev, BIO) and the DWBC time series, annual CTD measurements were complemented with Argo float measurements, which were used to calculate monthly averages. The Argo float measurements were much more abundant in the Labrador Sea, so that since 2002 several measurements per month were available there. In the DWBC, Argo floats were irregularly drifting through the considered area (see Figure 1.1b), but usually 3 or 4 months per year were covered by Argo float measurements, with the exception of only one Argo float measurement in the year 2002 and seven months covered with measurements in 2012. Due to its shallow depth, Argo floats just very rarely pass through the Flemish Pass. Therefore, the temporal resolution of the measurements there is limited to 3 - 4 CTD sections per year. However, all 3 regions show identical trends at the 95% confidence level in the evolution of the hydrographic properties (Figure 4.4), i.e. a warming trend of (0.3 $\pm$ 0.1)°C/decade and a salinification of 0.03 - 0.04 $\pm$ 0.01/decade (uncertainties denote standard errors). The ULSW of the Labrador Sea is colder than the ULSW observed in Flemish Pass and in the slope part of the DWBC during the whole period, and also fresher with some exceptions in 1995, 1997 - 1998 and 2003, while the ULSW volumes in Flemish Pass and in the slope DWBC have rather similar temperatures and salinities. This high similarity of the Flemish Pass and the slope DWBC ULSW shows clearly that the slope DWBC stays as a

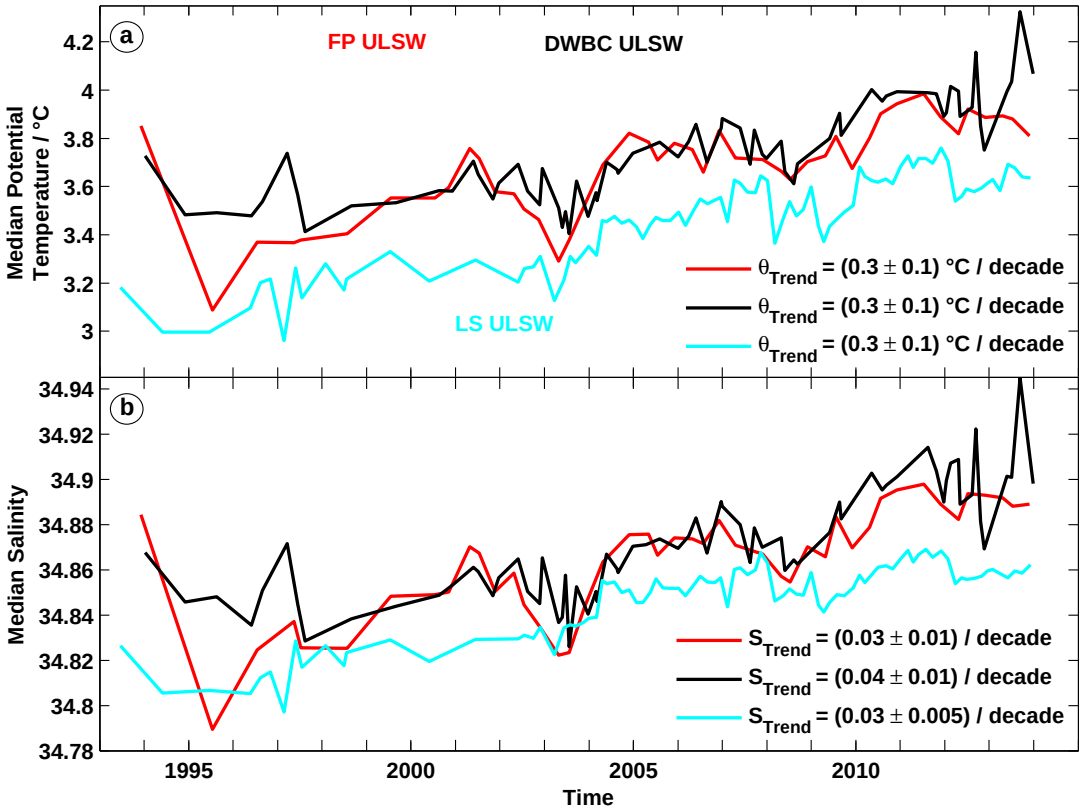

Figure 4.4: Time series of ULSW properties in Flemish Pass at 47°N (FP, red), in the DWBC east of Flemish Cap (black), and in the central Labrador Sea (LS, cyan) during 1993 - 2013. (a) Median potential temperature θ (°C) and (b) median salinity, seasonal cycle was removed.

whole closer to the boundary and does not interact with the NAC east of Flemish Cap at 47°N, which would elevate the temperatures and salinities in the slope DWBC compared to the Flemish Pass. However, interactions might still happen further south on the way around Flemish Cap, which is possibly the reason for the warmer and saltier water that recirculates northward in the eastern Flemish Pass as part of the anticyclonic gyre around Flemish Cap (see section 3.3.2). The interannual variability of potential temperature and salinity of ULSW observed in Flemish Pass and in the DWBC follows the general evolution in the Labrador Sea. For instance, the warming and salinification starting in the Labrador Sea in 1995, leveling off and increasing again in 2003 and decreasing in 2008, before it resumed to increase, is also apparent with a delay of a few months in the ULSW observed in the Flemish Pass and in the DWBC east of Flemish Cap. This delay cannot be specified more precisely due to the coarser time resolution at 47°N compared to

the Labrador Sea, but it points to LSW spreading from the Labrador Sea to 47°N within less than a year, in agreement with *Stramma et al.* (2004).
The high similarity in the evolution of ULSW in the Flemish Pass, in the Labrador Sea and in the DWBC provides evidence that the ULSW long term variability in the Flemish Pass as well as in the DWBC is remotely influenced by the hydrographic changes happening and observed in the Labrador Sea, which are in turn modulated through the impact of the adjacent North Atlantic basins. The signal is advected downstream without a noticeable weakening of the trends along the DWBC to 47°N. The generally higher temperatures and salinities of the southward flowing ULSW in the Flemish Pass and in the slope part of the DWBC at 47°N compared to the central Labrador Sea (Figure 4.4) indicate a persistent exchange between the exported ULSW and warmer and saltier water along the way south from the source region to 47°N with low long term variability. Individual CTD section snapshots (shown exemplary for cruise MSM12/3 in 2009 in Figure 4.5 and Figure 4.6) of the central Labrador Sea were compared to the DWBC at 53°N and 47°N, and the Flemish Pass at 47°N measured in the years 2009, 2011, and 2013 during the cruises MSM12/3, M85/1 (see Table 2.3) for related projects) and MSM28 (related project: RACE) to explore, where these interactions might occur. The data showed that the ULSW in the DWBC at 53°N was warmer and saltier than in the central Labrador Sea. This is clearly seen in the year 2009 comparing Figure 4.5a and b. In the central Labrador Sea (Figure 4.5a), ULSW temperatures are mostly colder than 3.5°C. At 53°N (Figure 4.5b), the temperatures of ULSW ranged between 3.5 up to 4°C, and thus were more similar to those of ULSW at the western boundary of the Labrador Sea, which in turn was warmer and saltier than its centre. Therefore, the warming and salinification observed at 53°N might have already happened in the Labrador Sea during the transition of ULSW formed in the convection area into the boundary current. *Straneo* (2006) found a lateral exchange between the center and the boundary current waters in the Labrador Sea, which induces the export of LSW out of the formation region and a shift of properties toward the warmer and saltier boundary current characteristics [*Straneo* (2006), *Yashayaev and Loder* (2009)]. The section data of 2009, 2011, and 2013 furthermore revealed that there was another increase in temperature and salinity between 53°N and 47°N. ULSW in Flemish Pass (without the northward flowing recirculation) and in the slope part of the DWBC at 47°N was warmer and more saline compared to 53°N (in 2009 by more than 0.15°C and 0.01, respectively, see

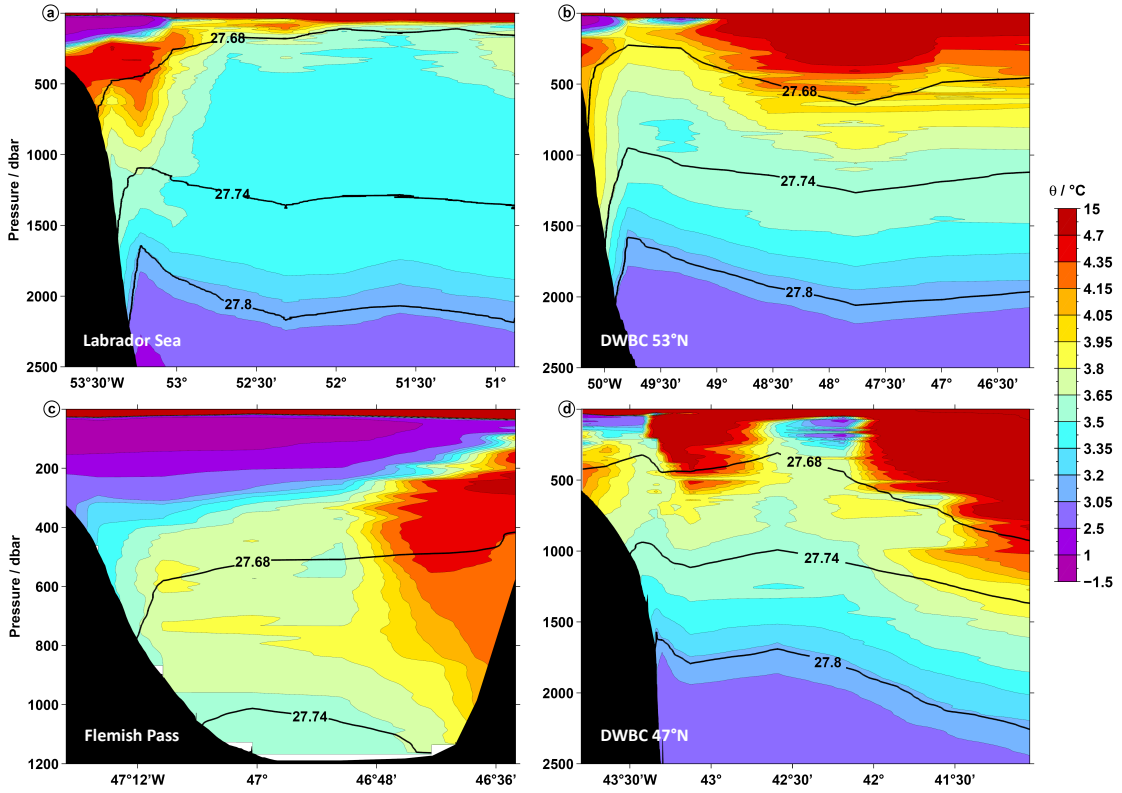

Figure 4.5: Sections of potential temperature θ (°C) measured during cruise MSM12/3 in 2009 in (a) the central Labrador Sea on the AR7W line, (b) in the DWBC at 53°N, (c) in Flemish at 47°N, and (d) in the DWBC at 47°N. Notice that the sharp drop of the hydrographic properties at western topography of the different sections is an artifact resulting from extrapolation of the data.

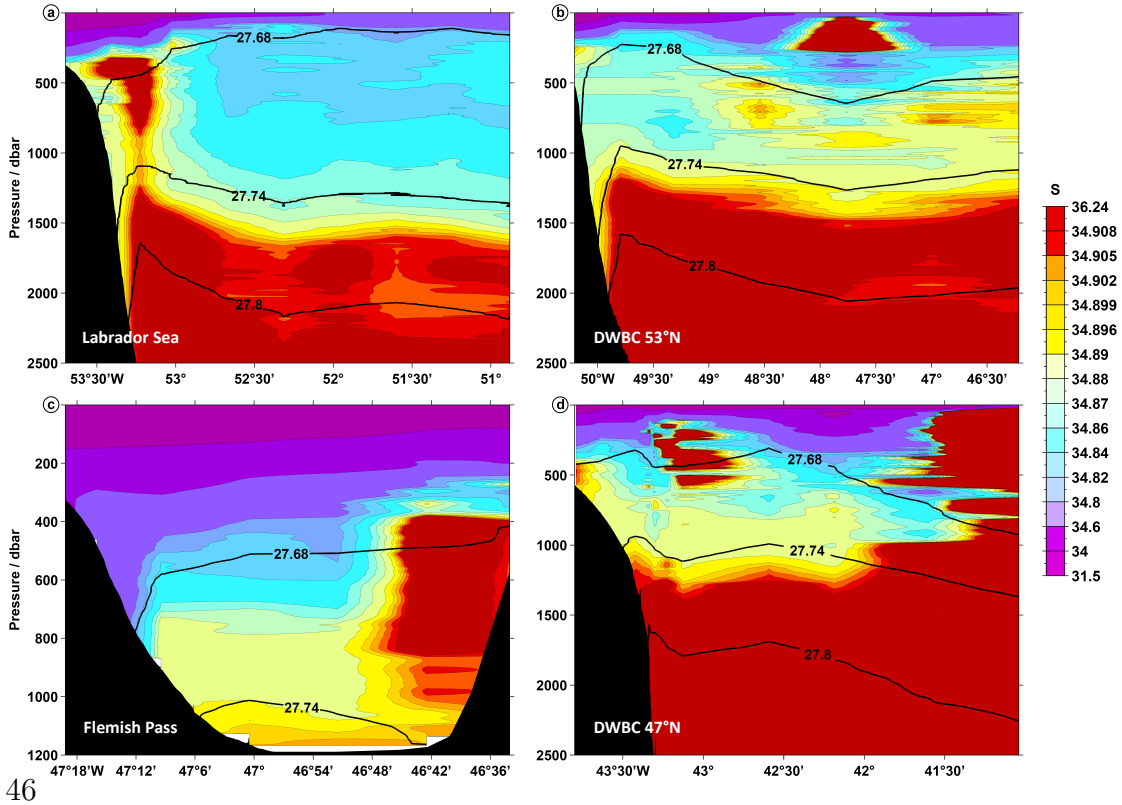

Figure 4.6: Same as in Figure 4.5, but for salinity.

Figure 4.5b, c, d, and Figure 4.6b, c, d). Located in between these areas is the Orphan Basin with the seamount Orphan Knoll situated northwest of 50°N, 45°W. There, part of the LSW is branching off on another export path towards the Mid-Atlantic Ridge [e.g. *Talley and McCartney* (1982), *Sy et al.* (1997), *Koltermann et al.* (1999), *Fischer and Schott* (2002), *Kieke et al.* (2009)] (Figure 1.1a). *Fischer and Schott* (2002) used profiling floats drifting in the DWBC to identify the whole area north of Orphan Knoll as a region of unorganized flow influenced by eddies. There, the floats were caught in eddies for several months and eventually arriving at the northern Flemish Cap. *Fischer and Schott* (2002) assumed that the eddies might mix the water masses of the DWBC and the NAC, which makes an anticyclonic loop known as the "Northwest Corner" in close proximity. It appears that due to this interaction with NAC water the DWBC gradually warms and becomes more saline in this area before splitting into a particular Flemish Pass branch and a DWBC branch for LSW transport, thus explaining the offsets in the different time series observed in the Labrador Sea and at 47°N.

4.3 The hydrographic evolution of ULSW in Flemish Pass in the context of multidecadal variability

In order to put the hydrographic variability of ULSW observed in the Flemish Pass into a multidecadal context, the respective observational time series of Flemish Pass are compared to hydrographic time series from the MIT/gcm model, which in addition covers a longer time frame from 1960 to 2009 with monthly data. Due to the model's offset in hydrographic properties discussed in chapter 3.3.1, the focus is on anomalies of median temperature and salinity of ULSW relative to the mean of 1994 - 2009, which is the overlapping time frame for the model and the observations in Flemish Pass (see Figure 4.7), the first observations were conducted in December 1993). A low-pass filter of 15 months was applied to the model data to remove the seasonal cycle. For 1994 - 2009, a trend analysis showed trends of observed and modeled hydrographic properties that agreed well. In both model and observations, a salinity increase of 0.03/decade is found (the respective standard errors are $\pm$ 0.01 for the model and $\pm$ 0.02 for the observations), and the warming trend of (0.3 $\pm$ 0.1)°C/decade seen in the model is statistically

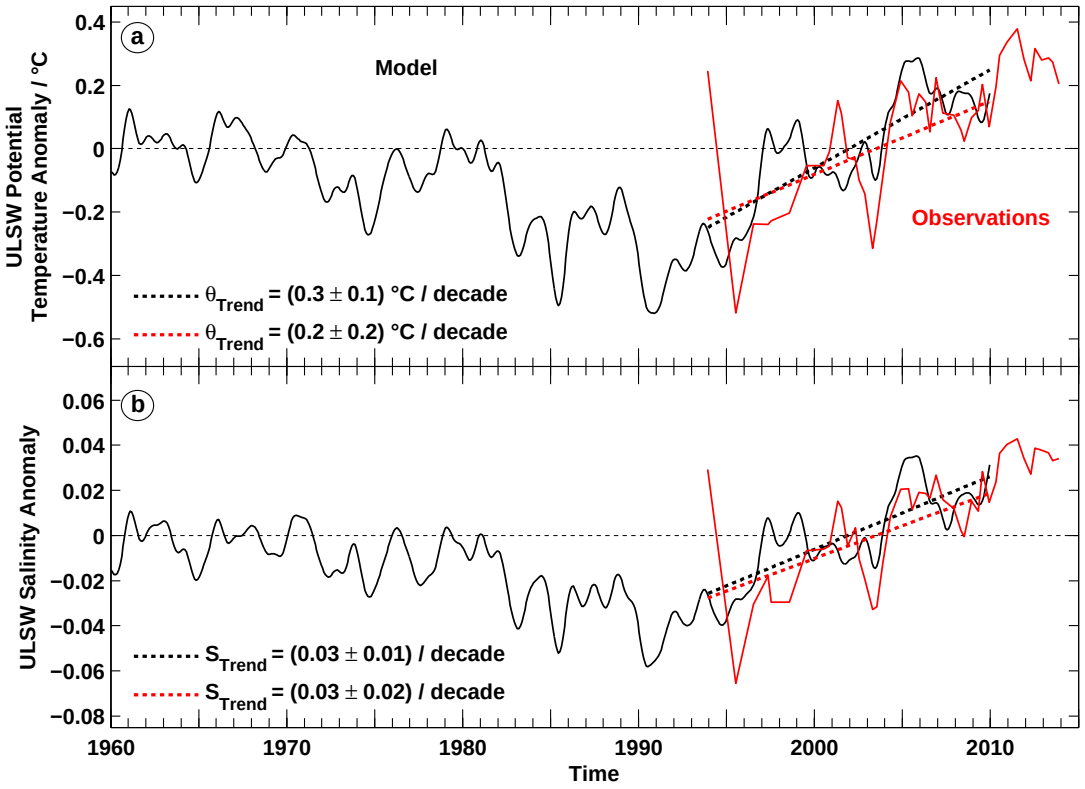

Figure 4.7: Time series of ULSW hydrographic anomalies in Flemish Pass at 47°N based on CTD measurements (red, seasonal cycle removed) and derived from the MIT/gcm model (black, 15 months low pass filtered). (a) Median potential temperature anomaly (°C) and (b) median salinity anomaly relative to the mean of the period 1994 - 2009. Dashed lines indicate trends during the overlapping period 1994 - 2009 of both time series.

the same as in the observations ((0.2 ± 0.2)°C/decade) at the 95% confidence level. The temperature and salinity anomalies in the model and in the observations are also rather similar in magnitude, ranging between −0.5 °C to 0.3°C and −0.065 to 0.035 respectively. The only exception is the first observational value in 1993, which is much higher in salinity and temperature than the model at this time. At the same time, higher temperatures and salinities were observed in both the central Labrador Sea and the DWBC at 47°N (Figure 4.4) as well, but the difference to the following years was not as extreme as in Flemish Pass. The section measured in Flemish Pass in 1993 was among the coarsest of all realizations, which may have an impact, but the data quality is assumed to be good as they were conducted and quality controlled in the framework of WOCE. Therefore,

it was included in the analysis. The model reproduced the trend found in the hydrographic observations in Flemish Pass well (see Figure 4.7) and is therefore used to extend the ULSW evolution of hydrographic properties back until 1960. This extension reveals that the trends observed in the Flemish Pass throughout the past two decades are rather part of a multidecadal cycle. Both temperature and salinity anomalies of the model ULSW are slightly positive in the 1960s. After 1970, the layer becomes colder and fresher, until a minimum is reached in the early 1990s, which coincides with the period of high convection activity in the central Labrador Sea when the coldest LSW was produced [e.g. *Lazier et al.* (2002), *Azetsu-Scott et al.* (2003)]. This is followed by warming and salinification since the mid-1990s, which corresponds to the observations in Flemish Pass.

4.4 Summary and discussion

In chapter 3 of this study, the hydrography and flow field of the Flemish Pass was investigated from ship based CTD and LADCP measurements with focus on the two different modes of Labrador Sea Water, namely ULSW and DLSW. The observed flow through Flemish Pass is mainly southward, with a northward recirculation around Flemish Cap in the east, which is warmer and saltier than the southward flow, possibly due to enhanced mixing with NAC water south of Flemish Cap. The southward flow in Flemish Pass accounts for a considerable amount of 15 - 27 % (-1.0 to -1.5 Sv) of the ULSW transport at 47°N, while most of the DLSW is carried with the DWBC east of Flemish Cap. Chapter 4 of this study furthermore examined the long-term hydrographic variability of LSW flowing through Flemish Pass. Significant warming and salinification trends of the LSW were found for the period 1993 to 2013, and meanwhile a locally increasing replacement of DLSW with the lighter ULSW mode was observed. These trends reflect closely the variability found in the formation region of LSW in the central Labrador Sea. There, several studies [*Azetsu-Scott et al.* (2003), *Stramma et al.* (2004), *Kieke et al.* (2006), *Rhein et al.* (2011), *Kieke and Yashayaev* (2015)] revealed a replacement of DLSW by ULSW with a strong anti-correlation between the evolution of the ULSW and DLSW layer thickness, which supports the findings for Flemish Pass. Results from the present study also agree with *Yashayaev and Loder* (2009) and *Kieke and Yashayaev* (2015), who observed a steady warming

and salinification in the central Labrador Sea during 2002 to early 2008 within the 1000 - 1500 m layer comprising the LSW convection depth. This general warming trend continued until 2014, but was interrupted during times of high convection activity in 2008, 2012 and 2014, while the salinification persisted until 2011/2012, and then started to decrease [*Kieke and Yashayaev* (2015), *Yashayaev et al.* (2015)]. *Khatiwala and Visbeck* (2000) and *Lazier et al.* (2002) explained the increasing temperatures and salinities in the central Labrador Sea as a result from an increasing contribution of warmer and more saline Atlantic waters through advection and lateral mixing by mesoscale eddies from the boundaries during weakening deep convection. *Yashayaev* (2007) and *Yashayaev et al.* (2007) linked the trends observed in the DLSW to Icelandic Slope Water, which is formed through mixing of Iceland-Scotland Overflow Water with the overlying Atlantic thermocline water near the Faroes, arriving in the Labrador Sea and replacing DLSW. With single point measurement mooring arrays distributed at 56°N, 55°N, 53°N, 46°N and 43°N, *Fischer et al.* (2010) traced the warming signal of LSW within the DWBC from the Labrador Sea to the Grand Banks following the pathway east of Flemish Cap. They inferred a warming trend of 0.5°C/decade within the DLSW in 1996 - 2009. Although different data and methods were used here and in the study of *Fischer et al.* (2010), the resulting trends agree in the order of magnitude, but are statistically different at the 95% confidence level, with a slightly lower trend of (0.3 ± 0.04)°C/decade observed in the hydrographic data of DLSW in Flemish Pass (Figure 4.3). Within the extended time frame of hydrographic model time series here presented, the observed trends in Flemish Pass are considered to be part of a multidecadal cycle. This is in agreement with the results of other studies. *Curry et al.* (1998) found that the hydrographic properties of LSW undergo pronounced variations on decadal time scales, primarily as a consequence of changes in the local atmospheric conditions associated with the North Atlantic Oscillation (NAO). *van Aken et al.* (2011) used a simplified heat budget model to show that the multidecadal temperature variability in the Labrador Sea mainly reflects the long term variation of the net heat flux to the atmosphere. *Yashayaev et al.* (2015) analyzed time series of hydrographic anomalies of LSW (500 - 1000 m layer averages) between 1950 and 2014, identified dominant time scales of hydrographic multidecadal variability of the order of 40 - 50 years, and linked respective changes to multidecadal variability in the NAO.

As the changes in the hydrographic properties of ULSW identified in Flemish Pass

between 1993 and 2013 were also observed upstream of Flemish Pass in the central Labrador Sea and in the DWBC east of Flemish Cap, the time series shown in Figure 4.4 provide evidence that the long term variability of ULSW in the Flemish Pass as well as in the DWBC is dominated by the changes in the LSW formation. This indicates that the LSW passing through Flemish Pass carries the anomalies from the formation region southward. On its southward pathway, the LSW warms and becomes more saline before arriving at 47°N, which possibly results from lateral exchange of water masses, while exiting the Labrador Sea [*Straneo* (2006)] and downstream on the way through the Orphan Basin [*Fischer and Schott* (2002)]. At 47°N, the hydrographic properties of LSW are very similar in the southward flow part of Flemish Pass and in the slope part of the DWBC. Imprints of interactions of the DWBC and the NAC at 47°N, which *Bower et al.* (2009) inferred from float experiments therefore do not appear in the slope part of the DWBC, but can be found in the rise part, which is warmer and more saline (see Figure 3.5). This was also observed by *Mertens et al.* (2014). Additionally, the model study of *Varotsou et al.* (2015) compared volume transports of ULSW from different sections crossing the DWBC at 53°N, at the northern and southern Flemish Cap, 47°N and at 45°N, and identified the region of most deflection from the DWBC to be located southeast of Flemish Cap. There, the loss of volume transport from deflection of the model DWBC between 47°N and the southern Flemish Cap was 1.6 Sv, while 1 Sv was lost to the interior between 53°N and the northern Flemish Cap, and 0.8 Sv between the northern Flemish Cap and 47°N. In conclusion, the Flemish Pass is an important LSW transport pathway besides the DWBC branch east of Flemish Cap, and an estimate of the southward deep water transport of the AMOC neglecting the Flemish Pass would be therefore incomplete. In addition to ship based measurements, sustained mooring records are needed to provide an insight into the short term and longer term variability of the LSW flow through Flemish Pass, as transport estimates derived from LADCP data only provide snapshots. Based on the available data of the Flemish Pass mooring array (see section 2.1.4), current and transport variability during July 2012 to April 2014 are investigated and discussed in the next chapters of this study. In the following, ULSW and DLSW are not analyzed separately from each other any more (with the exception of chapter 5.3). Instead, the Flemish Pass LSW is investigated as a whole, because the fraction of DLSW in Flemish Pass is small and the trends observed in the hydrography of both LSW modes were the

same.

5 Magnitude and variability of transports in Flemish Pass

This chapter will address research question 2 of this study: "What is the magnitude of transports and its associated variability for LSW passing through Flemish Pass? What is the amplitude of the seasonal cycle?" To answer these questions, time series of LSW transport were calculated based on the data of the Flemish Pass mooring array. First however, a more robust mean velocity field for the Flemish Pass was inferred from all current velocity ship measurements available to this study, and ship based transports were derived for comparison with the mooring based transports, which is described in section 5.1. The Flemish Pass velocity data from the IUP Bremen LADCP measurements in 2009 - 2013 presented in chapter 3.2 were therefore expanded by an LADCP section conducted in 2014, and available VmADCP sections (see table 2.1) measured in 2003, 2007, and 2009 - 2014.

The second section of this chapter describes how the time series of transport through Flemish Pass were derived by extrapolation of the mooring based flow field. The resulting transports are discussed and compared with the ship based estimates in section 5.3. In section 5.4, seasonal effects on the LSW transports are investigated and the amplitude of the seasonal cycle of the LSW transports is determined.

In the first mooring period (2012 - 2013), two ADCPs of type Long Ranger were deployed in Flemish Pass, and the mooring transports were derived from the best possible velocity field estimate based on the data of two instruments. One mooring (BM25/1) was located on the western slope of Flemish Pass, the other one (BM26/1) in the center (see Figure 2.1). In the second mooring period (2013 - 2014), only one mooring (BM25/2) could be redeployed. How much each mooring contributes to the magnitude of the transport signal is assessed in section 5.5. Afterward, the variability of the LSW transports through Flemish Pass is analyzed

in section 5.6.
The chapter is completed by an estimate of a top to bottom transport time series from the second mooring period. In 2013 - 2014, the Flemish Pass mooring array was complemented by a shallow mooring from Bedford Institute of Oceanography, Canada, which was deployed at 400 m depth on the western slope. With the additional data of this instrument (M1842), which was kindly provided for this study [B. Greenan, pers. communication], the top to bottom transport in Flemish Pass was calculated, which is presented in section 5.7. The data of M1842 was also used for another study investigating the spatial and temporal ocean variability on the northwest slope of Flemish Cap by *Layton* (2016). Lastly, a summary of the results will end this chapter.

5.1 Ship based mean flow field

In order to derive a robust mean velocity field as well as comparable transports from all VmADCP and LADCP sections conducted in Flemish Pass at 47°N by the IUP Bremen in 2003, 2007, and 2009 - 2014, the section area has to be identical for all cruises. However, the horizontal and vertical data coverage of the Flemish Pass differs between the individual sections. Horizontally, some of the measured sections do not totally cover part of the western or the eastern slope of Flemish Pass with measurements, as for instance the LADCP sections measured in 2009, 2010 and 2011 (see Figure 3.3). Concerning the VmADCP sections, the vertical range only covers 900 to 1000 m, and consequently the LSW layer is not fully captured by the measurements. Therefore, all LADCP and VmADCP sections were gridded linearly onto a regular grid of 1/20° horizontal resolution and 10 m vertical resolution. Then, the data was extrapolated to cover Flemish Pass down to the bottom between 46°24'W and 47°24'W. For the extrapolation, three different methods were considered:

1. Simple constant extension of the data.
2. Objective mapping, with influence and cutoff radii of 1/40° and 1/3°, respectively in the horizontal, and 15 m and 100 m, respectively in the vertical.
3. A gradient method, in which the data was vertically extrapolated based on the gradient of the adjacent 100 m of the velocity field, and horizontally based

on the gradient of the next five profiles.

All three different extrapolation methods yielded very similar velocity fields. In a visual comparison of the extrapolated VmADCP and LADCP sections, the objective mapping method was found to produce the most realistic looking extrapolations, while the gradient and the simple extension method produced more artifacts, therefore in the following, the transport estimates based on the objective mapping extrapolation will be presented.
Figure 5.1 shows exemplary the range of the gridded profiles and the area of the extrapolated velocity field of the VmADCP and LADCP section conducted at the same time during cruise MSM38. Generally, the velocity distribution of both sections is very similar as expected. A common feature for instance is the core of the shallow Labrador Current, which is displayed in both sections by intensified velocities up to $-30\,\mathrm{cm\,s^{-1}}$ over the western slope in the upper 200 dbar. The velocity field in the central Flemish Pass is similar in both sections as well, with velocities exceeding $-15\,\mathrm{cm\,s^{-1}}$ spreading from about 300 dbar down to the bottom. Due to the differences in the resolution of the original data, there are also some noticeable differences in the displayed velocity fields of the VmADCP and LADCP sections. In the VmADCP section (Figure 5.1a), the patch of elevated velocities in the center spreads further to the West than in the LADCP section.
Another visible difference is exhibited in the northward recirculation over the Flemish Cap. In the LADCP section, it extends to about 300 dbar, and it reaches velocities exceeding $20\,\mathrm{cm\,s^{-1}}$ in the uppermost 50 dbar, while in the VmADCP section the recirculation extends to about 400 dbar and reaches slightly lower velocities exceeding $15\,\mathrm{cm\,s^{-1}}$ in the upper 50 dbar. These discrepancies result from the high horizontal resolution of the VmADCPs, which recorded one profile per minute and therefore detect smaller scale velocity structures, which are not visible in the LADCP data.
Resulting from all extrapolated LADCP and VmADCP sections conducted between 2003 and 2014, the mean velocity field in Flemish Pass at 47°N is shown in Figure 5.2a). Compared to the average velocity field shown in chapter 3.2, which was based solely on LADCP measurements in 2009 - 2013 (Figure 3.2a), Figure 5.2a exhibits almost identical velocity structures (mind the different color scales). Both figures show two patches of elevated velocities over the western slope, one in the upper 200 dbar with high velocities exceeding $-20\,\mathrm{cm\,s^{-1}}$ indicating the core of the Labrador Current, and another deeper one in the LSW below 800 dbar

exceeding $-10\,\mathrm{cm\,s^{-1}}$. Apart from this, the general velocities in the LSW are lower than $-10\,\mathrm{cm\,s^{-1}}$. In the east, northward velocities mark the recirculation around Flemish Cap, limiting the southward transport through Flemish Pass in both figures.

The distribution of the standard deviations of the velocity measurements in Figure 5.2b shows that the variance of the flow field is highest in the upper layer at pressures of less than 200 dbar, over the eastern and western slope of Flemish Pass and near the bottom below 1000 dbar (standard deviations $>5\,\mathrm{cm\,s^{-1}}$). In the central Flemish Pass in the pressure range of 200 to 1000 dbar, the flow field exhibits less variance (standard deviations $<5\,\mathrm{cm\,s^{-1}}$).

The locations and range of the ADCP moorings are also indicated in Figure 5.2. In order to calculate mooring based transport time series, the Flemish Pass velocity field must be determined by extrapolation of the mooring data, which is explained in the next section.

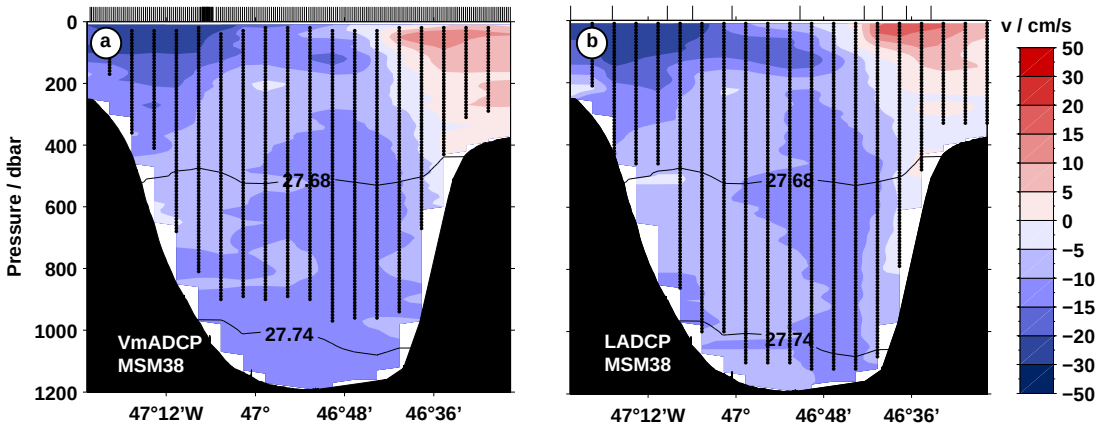

Figure 5.1: Meridional velocity distribution (cm/s) of the Flemish Pass at 47°N from (a) VmADCP measurements, and (b) LADCP measurements, which were conducted at the same time during cruise MSM38 in May 2014. The data of the measurements was gridded linearly, and then extrapolated by objective mapping. Ticks at the top of each plot indicate the original location of the measured velocity profiles, black dots display the gridded profiles, and the velocity contours exhibit the extrapolated velocity field.

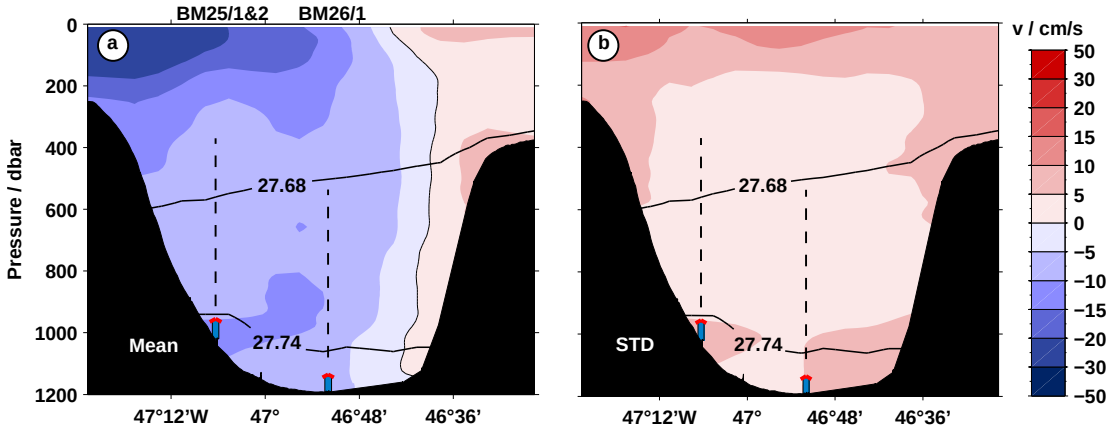

Figure 5.2: (a) Average meridional velocity distribution (cm/s) in Flemish Pass at 47°N derived from LADCP and VmADCP measurements in 2003, 2007, and 2009 - 2014. (b) Same as in (a), but standard deviations. Mooring locations are also shown: BM25/1 and BM25/2 respectively in the western Flemish Pass, and BM26/1 in the center. Dashed lines indicate the range of the ADCP measurements. Black lines indicate average ULSW isopycnals of hydrographic measurements in the deployment years 2012 - 2014.

5.2 Calculation of mooring based transports

5.2.1 LSW transports

To calculate mooring based LSW transports, the LSW layer area was estimated, and the mooring data was extrapolated to the boundaries limiting the area. In the vertical, the LSW layer is limited by the $\sigma_\theta = 27.68\,\mathrm{kg\,m^{-3}}$ isopycnal and the bottom topography. Horizontally, the velocity field in Flemish Pass is divided in the southward flow part, and the northward recirculation around Flemish Cap in the East. The Flemish Pass mooring array recorded measurements within the southward flow part of the LSW layer, but the northward recirculation was not covered by measurements. Therefore, the zero line of velocity separating the southward and northward flow in the east is a horizontal limit of the mooring based LSW transport. As the location of the zero velocity line is variable (see section 3.2.2), absolute geostrophic surface velocity data from satellite altimetry were used to approximate the location. The data provided by AVISO[1] (Archiving, Validation and Interpretation of Satellite Oceanographic data), specifically the product DT-MADT "all sat merged" (Delayed Time, Mean Absolute Dynamic

[1] http://www.aviso.altimetry.fr/

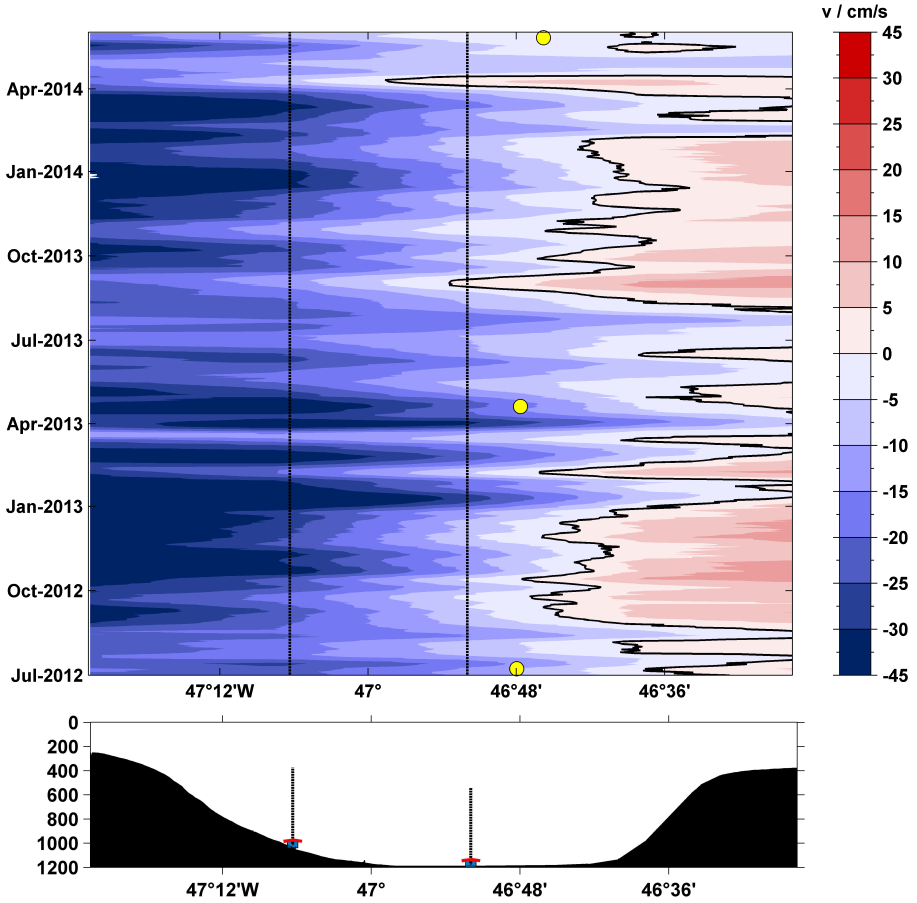

Figure 5.3: Location of the zero velocity line (solid black line) separating southward and northward flow in Flemish Pass at 47°N based on meridional surface velocity data from AVISO during the mooring period July 2012 - May 2014. Yellow markers indicate the position of the zero velocity line inferred from available LADCP/VmADCP sections. Dotted lines in the top panel mark the mooring locations in Flemish Pass. The bottom panel shows the Flemish Pass bottom topography and the location and range (dotted line) of the ADCPs.

Topography data from up to four satellites at a given time) is available in daily resolution on a 1/4° grid. To evaluate if the zero velocity line based on the AVISO data is a good approximation as a transport limit, a comparison was performed with the zero line location determined from the LADCP/VmADCP sections in Flemish Pass (Figure 5.3). The result was that the gridded product of AVISO did not agree very well with the ship based current measurements, the zero velocity line locations inferred from AVISO differ by 13 km or more from the location determined from the LADCP/VmADCP based near surface velocities. Therefore, the AVISO based zero velocity line location was not used as a time variable limit

of the LSW southward transport. Instead, the location of the zero velocity line was approximated from the average meridional current velocity field determined from the available LADCP/VmADCP measurements in Flemish Pass conducted between 2003 and 2014 (Table 5.3), which served as a fixed limit in the east for the mooring based transport estimates.
To infer the upper limit of the LSW layer in Flemish Pass, the location of the $\sigma_\theta = 27.68\,\mathrm{kg\,m^{-3}}$ isopycnal was estimated. The MicroCATs attached to the moorings only provide pointwise measurements of the near bottom hydrography. Therefore, a fixed location of the ULSW isopycnals was determined from the average density field of 9 hydrographic sections conducted in Flemish Pass in the years of the deployment period 2012 - 2014. The hydrographic measurements were restricted to these years to avoid biasing the transport limit as a result of the long term trend of warming and salinification described in chapter 4. To investigate if seasonal changes impact the LSW density layer, furthermore seasonal averages of the LSW layer were determined from the data conducted in spring, summer and winter during the deployment period. Transport time series were calculated based on both the fixed and the seasonal changing LSW layer areas, the results are compared and further discussed in section 5.4.
To calculate the transports, the current velocity field within the LSW layer was inferred based on the data of the moored ADCPs. Here, first the extrapolation of the velocity field based on two moorings will be described. This was the setting for the mooring period in 2012 - 2013 with one mooring on the western slope (BM25/1) of Flemish Pass and one in the center (BM26/1). There are different approaches to do the extrapolation. *Petrie and Buckley* (1996) for instance estimated mooring based transports in Flemish Pass simply by allowing the individual measurements to represent an area bounded by the surface, bottom, or half the distance to the nearest instrument. This approach was applied to the measurements of the Flemish Pass mooring array and the results were compared with the transport estimates from the LADCP sections conducted in 2012 and 2013 just before and after the mooring period. The mooring based transports overestimated the ship based transports by $-1.4\,\mathrm{Sv}$ and $-1.2\,\mathrm{Sv}$, respectively, which corresponds to an overestimation of the transport of 100% and 58% (compare table 5.3). Therefore, a more sophisticated approach of simple extrapolation following *Schott et al.* (1988) was used for the transport calculations. Figure 5.4 shows a schematic of this extrapolation approach. The data from BM25/1 was extrapolated westward

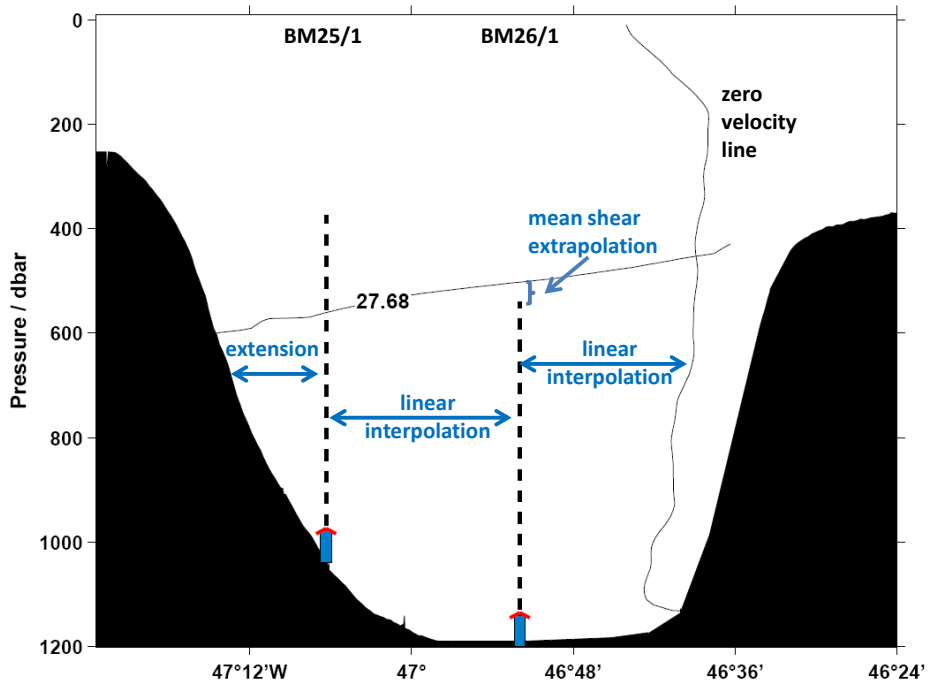

Figure 5.4: Schematic extrapolation of the Flemish Pass mooring data to the limits of the southward LSW flow following the method of *Schott et al.* (1988).

by simply extending the velocity measurements constantly toward the topography of the Grand Banks. Between both moorings, which were separated by a distance of 18 km, the velocity field was linearly interpolated. Another linear interpolation was applied between BM26/1 and the zero velocity line in the East. Furthermore, an extrapolation from the top value of BM26/1 to the upper limit of the LSW layer was performed using the mean shear of all depth bins. For this extrapolation, the current profiles at BM26/1 need to be nearly linear [*Schott et al.* (1988)], which was the case as shown in Figure 5.5. The flow at BM26/1 was in southwestward direction and very barotropic in both its meridional and its zonal component, in contrast to the mainly southward flow at BM25/1, which had a strong velocity shear in its meridional component. The velocity shear in the water column of the western Flemish Pass is induced by the shallow Labrador Current, which is intensified toward the Western boundary (see Figure 5.2a). Toward the bottom, the data from the deepest bin of each mooring were extended constantly.
For the second mooring period in 2013 - 2014, only one ADCP mooring was available to be redeployed. To asses how much a single mooring is contributing to the transport signal, transport time series based only on mooring BM25/1 and only on BM26/1 were calculated separately, and compared to the transport time series

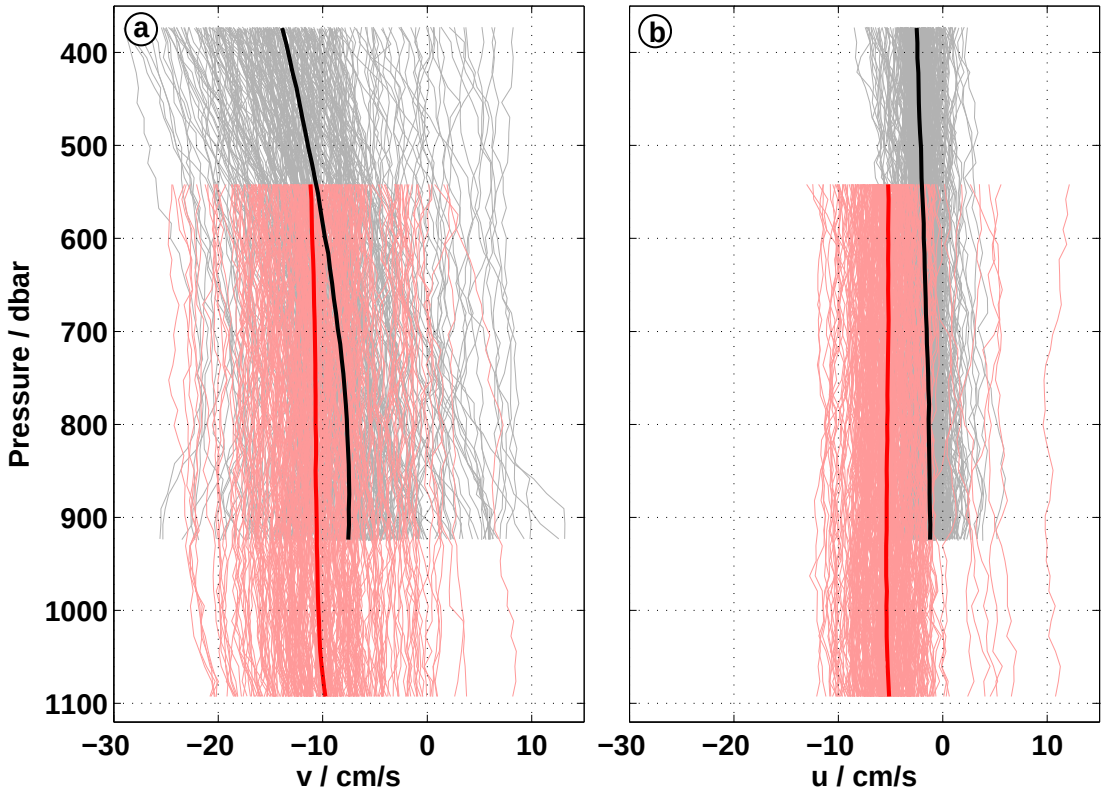

Figure 5.5: Velocity profiles (cm/s) measured by the ADCP of mooring BM25/1 in the western Flemish Pass (black - average profile, gray - daily averages) and of BM26/1 in the central Flemish Pass (red - average profile, light red - daily averages) during 2012 - 2013. (a) Meridional velocity, and (b) zonal velocity.

based on both moorings. To infer the single mooring transports, the data from mooring BM25/1 was extended constantly to the position of BM26/1, and then the extrapolations of the velocity field were performed as previously described, and vice versa. The resulting transport time series are discussed in section 5.5.
As there was an additional Canadian mooring deployed on the western slope of Flemish Pass (M1842) during July 2013 - July 2014, which measured the current velocities in the upper water column, it was possible to determine a top to bottom transport time series for the second mooring period. The derivation of the top to bottom transport is explained in the next section.

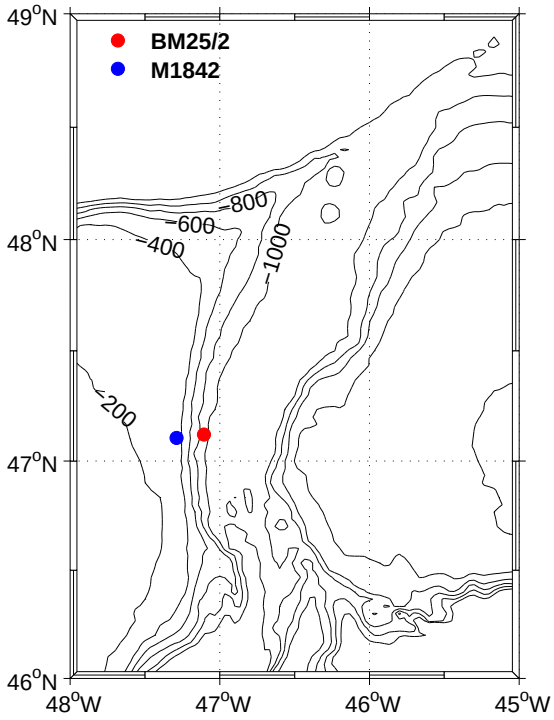

Figure 5.6: Flemish Pass mooring positions in 2013 - 2014. M1842 (blue) was deployed by the BIO, Halifax, and BM25/2 (red) by the joint project FLEPVAR of the IUP, Bremen, and IFM/CEN, Hamburg.

5.2.2 Top to bottom transports

As was shown in chapter 4, Flemish Pass is an important southward export pathway for LSW and part of the AMOC. Therefore, it is also important to determine a top to bottom estimate of the Flemish Pass transports. This was done for the first time by *Petrie and Buckley* (1996) based on moored current meter data of a period of only 3 month in 1985. It was now possible to calculate a top to bottom transport time series for July 2013 to April 2014, because the BIO, Canada, made the data of their shallow mooring M1842 available to this study. M1842 was located on the western slope of Flemish Pass at 400 m depth in a distance of 14 km to mooring BM25/2 (Figure 5.6), measuring the flow of the Labrador Current in the upper water column. Figure 5.7 shows the meridional and zonal velocity time series of the closest depths levels in BM25/2 and M1842 in comparison. The time series display expected differences in the flow as M1842 is located higher up on the shelf and therefore more dominated by the Labrador Current. Nevertheless, both time series have a similar range between +20 and $-40\,\mathrm{cm\,s^{-1}}$ in the meridional velocity component (Figure 5.7a). The average meridional velocities and standard

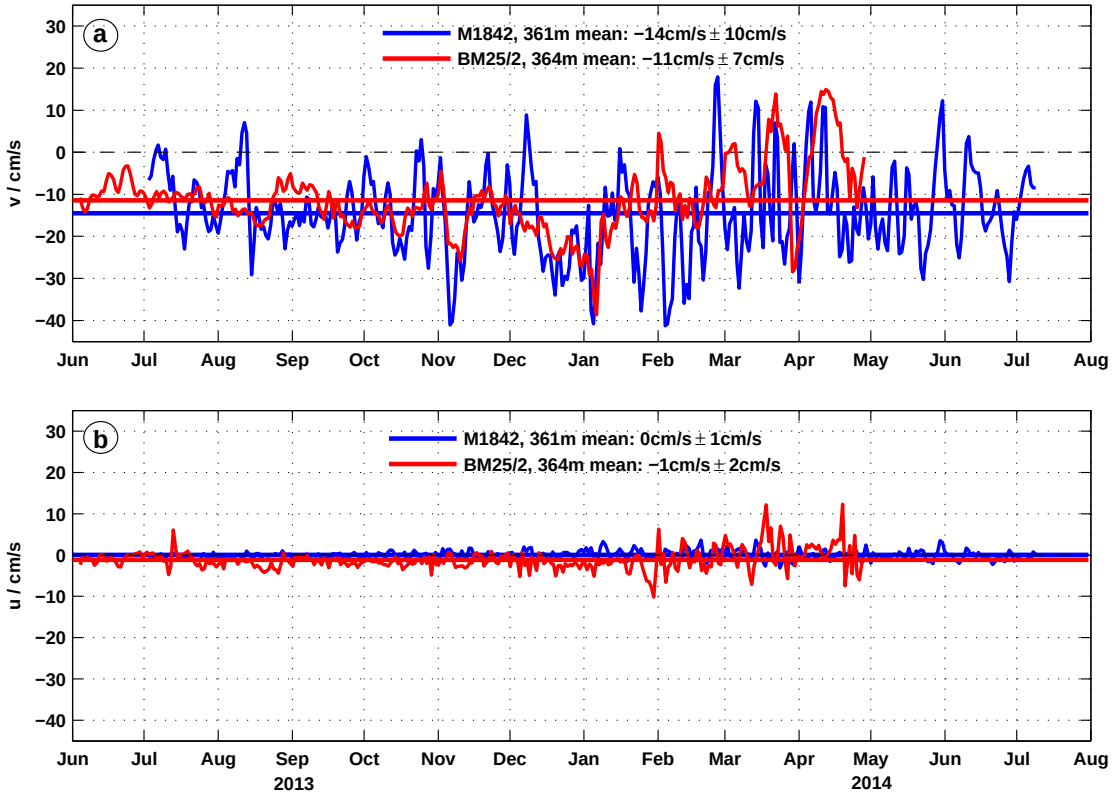

Figure 5.7: Velocity time series in June 2013 to April 2014 from the closest depth levels of the Flemish Pass ADCPs M1842 (blue) and BM25/2 (red). (a) Meridional velocity (cm/s) with mean value and standard deviation, and (b) zonal velocity, respectively.

deviations at M1842 are slightly higher than at BM25/2 ($-14\pm10\,\mathrm{cm\,s^{-1}}$, and $-11\pm7\,\mathrm{cm\,s^{-1}}$, respectively). Furthermore, several periods with correlating flow can be found, for instance in July 2013, between October 2013 and January 2014, and in March and April 2014. The overall correlation of both meridional velocity time series is weak (R = 0.3), but still statistically significant. The zonal velocity components (Figure 5.7b) of both time series were not significantly correlated, but they have in common that they are small compared to the meridional velocities, mostly not exceeding -5 to $5\,\mathrm{cm\,s^{-1}}$ and averaging to $-1\pm2\,\mathrm{cm\,s^{-1}}$ for BM25/2 and $0\pm1\,\mathrm{cm\,s^{-1}}$ for M1842, respectively.

Due to these results, the M1842 data was used in combination with the LSW layer transports based on BM25/2 to derive a top to bottom transport time series. The extrapolation of the mooring data is schematically shown in Figure 5.8. The data from BM25/2 was extrapolated as previously described for a single moor-

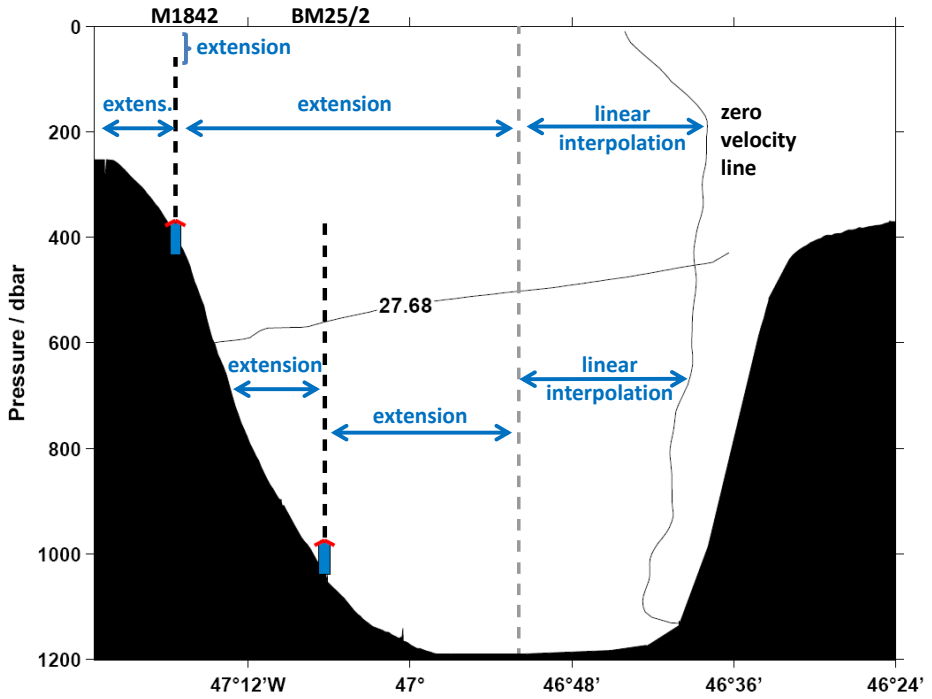

Figure 5.8: Schematic extrapolation of the Flemish Pass mooring data to estimate a top to bottom transport of the southward flow part in Flemish Pass during 2013/2014. Grey dashed line indicates the position of BM26/1 during the first mooring period (2012/2013).

ing based LSW transport, with the difference that the extrapolation of the data is continued above the LSW layer to a depth of 360 m, which is the range of BM25/2. Above, the velocity field is based on the data of M1842. The data was extended constantly westward to 47°23'W, the section limit of the extrapolated LADCP and VmADCP sections, and eastward toward the center of Flemish Pass to 46°51,58'W, the location where BM26/1 was located in the previous mooring period. Between 46°51,58'W and the location of the zero velocity line, the data was linearly interpolated. In the upper 60 m of the water column, the data of M1842 was extended constantly up to the surface. The combining of the M1842 and BM25/2 data produces a discontinuity at 360 m resulting from the different locations of the instruments. The differences in the meridional velocity component of the closest bins of both instruments were smaller than 5 cm s^{-1} for about 40% of the data, 43% of the data differed by 5 to 15 cm s^{-1}, and only 17% of the data had a difference larger than 15 cm s^{-1}. To reduce the discontinuity of the data, cubic smoothing splines were applied to the profiles between 260 and 460 m following *Roessler et al.* (2015). As an example, Figure 5.9 shows data profiles of

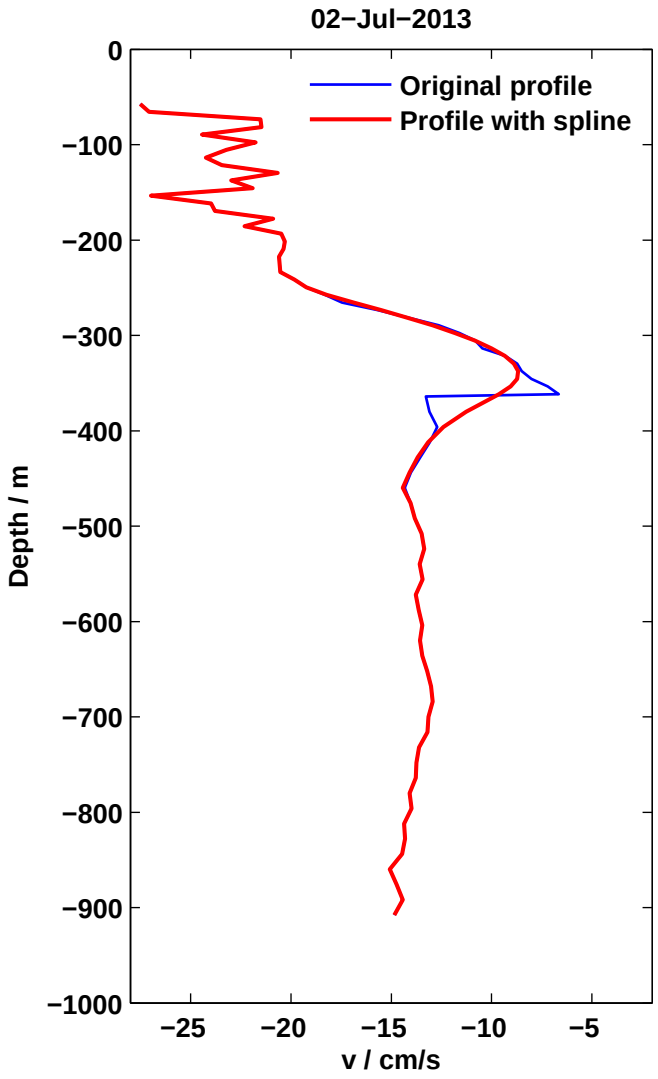

Figure 5.9: Original meridional velocity profiles (blue) measured by the ADCPs M1842 in the upper 360 m, and BM25/2 below 360 m on July 2 2013. In red, the same profiles are shown with an applied cubic smoothing spline between 260 and 460 m depth.

meridional velocity measured by both instruments on July 2 2013, and the applied cubic smoothing spline. A discontinuity between the velocity at the deepest bin of M1842 and the shallowest bin of BM25/2 is clearly visible at 360 m depth, the meridional velocities differ by about $7\,\mathrm{cm\,s^{-1}}$.

In the following section, the mooring based LSW and top to bottom transports are discussed and compared with the ship based estimates.

5.3 Transports through Flemish Pass from mooring and ship based estimates

In this section, the transport estimates of ULSW and DLSW are analyzed separately once again, as from the ship based current velocity measurements, transport estimates of the whole LSW layer could be only inferred from the LADCP data. The VmADCP data just covers the upper layer and the ULSW layer, DLSW transports would be based solely on extrapolation. Before the transport estimates are discussed, a short description will be given on how uncertainty estimates of the ship and mooring based transports were derived.

5.3.1 Uncertainty estimates

The uncertainty of the transport estimates was determined by error propagation from the uncertainty of the transport area and the uncertainty of the meridional velocity component (see equation 5.1).

$$\Delta T = \Delta A \cdot v + \Delta v \cdot A, \tag{5.1}$$

where ΔT is the transport uncertainty, A and ΔA are the transport area and its associated uncertainty, and v and Δv are the meridional velocity and the associated uncertainty of the velocity measurements.
The mooring transports of the different density layers in Flemish Pass were calculated based on the fixed limits of the average density field of 2012 - 2014 and the average zero velocity line separating southward and northward flow in the east determined from measurements in 2003, 2007, and 2009 - 2014 (see section 5.2.1). The uncertainty of the transport area was inferred from the variability of the density layer thickness in the vertical and from the horizontal variability of the zero velocity line based on the hydrographic and current velocity sections as shown in equation 5.2.

$$\Delta T = (\Delta A_{LT} + \Delta A_{ZL}) \cdot v + \Delta v \cdot A, \tag{5.2}$$

where ΔA_{LT}: uncertainty of the transport area due to variability of the density layer thickness, ΔA_{ZL}: uncertainty of the transport area due to variability of the zero velocity line.

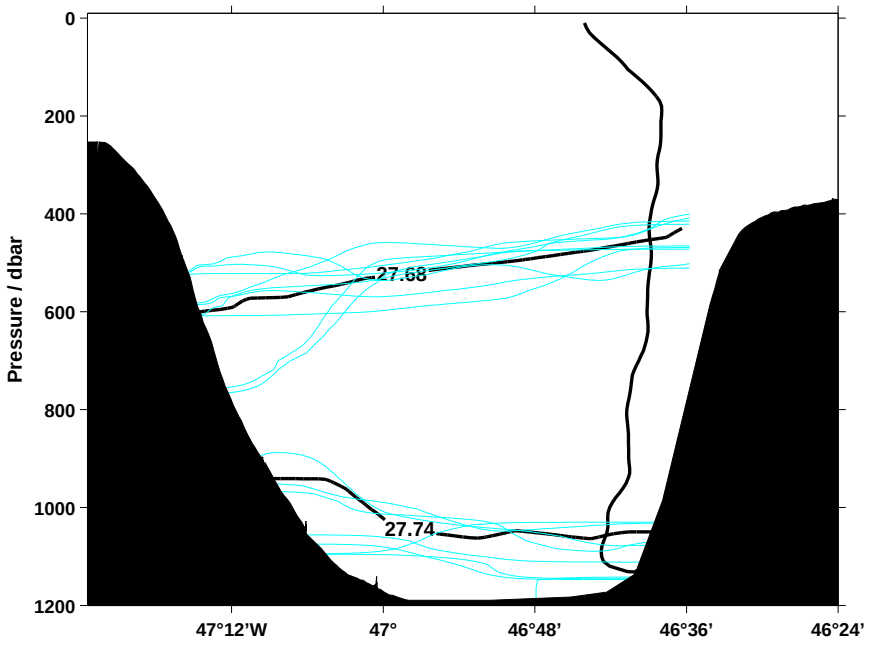

Figure 5.10: Schematic to infer the uncertainty of the transport area due to variability of the density layer thickness (ΔA_{LT}). Black lines indicate the fixed average density field and zero velocity line used to calculate layer transport estimates for the Flemish Pass southward flow. The uncertainty ΔA_{LT} is inferred from the standard deviation of the layer areas (upper layer, ULSW and DLSW layer, respectively) limited by the fixed zero velocity line in the east, and the ULSW isopycnals from the individual hydrographic sections in 2012 - 2014 (blue lines).

The variability of the density layer thickness of the considered hydrographic sections is shown in Figure 5.10, the different layer areas were estimated for each individual hydrographic section, and the fixed zero velocity line. The uncertainty ΔA_{LT} is the standard deviation of the layer areas. In the same way, ΔA_{ZL} was calculated as the standard deviation from the different layer areas limited by the zero velocity lines derived from each LADCP/VmADCP section (see table 2.1) and the fixed average ULSW isopycnals.
Following *Fischer et al.* (2015), Δv was estimated from the standard deviation of the flow in each density layer, divided by the square root of the degrees of freedom (DOF) to take into account statistical interdependency of the mooring measurements, $\Delta v = std(v)/\sqrt{DOF}$. The DOFs were determined from the first zero crossing of the autocorrelation function multiplied by two, as data are statistically independent after half a wavelength. The magnitudes of all variables to estimate the transport uncertainty according to equation 5.2 are given in table 5.1.

Table 5.1: Variables used to estimate the transport uncertainty for different density layers in Flemish Pass based on equation 5.2. A: transport area, ΔA_{LT} and ΔA_{ZL}: area uncertainty related to variability of the layer thickness and zero velocity line, respectively, std(v_1) and std(v_2): standard deviation of the mean meridional velocity component of each layer in the first (2012 - 2013) and second (2013 - 2014) mooring period, DOF_1 and DOF_2: degrees of freedom in the first and second mooring period, $\bar{v}_1$ and $\bar{v}_2$: layer average velocities of first and second mooring period, ΔT_1 and ΔT_2: transport uncertainty in the first and second mooring period. Upper layer: σ_θ <27.68 $\mathrm{kg\,m^{-3}}$, LSW layer: ULSW + DLSW layer, top to bottom: upper layer + ULSW + DLSW layer.

	ΔA_{LT} ($\mathrm{km^2}$)	ΔA_{ZL} ($\mathrm{km^2}$)	A ($\mathrm{km^2}$)	std(v_1) (m/s)	std(v_2) (m/s)	DOF_1	DOF_2	$\bar{v}_1$ (m/s)	$\bar{v}_2$ (m/s)	ΔT_1 ($\mathrm{Sv^2}$)	ΔT_2 ($\mathrm{Sv^2}$)
Top to bottom	0.0	4.0	49.6		0.06		26		0.18		1.3
Upper layer	1.5	2.5	24.9		0.07		26		0.23		1.3
ULSW layer	1.2	2.2	20.1	0.03	0.05	14	22	0.08	0.06	0.4	0.4
DLSW layer	1.8	0.7	4.6	0.04	0.05	18	26	0.07	0.05	0.2	0.2
LSW layer	1.5	2.6	24.6	0.03	0.05	14	22	0.08	0.06	0.5	0.5

Concerning the ship based transports, uncertainty estimates were derived following *Hall et al.* (2013) based on the following equation:

$$\Delta T = \Delta v \cdot A, \tag{5.3}$$

where Δv is the uncertainty of the meridional velocity measurements and A is the transport area. The magnitudes of Δv and A for the LADCP/VmADCP sections and the considered density layers are listed in table 5.2.

Table 5.2: Meridional velocity uncertainties (Δv) and density layer areas A used to calculate uncertainty estimates for the ship based transports with equation 5.3.1. The different layer areas are A_{TB}: top to bottom, A_{UL}: upper layer (σ_θ <27.68 kg m^{-3}), A_{ULSW}: ULSW layer, A_{DLSW}: DLSW layer. For cruises in which multiple Flemish Pass sections were measured, brackets in column one indicate the section number.

	A_{TB} (km^2)	A_{UL} (km^2)	A_{ULSW} (km^2)	A_{DLSW} (km^2)	Δv (m/s)
M59/2		27.1			0.03
MSM5/1		31.6			0.01
MSM12/3		24.1			0.02
MSM12/3	44.7	22.5	18.3	3.9	0.02
M82/2		26.5	19.9		0.01
M82/2	50.5	27.4	19.4	3.8	0.02
M85/1 (1)		28.8	19.7		0.02
M85/1 (2)		30.4	17.6		0.02
M85/1 (2)	52.3	30.1	18.9	3.3	0.02
MSM21/2 (1)		29.0	18.3		0.02
MSM21/2 (2)		26.3	18.7		0.02
MSM21/2 (2)	47.9	26.8	17.6	3.6	0.02
MSM27		33.5	22.0		0.02
MSM27	51.8	29.3	19.0	3.5	0.02
MSM28		27.2	22.7		0.03
MSM38		30.9	23.2		0.02
MSM38		27.8	23.5		0.02
MSM38	56.2	28.8	23.2	4.2	0.02

5.3.2 Transport estimates

The time series of LSW transports through Flemish Pass during July 2012 - April 2013 and June 2013 - May 2014, calculated based on the fixed average $\sigma_\theta = 27.68\,\mathrm{kg\,m^{-3}}$ isopycnal and the average zero velocity line is shown in Figure 5.11. In the first mooring period, transports range between -3.6 and $0.7\,\mathrm{Sv}$ with an average of $-1.9\,\mathrm{Sv}$. In the second period, in which the transport estimates are based only on the western slope mooring data, the transport range is -4.9 to $3.1\,\mathrm{Sv}$ with an average of $-1.4\,\mathrm{Sv}$. During both mooring periods, the strongest southward transports occur mainly during winter and spring, throughout December to April. In 2012, there is also an event of high southward transport ($-3.6\,\mathrm{Sv}$) in the middle of October. The LADCP sections conducted just before and after the first mooring period capture transports of $-1.4\,\mathrm{Sv}$ in July 2012 and $-2.1\,\mathrm{Sv}$ in April 2013. The magnitudes of the corresponding mooring and ship based transport estimates differ slightly, with a higher mooring based transport of $-1.6\,\mathrm{Sv}$ in the beginning of the first mooring period, and a lower one of $-1.7\,\mathrm{Sv}$ at the end. Even though there was just a short time gap of about two days each time between the mooring record and the ship based measurements, the discrepancies between transports are due to differences in the flow field, as Figure 5.12 shows. On July 10, 2012, the first day of the mooring period, BM25/1 measures low velocities smaller than $-5\,\mathrm{cm\,s^{-1}}$ over the western slope, while BM26/1 in the central Flemish Pass measures velocities between -5 and $-10\,\mathrm{cm\,s^{-1}}$. During the LADCP section conducted two days before, the LSW flow is higher over the western slope than in velocity distribution inferred from the moorings. Velocities exceeding $-5\,\mathrm{cm\,s^{-1}}$ extend from the western Flemish Pass to the center with just a narrow patch of velocities below $-5\,\mathrm{cm\,s^{-1}}$ just next to the position of BM25/1. East of the center, the flow field exhibits lower velocities smaller than $-5\,\mathrm{cm\,s^{-1}}$ and northward velocities from the recirculation around Flemish Cap in the LSW layer. The velocity distribution inferred from the mooring data on April 19, 2013, the last day of the mooring period, exhibits a slow reverse flow in the ULSW layer over the western slope down to a pressure of 800 dbar with velocities less than $5\,\mathrm{cm\,s^{-1}}$, and a stronger southward flow of up to $-15\,\mathrm{cm\,s^{-1}}$ in the central Flemish Pass. In the LADCP section carried out two days later, the reverse flow above 800 dbar over the western slope is replaced by a southward flow of less than $-10\,\mathrm{cm\,s^{-1}}$, and stronger flow of up to $-15\,\mathrm{cm\,s^{-1}}$ below 800 dbar which extends toward the central Flemish Pass. The differences in the mooring and ship based

velocity distributions indicate that the flow field in Flemish Pass is quite variable. The variability of the LSW transports will be discussed in detail at a later stage of this study (section 5.6), now the focus is on the comparison of the mooring and ship based transport estimates.

Table 5.3 shows all southward transport estimates from the LADCP/VmADCP measurements in Flemish Pass between 2003 and 2014, as well as average values from the mooring time records. The transport estimates are divided according to density layers, the upper layer ($\sigma_\theta < 27.68\,\mathrm{kg\,m^{-3}}$), the ULSW and DLSW layer and the entire water column (top to bottom). The ship based estimates of southward transport ranged between -2.1 to -5.4 Sv for the upper layer, between -1.1 to -2.4 Sv for the ULSW layer, between -0.1 to -0.4 Sv for the DLSW layer, and between -3.5 to -6.1 Sv for the top to bottom transport. From the VmADCP measurements of cruise MSM28 in June 2013, an even higher top to bottom transport through Flemish Pass is expected as the upper and ULSW layer transports together yield already -7.7 Sv, but no DLSW data was measured at that time.

The transport estimates of the upper and ULSW layer based on the VmADCP measurements usually deviated slightly from the LADCP based transport estimates (see table 5.3). These discrepancies result from the high horizontal resolution of the VmADCPs (about one profile per minute) in which smaller scale velocity structures are detected, which are not visible in the LADCP data, as well as from the extrapolation of the sections (section 5.1). The magnitudes of the

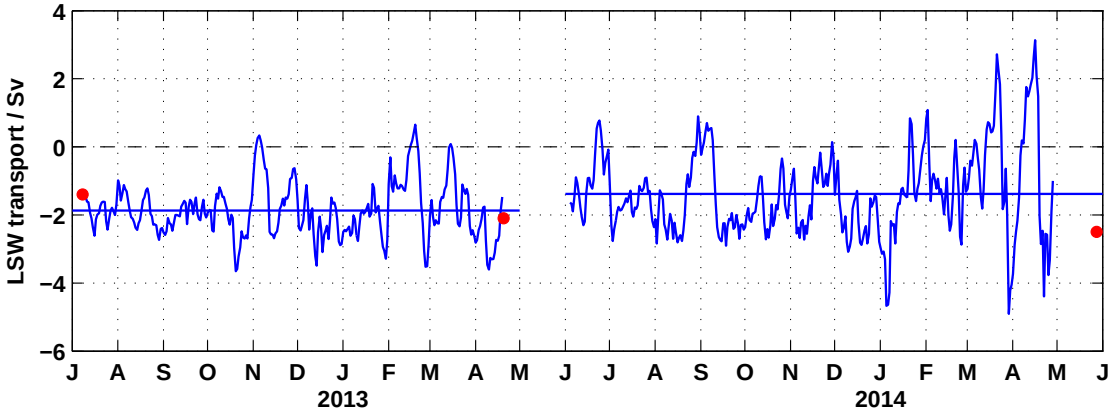

Figure 5.11: LSW layer transports (Sv) through Flemish Pass from mooring record of July 2012 to April 2013 and June 2013 to April 2014 based on a fixed $\sigma_\theta = 27.68\,\mathrm{kg\,m^{-3}}$ isopycnal boundary. Red dots mark ship based LADCP transport estimates.

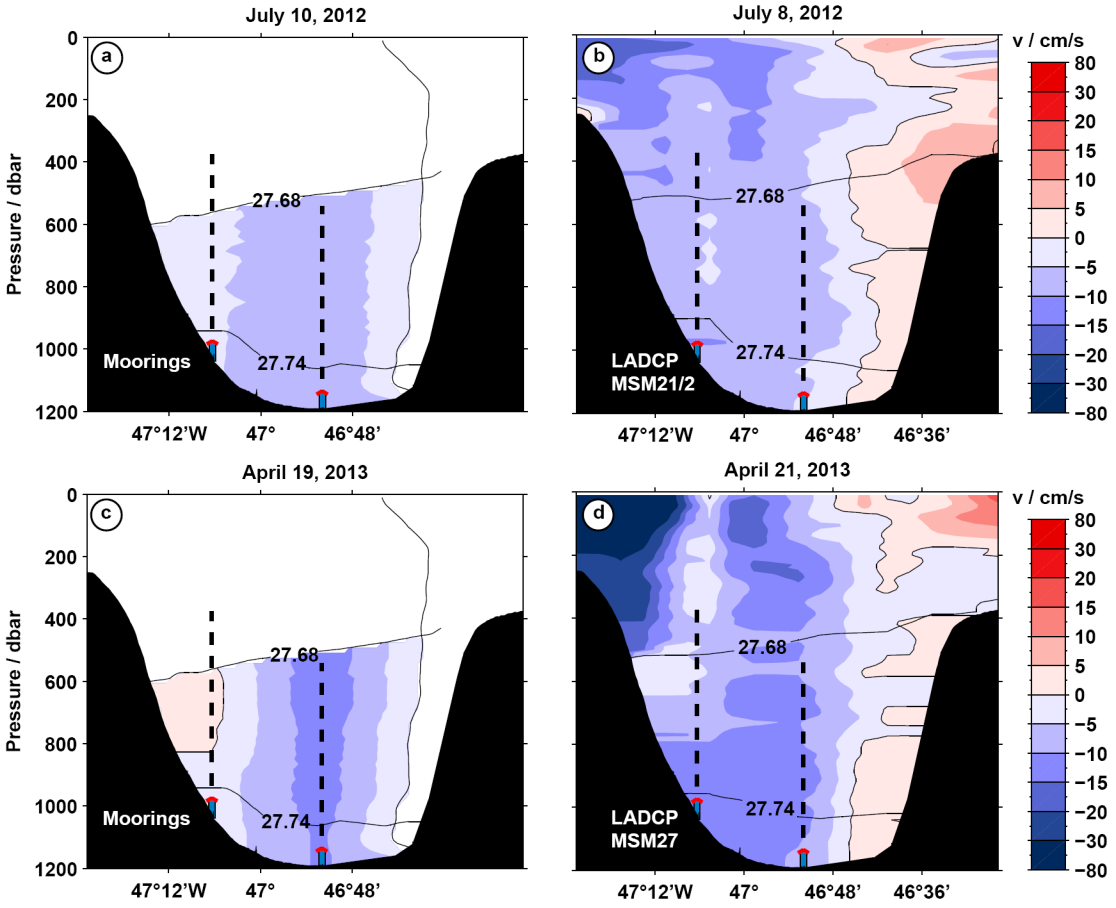

Figure 5.12: Meridional velocity distribution (cm/s) based on the mooring data at the first and last day of the mooring period (a,c), and based on the corresponding LADCP measurements (b,d). The zero velocity line in a) and c) is the average from all available Flemish Pass LADCP and VmADCP sections.

deviations were 0.5 Sv or less and therefore fall within the range of the transport uncertainties.

The average ship based transports of ULSW and DLSW agree very well with the average mooring based transports of the period 2012 to 2013 (−1.8 Sv (−0.3 Sv) and −1.7 Sv (−0.2 Sv), respectively for ULSW (DLSW)). The average mooring transport of 2013 to 2014, which was based on only one mooring, was slightly lower with −1.3 Sv for ULSW and −0.1 Sv for DLSW. It is likely that the transports inferred from only the western slope mooring BM25/2 underestimate the real transport slightly, which will be explained in more detail in section 5.5. Concerning the upper layer transport estimate (and as a consequence also the top to bottom estimate), the ship based average (−3.3 Sv) underestimates the mooring

Table 5.3: Estimates of the southward transport through Flemish Pass at 47°N based on shipboard and moored ADCP measurements for the upper layer (σ_θ <27.68 kg m^{-3}), ULSW and DLSW layer, and top to bottom (upper layer + ULSW + DLSW). The mooring transports were calculated based on seasonal average density layers of LSW. For cruises in which multiple Flemish Pass sections were measured, brackets in column one indicate the section number.

			Southward transports (Sv) and uncertainties			
Cruise	Date	Method	Upper layer	ULSW	DLSW	Top to bottom
M59/2	Aug 2003	OS 75	−2.8±0.8			
MSM5/1	Apr 2007	OS 75	−4.7±0.3			
MSM12/3	Jul 2009	OS 75	−3.2±0.5			
MSM12/3	Jul 2009	LADCP	−2.9±0.5	−1.5±0.4	−0.2±0.1	−4.6±0.9
M82/2	Aug 2010	OS 38	−2.6±0.3	−2.3±0.2		
M82/2	Aug 2010	LADCP	−2.8±0.4	−2.0±0.4	−0.2±0.1	−5.0±1.0
M85/1 (1)	Jul 2011	OS 75/OS 38	−3.4±0.4	−2.2±0.4		
M85/1 (2)	Jul 2011	OS 75/OS 38	−3.1±0.4	−1.7±0.4		
M85/1 (2)	Jul 2011	LADCP	−3.1±0.4	−1.6±0.4	−0.1±0.1	−4.8±1.0
MSM21/2 (1)	Jul 2012	OS 75/OS 38	−2.4±0.4	−1.5±0.4		
MSM21/2 (2)	Jul 2012	OS 75/OS 38	−2.6±0.4	−1.5±0.4		
MSM21/2 (2)	Jul 2012	LADCP	−2.1±0.4	−1.1±0.4	−0.3±0.1	−3.5±1.0
MSM27	Apr 2013	OS 75/OS 38	−4.1±0.4	−1.7±0.4		
MSM27	Apr 2013	LADCP	−4.0±0.4	−1.7±0.4	−0.4±0.1	−6.1±1.0
MSM28	Jun 2013	OS 75/OS 38	−5.4±0.7	−2.3±0.7		
MSM38 (1)	May 2014	OS 75/OS 38	−3.5±0.5	−2.2±0.5		
MSM38 (2)	May 2014	OS 75/OS 38	−3.1±0.5	−2.4±0.5		
MSM38 (2)	May 2014	LADCP	−3.1±0.5	−2.1±0.5	−0.4±0.1	−5.6±1.1
		Ship based mean	−3.3±0.4	−1.8±0.4	−0.3±0.1	−5.4±1.0
	2012 - 2013	Mooring mean		−1.7±0.4	−0.2±0.2	
	2013 - 2014	Mooring mean	−5.3±1.3	−1.3±0.4	−0.1±0.2	−6.7±1.3

based average (−5.3 Sv) by −2 Sv. As the ship measurements were only conducted during spring and summer, the reason for this underestimation is possibly a seasonal impact on the upper layer with higher transports during the other seasons. Upstream of Flemish Pass, *Fischer et al.* (2004) observed a seasonal cycle in the DWBC at 53°N, which was confined in the shallow Labrador Current, while they could not detect a seasonal signal in the deeper flow of the DWBC. The topic of seasonal effects on the transports through Flemish Pass are further analyzed in the next section.

5.4 Seasonal effects on LSW transports through Flemish Pass

There are two scenarios how the LSW transports in Flemish Pass could be affected by seasonal changes: Firstly, a seasonal change in the thickness of the LSW density layer would impact the transports. *Myers and Kulan* (2012) have found that transport estimates of the DWBC at 53°N are quite sensitive to seasonal and interannual variability in the structure of the density field used for the partitioning into density layers. Therefore, they suggested to use time-varying density fields whenever possible. Secondly, an increase or decrease of the LSW flow through Flemish Pass modulated by a seasonal cycle would affect the transports too. Upstream of Flemish Pass, at 53°N, *Fischer et al.* (2015) observed a seasonal cycle from current velocity time series of the DWBC, which was stronger near the surface than close to the bottom. To assess if the assumption of a fixed density layer for the calculation of mooring based LSW transports is a good approximation, the scenario of a seasonally changing density layer will be addressed here first. The other scenario will be discussed in section 5.4.4.

5.4.1 Seasonal changes of the LSW density layer based on shipboard hydrographic measurements

First, the ship based hydrographic measurements of Flemish Pass are used to investigate seasonal changes of the LSW density layer. The 9 hydrographic sections measured in Flemish Pass in 2012 - 2014 previously used to estimate the average LSW density layer as transport limits (section 5.2.1), were utilized here to derive seasonal averages for the measurements in spring (April, May), summer (June - August), and winter (November, December). In Figure 5.13a, the location of the seasonal and the average ULSW isopycnals are indicated. All average $\sigma_\theta = 27.68\,\mathrm{kg\,m^{-3}}$ isopycnals have an incline from East to West, while the $\sigma_\theta = 27.74\,\mathrm{kg\,m^{-3}}$ isopycnals have an incline from West to East. The location of the $\sigma_\theta = 27.68\,\mathrm{kg\,m^{-3}}$ isopycnal of spring and summer is quite similar. Both isopycnals are observed at a pressure of 340 dbar over the Flemish Cap, and decrease westward being separated by only 50 to 70 dbar to reach a pressure

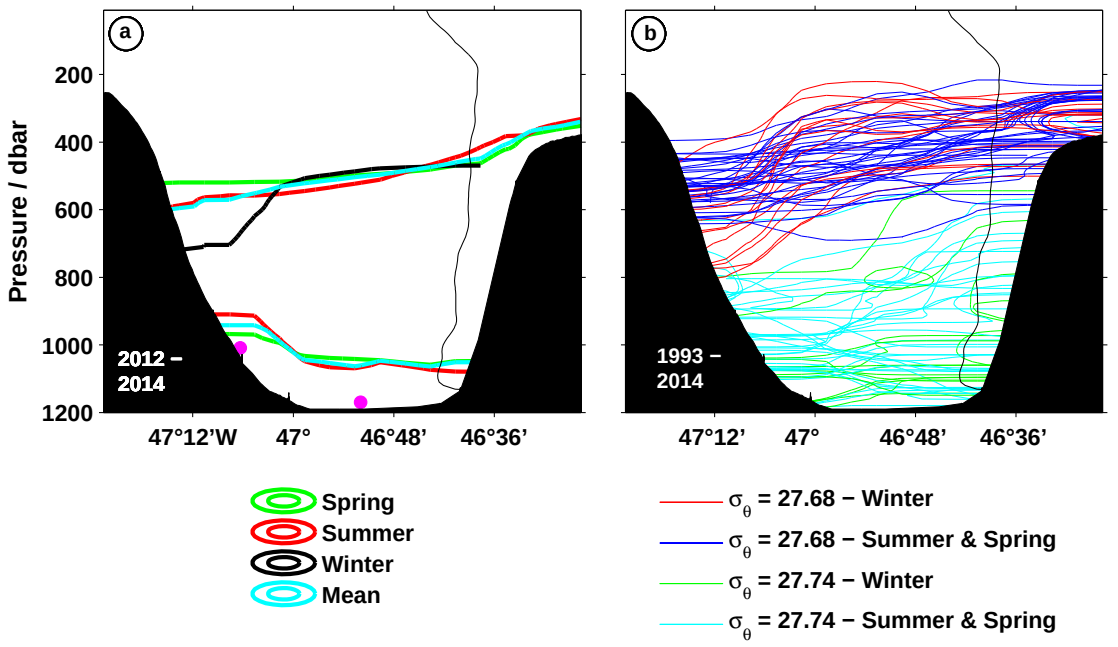

Figure 5.13: (a) Average ULSW isopycnals from measurements in spring (green), summer (red), winter (black) and all seasons (blue) for the period 2012 - 2014. Notice that there is no DLSW in the winter estimate. Pink dots indicate the MicroCAT locations of moorings BM25/1 and BM26/1. Vertical black line marks the zero velocity line. (b) ULSW isopycnals from individual hydrographic sections conducted during 1993 - 2014.

of 520 dbar (spring) and 590 dbar (summer) at the western slope. In the winter sections, no measurements have been conducted over the Flemish Cap, therefore the $\sigma_\theta = 27.68\,\mathrm{kg\,m^{-3}}$ winter isopycnal only extends to 46°39'W. In the central Flemish Pass, the winter isopycnal is located at a pressure of about 500 dbar similar to the spring isopycnal, but distinctly differs in location in the western Flemish Pass. At the western slope, it is located at 710 dbar, which is 150 to 200 dbar deeper than the summer and spring isopycnal. Toward the central Flemish Pass, it has a steep increase to about 530 dbar at 47°W. Due to the lowered isopycnal, the LSW layer has a reduced area over the western slope in winter compared to the spring and summer seasonal density layers.

Concerning the seasonal $\sigma_\theta = 27.74\,\mathrm{kg\,m^{-3}}$ isopycnals, there is a 60 dbar difference in depth between the summer and spring estimate over the western slope, while in the central and eastern Flemish Pass they differ by about 30 dbar. Notice that there is no DLSW in Flemish Pass in the winter estimate, due to a lowering of the average $\sigma_\theta = 27.74\,\mathrm{kg\,m^{-3}}$ winter isopycnal.

The ULSW isopycnals averaged over all seasons follow very closely the shape of the spring and summer ULSW isopycnals, only deviating by 20 to 70 dbar to each one. This is due to the fact that of the 9 hydrographic sections, 3 were conducted in spring, 4 in summer, and only 2 in winter. Transport estimates based on the fixed average ULSW isopycnals would therefore overestimate the transports in the winter months. The dropping of the $\sigma_\theta = 27.68\,\mathrm{kg\,m^{-3}}$ isopycnal over the western slope in winter is a phenomenon, that is not just occurring during the period 2012 - 2014. Figure 5.13b compares the summer and spring ULSW isopycnals with the winter isopycnals for all sections measured in 1993 - 2014. The ULSW isopycnals from the early 1990s and the recent ones have a wide range of more than 200 dbar in their location resulting from the warming and salinification trend of LSW (see chapter 4). Nevertheless, the stronger dropping of the $\sigma_\theta = 27.68\,\mathrm{kg\,m^{-3}}$ isopycnals in winter over the western slope as compared to the summer and spring isopycnals is clearly visible.
As the average isopycnals based on all seasons of 2012 - 2014 do not represent the LSW density layer very well during winter, LSW transport estimates based on the seasonal density limits were also considered. To study in more detail how seasonal changes affect the hydrographic properties of the deep water in Flemish Pass and to identify when seasonal changes take place, the MicroCAT data of the Flemish Pass moorings 2011 - 2013 are analyzed in the following section.

5.4.2 Seasonal changes based on MicroCAT time series, 2011 - 2013

The MicroCATs of the Flemish Pass moorings recorded time series of near bottom temperature and salinity. During the pilot array period 2011 - 2012, two MicroCATs were deployed in the central Flemish Pass at a pressure of 1068 and 1153 dbar. In 2012 - 2013, one MicroCAT was attached to the western slope mooring BM25/1 at a pressure of 956 dbar and another one at BM26/1 in the central Flemish Pass at a pressure of 1126 dbar (see table 2.2). From the measured temperatures and salinities, time series of potential density σ_θ were calculated. In a harmonic analysis, the seasonal cycle of the hydrographic properties was estimated. Figure 5.14 shows the time series and seasonal cycles during 2012 - 2013. Seasonal changes are clearly visible in the density time series (Figure 5.14a).

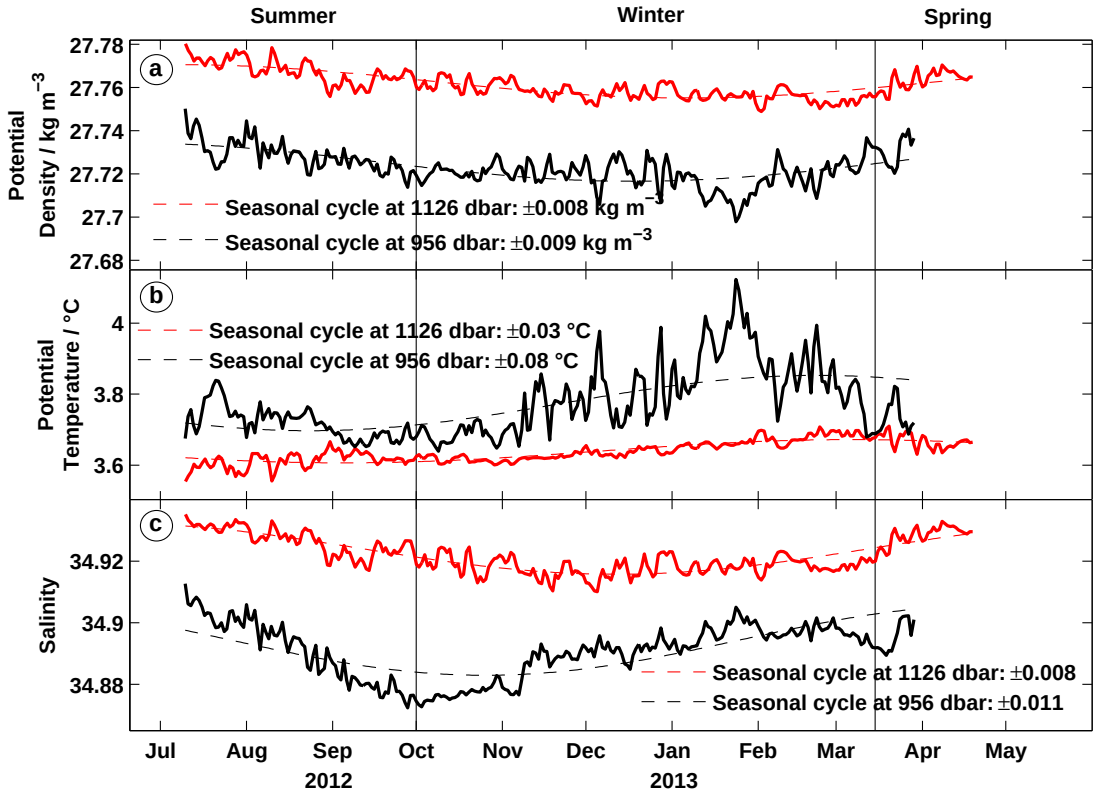

Figure 5.14: Hydrographic time series (40 h low pass filtered, daily averages) from MicroCAT records in BM25/1 (black) and BM26/1 (red) between July 2012 to April 2013. (a) Potential density (kg m^{-3}), (b) potential temperature, and (c) salinity. Note that the time series from BM25/1 end in March 2013 due to a sensor failure. Vertical black lines indicate the time periods, in which the seasonal average LSW density layers were applied to calculate transports, as described in the text.

The magnitude and the temporal evolution of the seasonal cycles was very similar at both moorings. The magnitude of ±0.008 and ±0.009 kg m^{-3} corresponds to a change in isopycnal depth of about 80 m in the water column. Concerning the temporal evolution, the highest densities (about 27.74 kg m^{-3} at BM25/1 and 27.78 kg m^{-3} at BM26/1) occurred during the summer months July and August 2012, followed by a decrease in density until the beginning of October. Between October 2012 and early March 2013, the densities stayed low, oscillating around 27.76 kg m^{-3} at BM26/1, and 27.72 kg m^{-3} at BM25/1. The density time series at BM25/1 exhibits a further drop to a minimum density of 27.7 kg m^{-3} in January 2013. After March 15, 2013 until the end of the time series, the densities increased again. In the temperature time series, a slightly stronger seasonal cycle

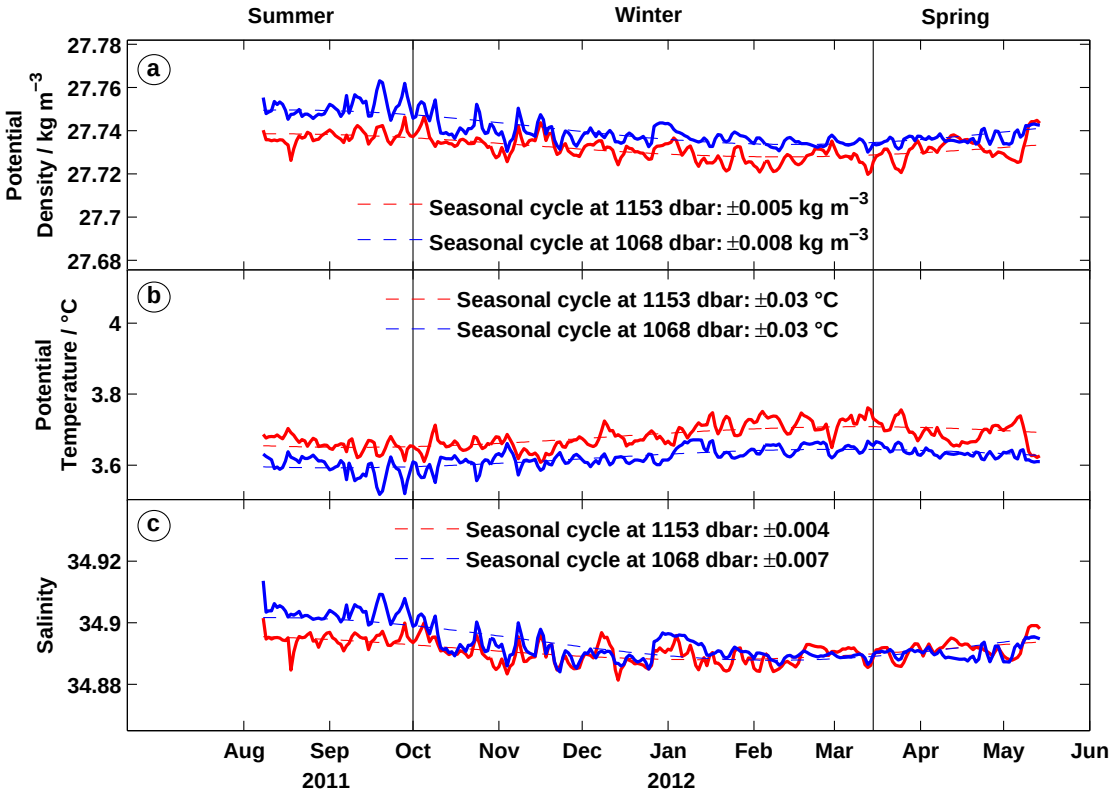

Figure 5.15: Hydrographic time series (40 h low pass filtered, daily averages) from MicroCAT records of the pilot mooring in the central Flemish Pass (same position as BM26/1) between August 2011 to May 2012 at two depths levels: 1068 dbar (blue) and 1126 dbar (red). (a) Potential density (kg m^{-3}), (b) potential temperature, and (c) salinity. Vertical black lines are the same as in Figure 5.14.

was observed at BM25/1 (±0.08 °C) than at BM26/1 (±0.03 °C, Figure 5.14b). The lowest temperatures occurred at both moorings during summer and early autumn 2012. At BM25/1, temperatures varied between 3.65 to 3.75 °C from July throughout October. Meanwhile at BM26/1, temperatures of 3.6 °C were observed. Between November 2012 and late January 2013, the temperatures at BM25/1 were increasing and more variable, ranging between 3.70 to 4.10 °C. Afterward, the temperatures decreased again. The temperatures at BM26/1 were increasing during the winter months as well, and reached a maximum of about 3.7 °C in February.

Similar to the temperatures, the magnitude of the seasonal cycle of salinity at BM26/1 was slightly weaker (±0.008) than at BM25/1 (±0.011, Figure 5.14c). The temporal evolution of the seasonal cycle at BM26/1 mirrors the one of the

density time series, with the highest salinities occurring in the summer months July and August 2012, and the lowest in the winter months November 2012 - January 2013. The salinity time series recorded at BM25/1 displayed high salinities ranging from 34.89 to 34.91 throughout most of the summer (July and August 2012) as well as winter and spring (November 2012 - end of March 2013), and the lowest salinities occurred between September and November.

Based on the seasonal evolution of the density time series in 2012 - 2013, the seasonal changes between summer, winter and spring (the three seasons in which ship based hydrographic measurements were conducted in Flemish Pass), were identified as follows: Summer ending at September 30, 2012, and winter ending at March 15, 2013 (Figure 5.14). These dates were used to calculate an LSW transport time series based on the seasonal averaged LSW isopycnals (section 5.4.1), which is further discussed in the following section 5.4.3.

The hydrographic time series and seasonal cycles of 2011 - 2012 estimated from the pilot mooring MicroCATs (Figure 5.15) support the results of 2012 - 2013. The magnitudes of the seasonal cycles of the shallower MicroCAT deployed at a pressure of 1068 dbar were almost identical to those at the MicroCAT in BM26/1. Both had a seasonal cycle of $\pm 0.008\,\mathrm{kg\,m^{-3}}$ for density (Figures 5.14a and 5.15a), $\pm 0.03\,^{\circ}\mathrm{C}$ for temperature (Figures 5.14b and 5.15b), and ± 0.007 (pilot mooring) and ± 0.008 (BM26/1) for salinity (Figures 5.14c and 5.15c). In comparison, the seasonal cycle magnitudes at the deeper MicroCAT of the pilot mooring (1153 dbar) were slightly weaker for density ($\pm 0.005\,\mathrm{kg\,m^{-3}}$) and salinity ($\pm 0.004$), but the same for temperature ($0.03\,^{\circ}\mathrm{C}$). The highest densities and salinities and lowest temperatures occurred in summer (August and September 2011, Figure 5.15), and the lowest densities and salinities and highest temperatures in winter (January to March 2012), similar to the time series at BM26/1. However, the onset of the seasonal change happened about a month later in 2011 than in 2012. The decrease in density and salinity and the increase in temperature during the transition from summer to winter did not start before October in 2011, while in 2012 it was observed already in September.

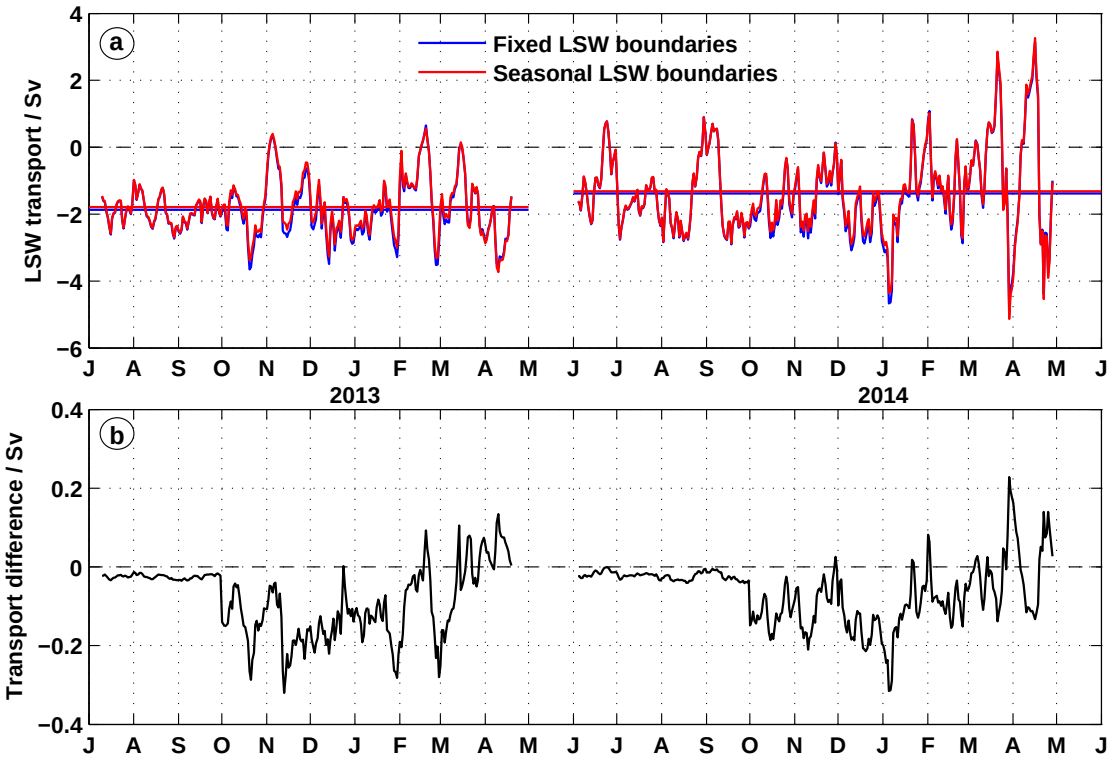

Figure 5.16: (a) LSW layer transports (Sv) through Flemish Pass from mooring record of July 2012 to April 2013 and June 2013 to April 2014 based on a fixed isopycnal boundary (blue) and based on seasonal isopycnal boundaries (red). (b) Difference of transports based on a fixed isopycnal boundary and based on seasonal isopycnal boundaries. Negative differences indicate that the transports based on the fixed isopycnal boundary are higher.

5.4.3 Flemish Pass transport time series based on fixed and seasonal LSW density limits

Based on the results from the MicroCAT time series, the seasonal average isopycnals shown in Figure 5.13a were applied in the following time frames to calculate the LSW transports: the average summer isopycnal in June throughout the end of September, the winter isopycnal from October until the middle of March, and the spring isopycnal from the middle of March until the end of the record.

The time series of LSW transports through Flemish Pass during July 2012 - April 2013 and June 2013 - May 2014, determined from both, the fixed average LSW layer and from the seasonal average LSW layers are shown in Figure 5.16a. As the discrepancies of both time series are rather small, the transport differences of the

time series are displayed in Figure 5.16b. In summer and winter, the transports based on the seasonally varying LSW layers are mostly lower than the transports based on the fixed LSW layer (Figure 5.16b), and mostly higher for the spring months between middle of March to May. The smallest differences of less than $-0.05\,\mathrm{Sv}$ occur during summer. Then, the fixed average $\sigma_\theta = 27.68\,\mathrm{kg\,m^{-3}}$ isopycnal is located very close to the summer $\sigma_\theta = 27.68\,\mathrm{kg\,m^{-3}}$ isopycnal (Figure 5.13a), and therefore the LSW layer thickness is almost the same.
The positive transport differences in spring of 0.1 Sv in the first mooring period and of up to 0.2 Sv in the second mooring period (Figure 5.16b) result from a slightly shallower location of the spring isopycnal over the western slope compared to the fixed average isopycnal (Figure 5.13a), it therefore limits a somewhat larger LSW transport area.
During winter, the highest differences between the fixed and seasonal layer transport estimates manifested as expected, resulting from the change in layer thickness over the western slope (Figure 5.13a). The differences are mostly smaller than $-0.2\,\mathrm{Sv}$, but also reach up to $-0.3\,\mathrm{Sv}$ during short events in October and November 2012, January and February 2013, and January 2014. A difference of $-0.3\,\mathrm{Sv}$ corresponds to about 20% of the mean transport, and $-0.2\,\mathrm{Sv}$ corresponds to about 14%. This is a considerable overestimation of the winter transports, if the fixed isopycnal boundary is used for the transport calculation. These results agree with the results of *Myers and Kulan* (2012), who found that density layer transport estimates of the DWBC at 53°N are quite sensitive to seasonal variability of the density field. However, the difference of $-0.3\,\mathrm{Sv}$ in the Flemish Pass transport based on the fixed and on the seasonal variable density limit is still well within the range of the estimated LSW transport uncertainty of $\pm 0.5\,\mathrm{Sv}$ (see table 5.3). Therefore, the effect of seasonally changing density limits on the LSW transport is considered negligible in this case. For this reason, in the following, the results based on the fixed average isopycnal boundary will be further analyzed and discussed. In the next section, the impact of seasonal changes of the flow on the Flemish Pass transports is investigated.

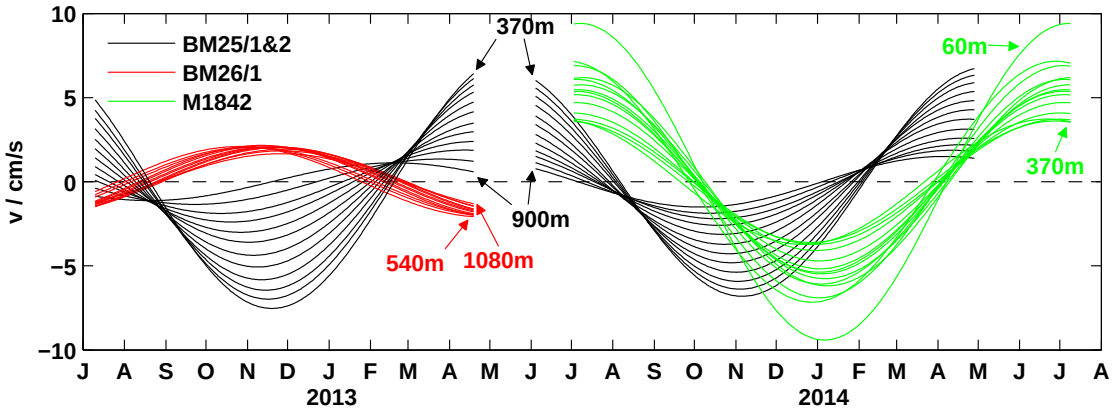

Figure 5.17: Amplitudes of the seasonal cycle of the meridional current velocity at different depth bins of the Flemish Pass moorings BM25/1 & 2 (black), BM26/1 (red), and M1842 (green). For clarity, only every third depth bin is displayed. Approximate depths of the shallowest and deepest bins are indicated by text arrows. Note that the seasonal cycle amplitudes are depth dependent at the western slope moorings BM25/1 & 2 and M1842, with the smallest amplitudes at the deepest bins, and increasing amplitudes toward shallower depths.

5.4.4 Seasonal changes in the LSW flow through Flemish Pass

The previously mentioned scenario of a seasonal impact on the flow through Flemish Pass affecting the LSW transports was investigated by performing a harmonic analysis of the current velocity data of the Flemish Pass moorings, and also of the transport time series. Figure 5.17 shows the amplitudes of the seasonal cycle of the meridional current velocity at different depth bins of the moorings. The minimum and maximum of the seasonal cycle amplitudes correspond to an increase and a decrease of the southward flow, respectively. Interestingly, there is a depth dependent change in the amplitudes of the seasonal cycles at the western slope moorings BM25/1 and BM25/2 (Figure 5.17). At the deepest bins in a depth of about 900 m, the seasonal cycles were very weak with amplitudes of about $\pm 1\,\mathrm{cm\,s^{-1}}$ during both mooring periods. During 2012 - 2013, the minimum of the seasonal cycle occurred in August 2012, and the maximum in February (BM25/1). In 2013 - 2014 (BM25/2), the maximum and minimum of the seasonal cycle at 900 m depth were delayed about two month compared to the first mooring period and exhibited in October and April, respectively. With decreasing water depth, the seasonal cycle amplitude increased to about $\pm 7\,\mathrm{cm\,s^{-1}}$ at 370 m depths during

2012 - 2013 (BM25/1). Furthermore, a phase shift of three months occurred, so that the minimum of the seasonal cycle was in November instead of August. In 2013 - 2014, the seasonal cycles at BM25/2 display a very similar increase in amplitude with decreasing depths to $\pm 7\,\mathrm{cm\,s^{-1}}$, with a slightly weaker phase shift of one month, so that the minimum of the seasonal cycle occurred in November as well. The difference of the seasonal cycles of shallow and deeper depths at the western slope moorings is most likely a result of the very baroclinic flow field in the western Flemish Pass, induced by the shallow Labrador Current (see section 5.2.1, Figure 5.5). The closer the proximity to the core of the Labrador Current was in the flow field, the higher was the seasonal impact on the flow at the western slope. The amplitude of $\pm 7\,\mathrm{cm\,s^{-1}}$ at 370 m depth matches a result from *Fischer et al.* (2004), who investigated seasonality in the flow of the DWBC at 53°N based on a harmonic analysis of current velocity mooring data. They found a seasonal cycle amplitude of $\pm 7\,\mathrm{cm\,s^{-1}}$ in the near surface layer of the Labrador Current.
Corresponding results were found from the data of the shallow Canadian mooring M1842, which was located higher up on the western slope during 2013 - 2014, and measured the current velocity in the Labrador Current. The meridional velocity data displayed the same tendency of increasing amplitudes of the seasonal cycle with shallower depths, ranging between $\pm 4\,\mathrm{cm\,s^{-1}}$ at 370 m depth, and $\pm 9\,\mathrm{cm\,s^{-1}}$ at 60 m depth. There was no phase shift in the seasonal cycles of the different depth bins, the minimum occurred in January, and the maximum in July.
In the central Flemish Pass (BM26/1), the seasonal cycles during 2012 - 2013 were quite weak, but comparable at all depth bins with amplitudes of about $\pm 2\,\mathrm{cm\,s^{-1}}$. This can be attributed to the barotropic flow field in the center (see section 5.2.1, Figure 5.5). The only difference between shallower depths (minimum 540 m) and deeper depths (maximum 1080 m) was a slight phase shift of the maximum of the seasonal cycle from October to November. Note that the maximum of the seasonal cycle at BM26/1 occurred at the same time as the minimum of the seasonal cycle at BM25/1. *Fischer et al.* (2004) observed a seasonal cycle in the DWBC at 53°N that was confined in the shallow Labrador Current, while they could not detect a seasonal signal in the deeper flow of the DWBC. Based on longer mooring time series data of nine years in total, *Fischer et al.* (2015) found a weak seasonal cycle also in the deep flow of the DWBC. Performing an analysis of the seasonality of the intra seasonal boundary current variability, they were able to detect a seasonal cycle, which had a phase shift compared to the seasonal cycle of the Labrador

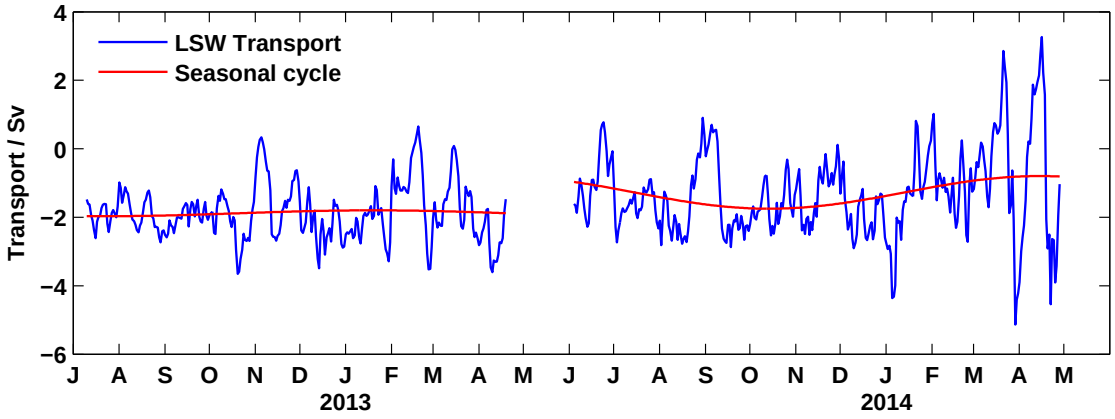

Figure 5.18: LSW transport time series (blue) and seasonal cycles (red) during July 2012 - April 2013, and June 2013 - April 2014.

Current. *Fischer et al.* (2015) could only find the deep seasonal cycle at one mooring (K9) of their mooring array, and they considered the signal as rather weak, but they suggested that this result could stimulate a future discussion about deep seasonal cycles in the subpolar North Atlantic. The seasonal cycles found in the deep flow through Flemish Pass at BM26/1 were quite weak as well, and also had a phase shift compared to the Labrador Current. In this way, the results of the Flemish Pass point to a confirmation of the observations of *Fischer et al.* (2015).
To assess how the seasonal cycle in the flow affected the transport of LSW through Flemish Pass, a harmonic analysis of the transport time series was performed. Figure 5.18 shows the transport time series of both mooring periods 2012 - 2013 and 2013 - 2014, and the estimated seasonal cycles. During the first mooring period, the LSW transports were estimated based on both the western slope mooring BM25/1, and the central Flemish Pass mooring BM26/1. The seasonal cycle of the transport time series had a very small amplitude of about ± 0.1 Sv, with a minimum in July and a maximum in January. The different seasonal cycles at BM25/1 and BM26/1 appear to superpose in a way that the seasonal signal is almost canceled out. During the second mooring period, the LSW transports were calculated based on only the western slope mooring BM25/2. Therefore, the transport time series in 2013 - 2014 had a seasonal cycle with a larger amplitude of ± 0.5 Sv.
After the seasonal effects on the LSW transports through Flemish Pass were discussed in detail in this section, the following section deals with the impact of a single mooring vs. two moorings as the basis for the calculation of LSW transports.

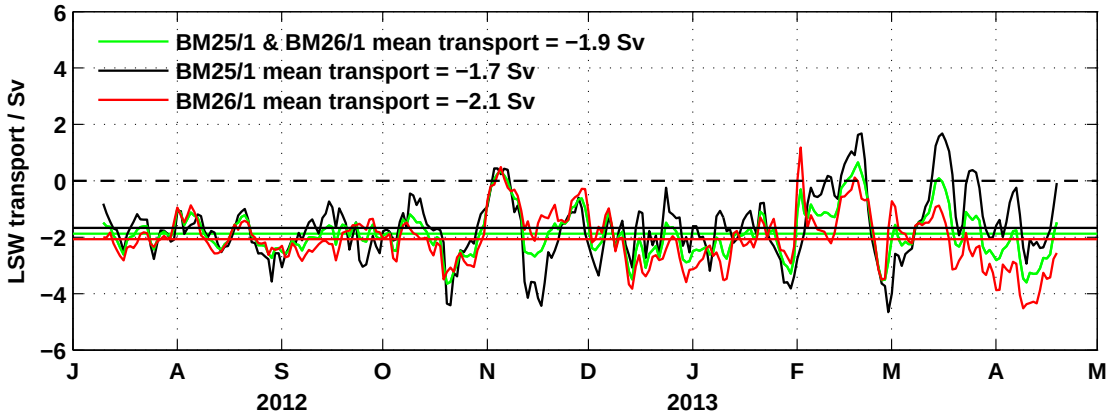

Figure 5.19: LSW layer transports (Sv) through Flemish Pass from mooring record of July 2012 to April 2013 inferred from both moorings BM25/1 and BM26/1 (green), based only on mooring BM25/1 (black), and based only on mooring BM26/1 (red).

5.5 Transports from one vs. two moorings

In this section, the LSW transport time series of the first mooring period (2012 - 2013), which was calculated based on two moorings deployed in Flemish Pass (BM25/1 and BM26/1), is compared to single mooring transport time series based on only BM25/1 and only BM26/1, to assess how much each mooring contributes to the magnitude of the transport signal. The three different transport time series are shown in Figure 5.19. Both single mooring transport time series were as expected highly correlated with the two mooring transport time series. The correlation of the BM26/1 based time series with the two mooring time series was slightly higher (R = 0.85) than the one of the BM25/1 based time series (R = 0.80). On average, the single mooring transports based on BM25/1 underestimate the transports based on both moorings by 0.2 Sv (mean transport of −1.7 Sv for just BM25/1, and −1.9 Sv for both moorings), while the single mooring transports based on BM26/1 overestimate the transports based on both moorings by 0.2 Sv (mean transport of −2.1 Sv for just BM26/1). This implies that the transport estimates of the second mooring period in 2013 - 2014 are potentially slightly too low on average, as they were calculated based on only the western slope mooring

BM25/2. However, in the range of the LSW transport uncertainty (±0.5 Sv, see table 5.3), this deviation is really small and therefore negligible. The contribution of the two single moorings to the transport signal is therefore rather balanced. Only in certain events of high southward transport or strong transport reduction, the single mooring transport based on BM25/1 is overshooting the other two time series considerably. For example in October and November 2012, and in January and February 2013, the BM25/1 based transport time series exhibits the highest southward transport estimates of about 4 Sv, and is overestimating the two mooring time series by up to 2 Sv. In February, March and April 2013, there were strong reductions and sometimes even transport reversals, which were also more intense in the BM25/1 based time series, reaching up to 1.6 Sv of northward transport and deviating by about 1.5 Sv from the two mooring time series. This indicates that in particular events, something is occurring in the flow of the western Flemish Pass, maximizing or minimizing the transport there, which does not occur in the center. This phenomenon is further investigated in the next section 5.6, which investigates LSW transport variability, and also later on in this study in section 6.2.

5.6 Transport variability of LSW

The two time series of LSW transports through Flemish Pass between July 2012 and April 2014, which were already shown in Figure 5.11, are displayed and discussed here again under the aspect of transport variability (Figure 5.20). During the first mooring period in July 2012 to April 2013, the LSW transport time series appears to divide in two phases. In phase one, during the summer time and early autumn (July to middle of October), the LSW transports lightly oscillated around the mean value of −2 Sv, while values between −1 Sv and −2.7 Sv were reached. In the middle of October, phase two began, comprising the autumn and winter month until the end of the mooring record. This phase was characterized by strong variability with transports up to −3.5 Sv, for instance in October and December 2012, and in February and April 2013, but also by strong transport reductions which even turned into current reversals within the LSW layer twice, in November 2012 and February 2013. The northward transports in these two events were 0.3 and 0.7 Sv in November and February, respectively.

During the second mooring period in June 2013 to April 2014, the two different

phases of lower and higher variability are also observed. However, the phase of lower variability with LSW transports between −1 Sv and −3 Sv exceeds the summer month and continues on until the end of December, but is disrupted several times by events of strong transport reductions or reversals, for instance in June, September and November 2013. During the second phase, transport maxima up to −4.8 Sv occurred in January, March and April 2014, while transport reversals reached northward LSW transports of 1 Sv to 3 Sv in late January/early February, and March and April 2014.

A spectral analysis was carried out to identify the characteristic time scales of the LSW transports in Flemish Pass. The transport time series were zero padded to the next higher order of magnitude of 2 to ensure that all measurements were included to derive the spectra. Figure 5.21a shows the raw spectra derived via Fast Fourier Transformation (FFT) of the LSW transport time series of both mooring periods. The raw spectra are fairly noisy and show the highest variance in the short term range of less than 50 days. The maximum variance occurred in a period band of 20 to 50 days in both mooring periods. In the second mooring period (2013 - 2014), the variance is significantly higher than in the first one (2012 - 2013), reaching maxima of up to 1.4 Sv^2 as compared to 0.6 Sv^2. Toward time scales longer than 50 days and shorter than 20 days, the variance decreases, with the exception of another maximum of 1 Sv^2 that occurred in the 5 - 10 days range in 2013 - 2014. On time scales longer than 130 days, there is barely any variance. To reduce the noise and uncertainty of the raw spectra, spectral estimates were

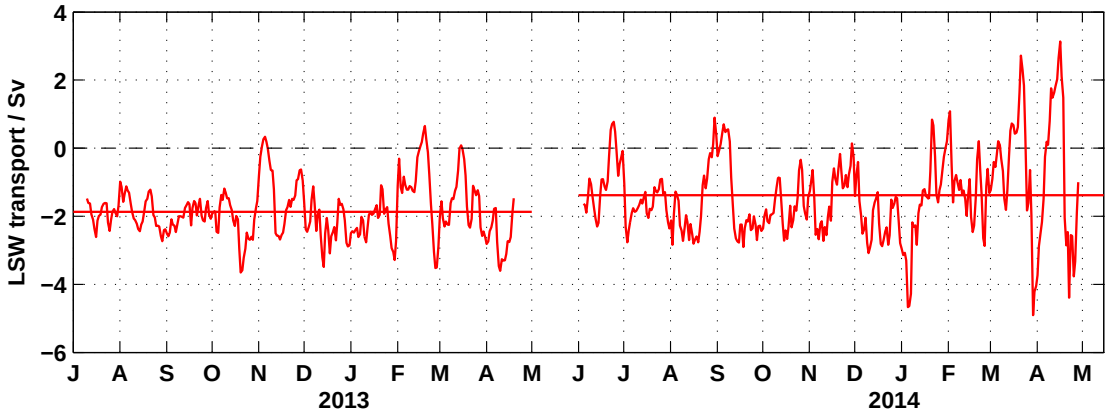

Figure 5.20: LSW layer transports (Sv) through Flemish Pass from mooring record of July 2012 to April 2014, same as in Figure 5.11.

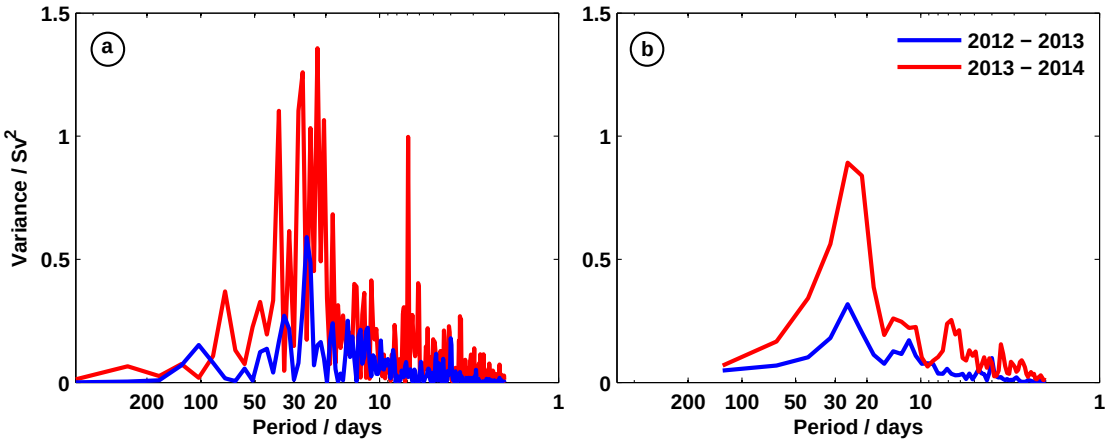

Figure 5.21: LSW transport spectra of the first mooring period in 2012 - 2013 (blue), and of the second mooring period in 2013 - 2014 (red). Variance-preserving (a) raw spectra, and (b) Welch spectra (128 day segments, 64 day overlap).

calculated by Welch's method [*Welch* (1967)]. In the Welch method, a spectral estimate is determined by dividing the time series into segments with 50% overlap, these segments are windowed with a Hamming window, and for each segment a spectral estimate is calculated via FFT. The spectral estimates of the segments are then averaged. Based on the results of the raw spectra, a window length of 128 days and 64 days overlap was chosen with a focus on the shorter time scales. This window length excludes longer term variability. The resulting variance-preserving Welch spectra of LSW transport are more smooth and have reduced variance compared to the raw spectra (Figure 5.21b). Both mooring periods have their variance maxima in the 20 to 50 days range as expected. The spectrum of the 2012 - 2013 time series reaches a maximum variance of 0.3 Sv^2, the spectrum of 2013 - 2014 has a maximum of 0.9 Sv^2. Both spectra decline for time scales longer than 50 days. In the shorter period range, both spectra display another variance plateau of about 0.2 to 0.25 Sv between 10 to 20 days. The variance in 2012 - 2013 decreased toward shorter periods, while the spectrum of 2013 - 2014 exhibits more variance of about 0.25 Sv^2 between 5 and 10 days. The processes that might cause the strong short term variability and even reverse the LSW transports in Flemish Pass are further analyzed in chapter 6. Before, the current chapter is completed by a section about the top to bottom transports through Flemish Pass.

5.7 Top to bottom transports through Flemish Pass during 2013 - 2014

The time series of top to bottom transports through Flemish Pass from July 2013 to April 2014 are shown in Figure 5.22 in comparison to the LSW and upper layer (σ_θ <27.68 kg m^{-3}) transports. Due to the extrapolation of the velocity field (see section 5.2.2), it is to be expected that the upper layer transport is overestimated as the shallow western slope mooring M1842 was positioned to measure the core of the fast flowing Labrador Current, and its data was constantly extended to the central Flemish Pass. In contrast, the LSW layer transport based solely on the data of the western slope mooring BM25/2 is expected to be slightly underestimated on average, as was previously discussed in section 5.5. The transport area of the top to bottom southward flow through Flemish Pass is about 50 km^2, with about 25 km^2 contributed by each the upper layer and the LSW layer.
The top to bottom transport estimates range between −15 Sv of southward transport in January 2014 and total transport reversal of 1 Sv in April 2014, with an average transport of −6.7 Sv. A rough estimate of the top to bottom transport in Flemish Pass of −6.3 to −9.8 Sv was previously calculated by *Petrie and Buckley* (1996) based on a 3 month mooring record of the upper 350 m during October 1985 to January 1986, combined with additional archived current meter data. The magnitude of the average top to bottom transport (−6.7 Sv) based on the longer time series of the Flemish Pass mooring array in 2013 - 2014 agrees well with the lower estimate of −6.3 Sv of *Petrie and Buckley* (1996). However, the more recent observations revealed a larger range (−15 to 1 Sv) of the top to bottom transport in Flemish Pass, which however might be overestimating the transports as it was determined only based on the western slope moorings. *Mertens et al.* (2014) investigated the top to bottom transport of the DWBC east of Flemish Cap at 47°N. They derived an average top to bottom transport of −37.3 Sv based on LADCP measurements between 2003 and 2011 for the slope and rise part (see Figure 3.2b) of the DWBC. Considering a total southward top to bottom transport of −44 Sv (−6.7 Sv and −37.3 Sv) across 47°N in the Flemish Pass and in the DWBC based on the combined estimates, about 14% are through the shallow Flemish Pass.

The top to bottom transport time series is highly correlated with both, the LSW transport time series (R = 0.84) and the upper layer transport time series (R = 0.91). The upper layer transports were stronger than the LSW transports, with

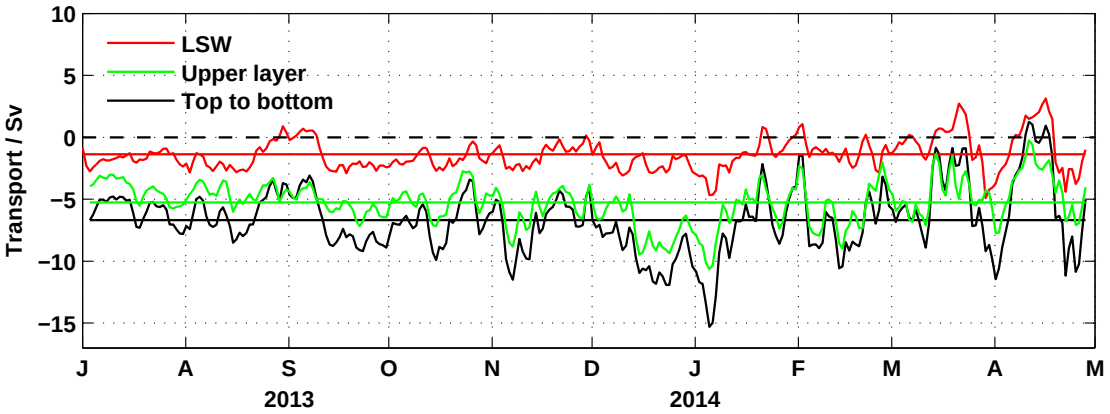

Figure 5.22: Time series of transport [Sv] in the LSW layer (red), upper layer (σ_θ <27.68 kg m^{-3}, green), and from surface to bottom (black) during July 2013 to April 2014.

an average of −5.3 Sv compared to −1.4 Sv (LSW), resulting from the fast flow of the shallow Labrador Current within the upper layer.

The temporal evolution of the LSW transport generally followed the evolution of the upper layer transport, but manifested a short time delay of a few days, which might be caused by drag of the Labrador Current on the deeper water masses. Some noticeable exceptions to this behavior occurred however. For instance, in late August to early September 2013, the LSW transports exhibited an oscillation, with a change in transport from −3 Sv to northward transports of 1 Sv, then followed by increasing transports reaching about −3 Sv again. The same oscillation is observed in the top to bottom transports with a magnitude of about 4 Sv, while the upper layer transports just lightly vary between −5 Sv and −3.5 Sv. During this phase, the top to bottom transport was therefore clearly dominated by processes happening in the LSW layer. Another exception occurred in late March/early April 2014. Then, the upper layer transports were delayed a few days compared to the LSW transports.

5.8 Summary

This chapter addressed research question 2 of this study: "What is the magnitude of transports and its associated variability for LSW passing through Flemish Pass?

What is the amplitude of the seasonal cycle?" based on the data of the Flemish Pass mooring array as well as hydrographic and current velocity ship measurements. Concerning the magnitude of the southward LSW transports, an average of -1.9 ± 0.5 Sv was estimated for the first mooring period in 2012 - 2013 based on two moorings deployed in Flemish Pass. A slightly lower value of -1.4 ± 0.5 Sv was found for the second mooring period in 2013 - 2014, which was based on the data of only one mooring located at the western slope. The range of the calculated LSW transports showed that in extreme events, very high southward transports of almost -5 Sv were reached, as well as complete transport reversals of up to 3 Sv. Seasonal effects on the LSW transports were investigated based on both, the variability of the density field in Flemish Pass, as well as seasonality in the southward flow through Flemish Pass. *Myers and Kulan* (2012) have found that transport estimates of the DWBC at 53°N are quite sensitive to seasonal and interannual variability in the structure of the density field used for the partitioning into density layers. Concerning Flemish Pass, a seasonal difference in the density field between spring, summer and winter was measurable, the effect on the LSW layer transports of less than -0.3 Sv is negligible though in the range of the transport uncertainty (±0.5 Sv).

The seasonal cycle of the flow through Flemish Pass was found to be dependent on the depth and the velocity structure of the flow. The western Flemish Pass has a baroclinic velocity structure with a strong velocity shear induced by the Labrador Current (see section 5.2.1, Figure 5.5). There, the seasonal cycle amplitude was increasing with decreasing water depth, from $\pm1\,\mathrm{cm\,s^{-1}}$ at 900 m depth up to $\pm7\,\mathrm{cm\,s^{-1}}$ at 370 m and almost $\pm10\,\mathrm{cm\,s^{-1}}$ near the surface in the shallow Labrador Current. In the central Flemish Pass, the seasonal cycle of the flow was not depth dependent due to the barotropic velocity structure and had a small amplitude of about $\pm2\,\mathrm{cm\,s^{-1}}$ between 540 and 1080 m. Between the seasonal cycles of the flow in the western and central Flemish Pass, there was a phase shift of about 6 month. These results agree with observations of *Fischer et al.* (2004) and *Fischer et al.* (2015), who found a pronounced seasonal cycle in the DWBC at 53°N that was confined in the shallow Labrador Current, while they detected a very weak seasonal cycle also in the deep flow of the DWBC. The LSW transports through Flemish Pass were derived based on two moorings in the first mooring period 2012 - 2013, one located in the center, and one located at the western slope. Due to a phase shift in the seasonal cycles from the western and central

Flemish Pass, the net effect on the transport was very small (± 0.1 Sv). In the second mooring period 2013 - 2014, the transports were derived based on only the western slope mooring and therefore the seasonal cycle of the LSW transport time series was more pronounced (± 0.5 Sv).
The investigation of LSW transports in Flemish Pass was complemented through an estimate of a top to bottom transport time series during 2013 - 2014, which was possible due to additional current velocity data of the upper layer (σ_θ $<27.68\,\mathrm{kg\,m^{-3}}$) from a shallow Canadian mooring deployed on the western slope of Flemish Pass. The average top to bottom transport of 2013 - 2014 was -6.7 Sv. This result agrees with a historical estimate of *Petrie and Buckley* (1996), who calculated a top to bottom transport in Flemish Pass of -6.3 to -9.8 Sv.
A spectral analysis of the variability of the LSW transport in 2012 - 2013 and 2013 - 2014 revealed high intra-seasonal variability in Flemish Pass with the strongest signal in the 20 - 50 day period range. On time scales longer than 100 days, barely any variance was observed. In the next chapter, the variability of the flow through Flemish Pass will be analyzed in detail on a spatial and temporal scale, and local processes that might drive the variability will be investigated.

6 Local processes and their influence on the LSW variability

This chapter addresses the research question 3 of this study: "Which processes drive the variability of the LSW flow through Flemish Pass?". As discussed in section 5.6, the southward LSW transport through Flemish Pass is impacted by strong reductions in transport, which occasionally even turn into complete reversals of the net transport. Here, these peculiar events are further analyzed on a spatial and temporal scale. The spatial analysis was performed to reveal if the flow reversals extend throughout the whole LSW layer or if there were localized patches of strong northward transport which reverse the net LSW transport (see section 6.2.1). Concerning the temporal scale, a spectral analysis was carried out to identify the characteristic time scales of the LSW flow variability (see section 6.2.2) at each mooring. Furthermore, two processes were investigated, which are likely to induce the observed transport reversals in the LSW layer:

1. **An increase and widening of the recirculation around Flemish Cap.** A widening of the recirculation around Flemish Cap could suppress the southward flow part by extending further into Flemish Pass. This process is examined in section 6.1.

2. **Topographic Rossby waves (TRWs).** TRWs are large scale transverse waves with wavelengths up to hundreds of kilometers, which are observed particularly over the continental slope [*Gill* (1982)]. A characteristic feature of TRWs is decreasing energy with increasing height off the bottom because of the increased stratification [*Pickart and Watts* (1990)]. Several studies [e.g. *Johns and Watts* (1986), *Pickart and Watts* (1990), *Mertens et al.* (2014), *Fischer et al.* (2015)] document the impact of TRWs on the variability of the DWBC up- and downstream of Flemish Pass. *Pickart and Watts* (1990) for instance observed periodic flow reversals at Cape Hatteras and

linked these to TRWs with a 40 day period. TRWs as a driving factor for the Flemish Pass current reversals are investigated in section 6.2.

6.1 Does the recirculation around Flemish Cap induce LSW transport reversals?

The northward recirculation in the eastern Flemish Pass is variable in its strength and spatial extent, as was discussed in chapter 3.2.2. Therefore, a possible mechanism to induce the observed transport reversals in Flemish Pass (chapter 5.6) is an increase and widening of the recirculation into the central Flemish Pass, thereby suppressing the southward flow part. However, most of the observed reversal events occurred between November and May, a season in which, according to literature [e.g. *Kudlo et al.* (1984), *Colbourne and Foote* (2000)], the anticyclonic gyre circulation around Flemish Cap is more likely to break down due to heavy wind forcing from storms. Nevertheless, the available MicroCAT data from the first mooring period in 2012 - 2013 (the MicroCAT from the second mooring period was lost unfortunately) was analyzed to identify any increase in temperature and salinity coinciding with the current reversals, which would be expected if the warmer and saltier recirculation extended further into the Flemish Pass. Figure 6.1 shows time series of temperature and salinity anomalies (relative to the mean of the time series) from the MicroCAT of mooring BM25/1 at the western slope of Flemish Pass at 977 dbar and of mooring BM26/1 in the central Flemish Pass at 1095 dbar, in comparison to the velocity time series of the ADCP bin of each mooring, which was closest to the respective MicroCAT.

At the western slope (BM25/1), the anomalies range between -0.13 to $0.35\,°C$ for temperature and -0.02 to 0.02 for salinity. Minimum temperatures and salinities occur in September and October, and maximum temperatures and in January. Salinities are at maximum in January and July (Figure 6.1a, b). Some smaller temperature and salinity maxima can be furthermore found in December and February. The velocity time series from the western slope in comparison shows northward flow in November, February and March, reaching velocities of 5 to $13\,cm\,s^{-1}$ (Figure 6.1c). Only in February, the northward flow coincides with elevated temperatures and salinities. Much less northward flow events occurred in the center of Flemish Pass (BM26/1), only two short events are displayed in

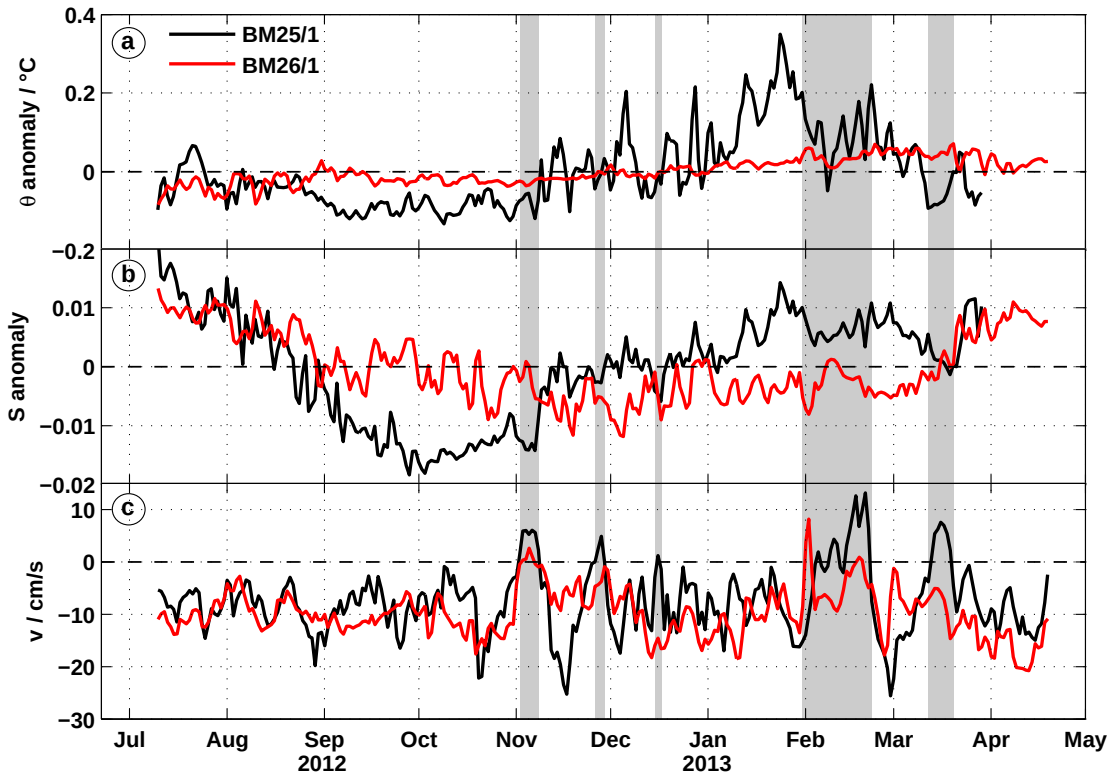

Figure 6.1: Time series (40 h low pass filtered, daily averages) from mooring BM25/1 in the western Flemish Pass (black) and mooring BM26/1 in the central Flemish Pass during July 2012 to April 2013. (a) Potential temperature (θ / °C) anomalies (respective to the mean of the time series), (b) salinity anomalies from MicroCAT data, and (c) meridional velocities (cm/s) from the ADCP bin closest to the MicroCAT of the respective mooring. Events of northward flow are shaded in gray.

November and early February with velocities of 3 and 8 cm s^{-1}, respectively. These two events of current reversal show no connection to the temperature and salinity anomalies. The bottom water of the central Flemish Pass has a lower range of temperature anomalies (−0.08 to 0.07 °C) compared to the western slope, and the anomalies are mostly negative until December and mostly positive afterward. The salinity anomalies are slightly lower as well, ranging between −0.01 to 0.01 with the highest values in July and April, and the smallest values in November and December.

To define criteria of temperature and salinity that would indicate a westward extension of the recirculation as measured by the MicroCATs, temperature and salinity gradients between the western and the central Flemish Pass in near bottom level (>870 m depth) were investigated from the ship based hydrographic

measurements conducted in Flemish Pass between 2009 and 2014 (table 2.3). Older cruises were not included for this analysis because of the longterm change observed in the hydrographic properties in Flemish Pass (chapter 4). For a few cruises (TL39890, MSM12/3, and HU20112, see table 2.3), high gradients of up to to 0.2 °C and 0.02 were found for temperature and salinity, respectively. In case of cruise MSM12/3, the available LADCP data revealed a pronounced recirculation with strong northward flow (see Figure 3.3b). For cruise TL39890 and HU20112, no velocity data was available. In most other sections, the temperature and salinity gradients were less pronounced and the northward flow of the recirculation was weaker (see Figure 3.3c - f). The average temperature and salinity gradients of all sections measured in 2009 - 2014 were 0.04 °C and 0.004, respectively. In mid February 2013 (Figure 6.1), temperature anomalies of 0.2 °C and above average salinity anomalies of 0.01 at the western Flemish Pass MicroCAT (BM25/1) fulfill the gradient criteria of the recirculation. However, there is no sign of recirculation at the same time in the central Flemish Pass (BM26/1), neither in the flow, nor in temperature and salinity. For this reason, there is no evidence that a westward extension of the recirculation drives the current reversal in February 2013 in the western Flemish Pass. In the following, another possible driving mechanism is investigated.

6.2 LSW flow variability in Flemish Pass and topographic Rossby waves

6.2.1 Spatial scale of the LSW flow reversals

To find out, if the flow reversals extend throughout the whole Flemish Pass LSW layer or if they are localized, current velocity vector time series of the different depth bins of the ADCP mooring data were examined. In Figure 6.2, three different depth levels are exemplary shown, the bottom level, an intermediate level and the shallowest level of each ADCP in BM25/1, BM25/2 and BM26/1. In the first mooring period in 2012 - 2013, the current reversals at BM25/1 in the western Flemish Pass are clearly visible in the deepest level (914 m depth, Figure 6.2c) in November 2012, and February and March 2013. A comparison with the other two

depth levels (Figure 6.2a, b) reveals that the strength of the current reversals is decreasing with decreasing depth. In the intermediate depth (658 m, Figure 6.2b), only two of the three events of current reversals observed during the first mooring period occurred, one in February 2013, which is clearly less intense than at the deeper level, and one in March 2013. At the shallowest level (370 m, Figure 6.2a), very diminished northward flow events are visible in March and April 2013. During

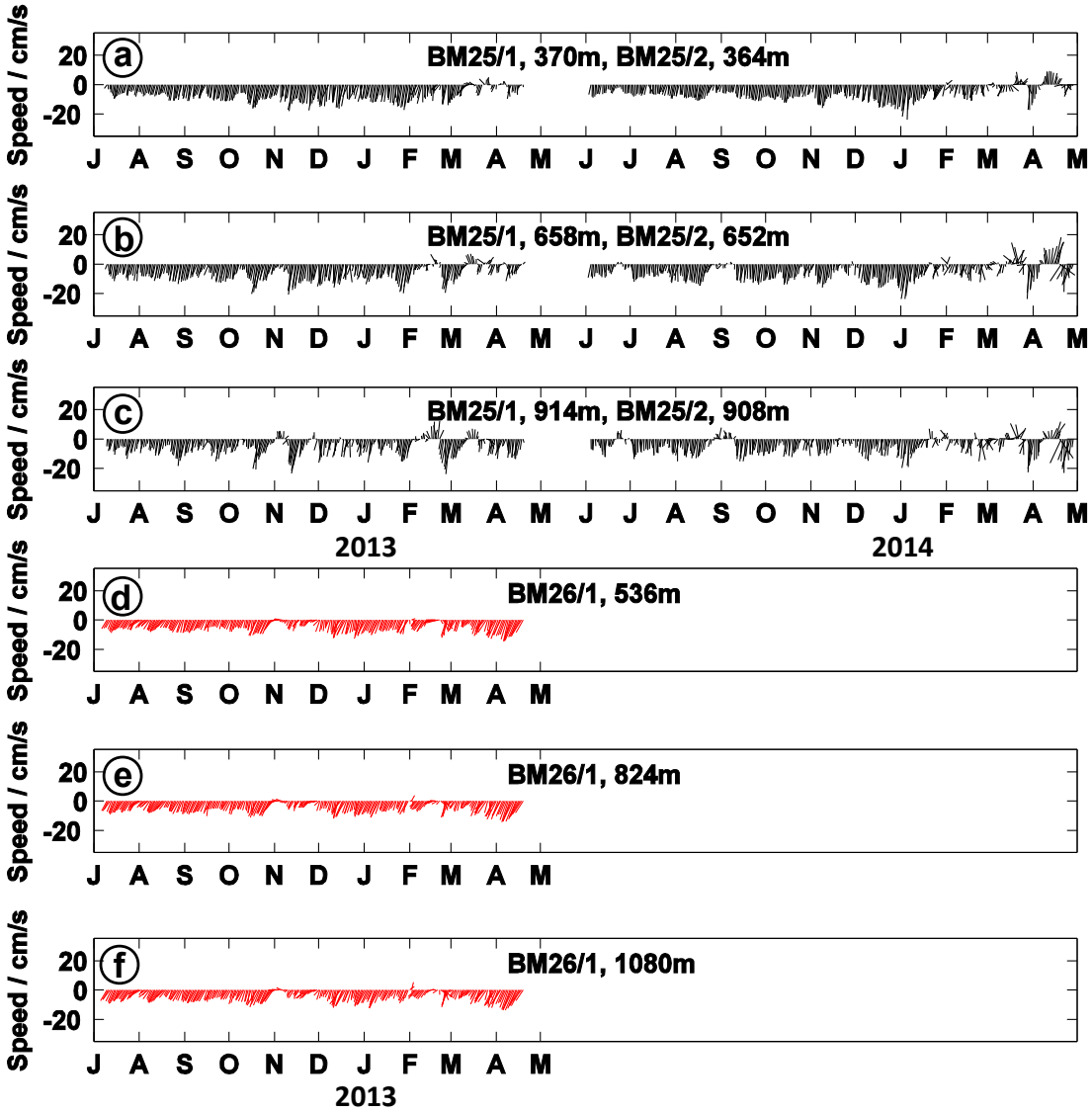

Figure 6.2: Time series of current vectors (40 h low pass filtered, daily averages) in three different depth levels: a) Bottom level, b) intermediate level, and c) shallowest level in the range of the ADCP at BM25/1 in the western Flemish Pass. d), e), and f) the same, but for BM26/1 in the central Flemish Pass.

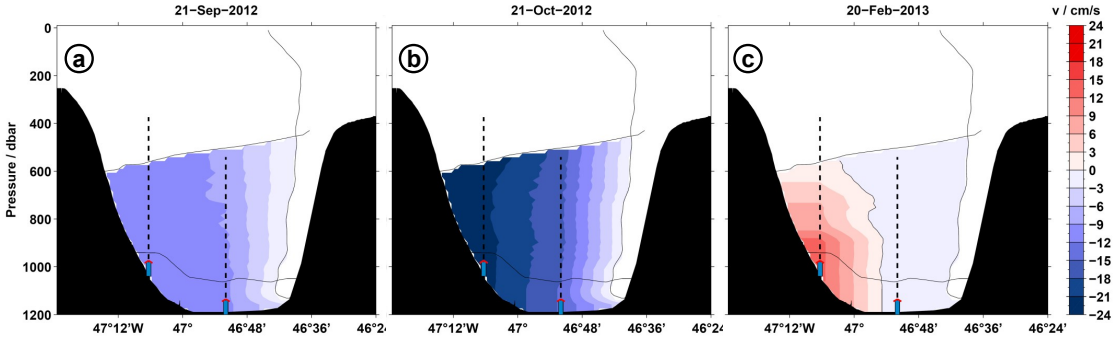

Figure 6.3: Velocity distribution of LSW in Flemish Pass from the ADCPs of moorings BM25/1 and BM26/1 for three events in the first mooring period 2012 - 2013 (see Figure 5.20): a) representing average LSW transport (−1.9 Sv), b) maximum transport (−3.6 Sv), and c) transport reversal (0.7 Sv).

the second mooring period in 2013 - 2014, the same phenomenon of bottom intensified current reversals occurred. In the deepest level (908 m depth, Figure 6.2c), northward flow events occurred in June and September 2013, and between January and April 2014. With the exception of the current reversals in March and April 2014, which are strongest in the intermediate depth (652 m depth, Figure 6.2b), all other northward flow events strongly decreased toward shallower depths. In the time series from BM26/1 in the central Flemish Pass (536 m, 824 m, and 1080 m, Figure 6.2d, e, f), only two events of current reversal can be observed in November 2012 and February 2013, which are less intense than at the western slope, but a decrease in strength from the bottom to the shallowest level is also obvious.

The spatial velocity distribution in the Flemish Pass LSW layer during an event of transport reversal from the first mooring period 2012 - 2013 is exemplary shown in Figure 6.3c, in conjunction with the velocity distributions for an event representing a) average transport (−1.9 Sv, see Figure 5.20), and b) maximum transport. Interestingly, the velocity distributions in all three events are intensified toward the western slope with higher southward velocities in the case of the average and maximum transport event (Figure 6.3a, b) compared to the center, and northward velocities in the case of the transport reversal (Figure 6.3c). The transport reversal appears to originate from the bottom of the western slope at about 47°08'W, where the northward velocities are strongest, exceeding 12 cm s^{-1}. The role of the western slope and the variability inducing processes, which cause the current reversals, will be analyzed in the following sections.

6.2.2 Temporal scale of the flow variability in Flemish Pass

In order to identify the characteristic time scales of the LSW flow variability, a spectral analysis of the velocity data recorded by the Flemish Pass ADCP moorings BM25/1, BM26/1, and BM25/2 was carried out. Furthermore, the data of the shallow mooring M1842 was analyzed and compared to the results of the deep moorings, to evaluate if the variability of the upper layer has an impact on the deep flow. Spectral estimates were calculated by Welch's method [*Welch* (1967)]. A Hamming window length of 128 days and 64 days overlap was chosen following *Fischer et al.* (2015). The velocity time series were zero padded to the next higher

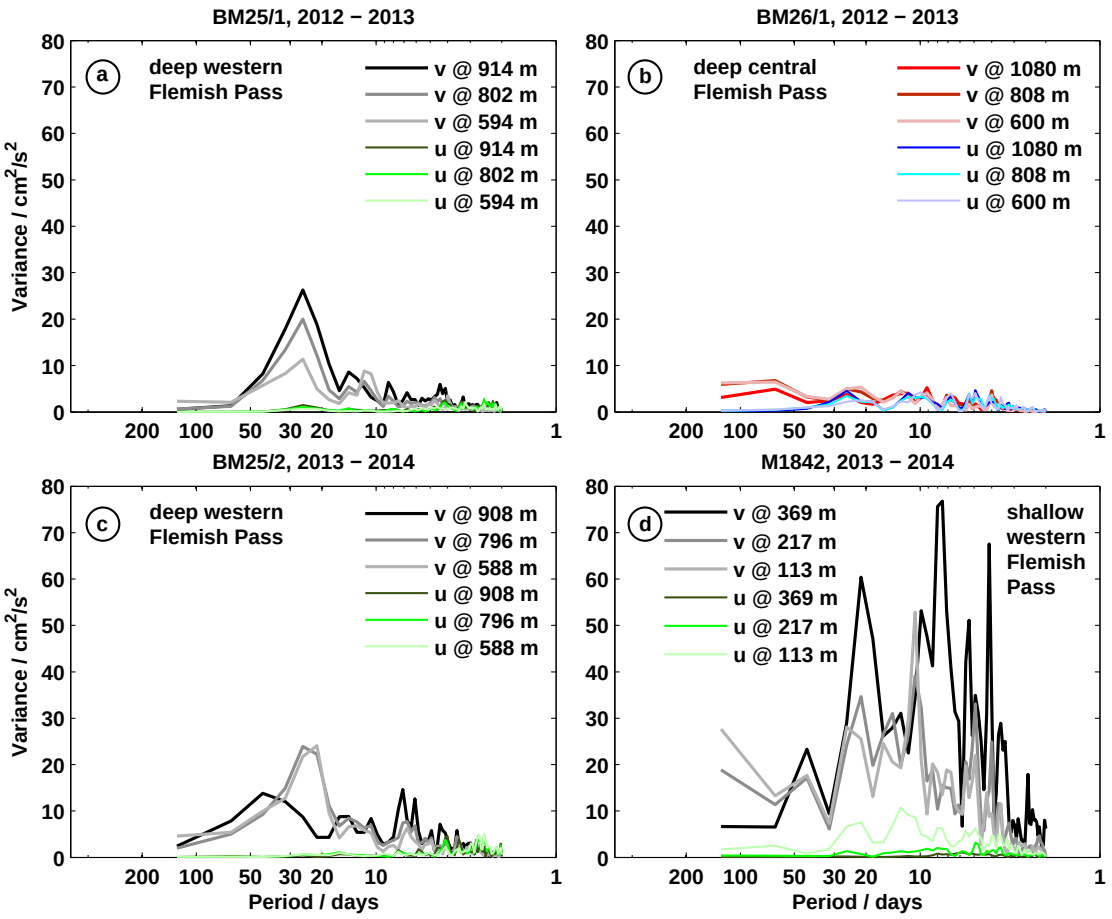

Figure 6.4: Variance-preserving Welch spectra (128 day segments, 64 day overlap) of meridional (v) and zonal (u) velocity recorded at three different depth levels by the moored ADCPs located at the western slope (indicated by gray and green colors) of Flemish Pass (a) BM25/1, c) BM25/2 and d) M1842) and in the center (b) BM26/1 (red and blue colors).

order of magnitude of 2 to ensure that all measurements were included to derive the spectra. The resulting variance-preserving Welch spectra of the meridional and zonal velocity are shown in Figure 6.4, exemplary at three different depth levels, the deepest bin of each instrument, an intermediate bin, and the shallowest bin. At the western slope (Figure 6.4a, c, and d), the zonal velocity component has much less variance than the meridional component in the deep water as well as in the upper water column, as a result of the topographic boundary. In 2012 - 2013, a characteristic feature of the variability at the western slope (BM25/1, Figure 6.4a) is that the highest variance was detected at the bin closest to the bottom, and the variance is decreasing with decreasing depth. The increase in energy with depth is a characteristic sign of bottom trapped TRWs [e.g. *Pickart and Watts* (1990)]. The strongest signal is in the 20 - 50 day period band with a maximum variance of about $26\,\mathrm{cm^2\,s^{-2}}$ at 26 days at the deepest bin and about $11\,\mathrm{cm^2\,s^{-2}}$ at the shallowest bin. There was barely any variance for periods longer than 50 days. A smaller, also bottom intensified maximum occurred in the 10 - 20 days range, peaking at 14 days in the deepest level at $8\,\mathrm{cm^2\,s^{-2}}$ and decreasing to $4\,\mathrm{cm^2\,s^{-2}}$ in the shallowest level. In the high frequency range (periods lower than 10 days), there are two small peaks with a variance of less than $6\,\mathrm{cm^2\,s^{-2}}$ at 8 and 4 day periods.

In the central Flemish Pass (BM26/1, Figure 6.4b), variances are much smaller (less than $7\,\mathrm{cm^2\,s^{-2}}$), not bottom intensified, and the variance of the zonal velocity component is comparable in magnitude with the meridional component for periods of less than 30 days. In comparison to the western slope (Figure 6.4a), the zonal velocity component has more variance in the central Flemish Pass, which probably results from the lack of a topographic boundary. The highest variance of $7\,\mathrm{cm^2\,s^{-2}}$ occurred between 50 - 100 days, slightly smaller variances are displayed between 20 - 30 days, 10 - 20 days, and on time scales of less than 10 days.

In 2013 - 2014, mooring data was only recorded on the western slope. In the range of BM25/2 (Figure 6.4c), the highest variance occurred again in the 20 - 50 days period range. The maximum variance of about $24\,\mathrm{cm^2\,s^{-2}}$ in both the intermediate and shallow depths levels is displayed at 26 days. At the deepest level, the maximum of $14\,\mathrm{cm^2\,s^{-2}}$ was shifted to a 42 days period. Therefore, in contrast to the previous year, the signal is not bottom intensified. Smaller, bottom intensified variances of less than $8\,\mathrm{cm^2\,s^{-2}}$ occurred in the 10 - 20 days comparable to the previous year. A higher, bottom intensified peak of up to $15\,\mathrm{cm^2\,s^{-2}}$ is exhibited

in the high frequency range 5 - 10 days. For periods longer than 50 days, the variance decreased toward zero.
Concerning the shallow western slope mooring M1842 (Figure 6.4d), the characteristic time scales in the spectra differ from the deep water flow especially for periods of less than 12 days, indicating that in the shallow water range other processes are occurring. Generally, the variances are much higher than at BM25/2. For periods of less than 50 days, the highest variance occurred at the deepest level (369 m), therefore the signal is bottom intensified indicating the presence of bottom trapped TRWs. The maximum variance of 77 $cm^2\,s^{-2}$ is displayed in the 5 - 10 days period range. Further high variance peaks of 50 to 70 $cm^2\,s^{-2}$ were reached at periods lower than 5 days and in the 15 - 30 days range. *Layton* (2016) also investigated the data of M1842 in comparison with mooring data of the northern entrance of Flemish Pass at about 48°N, and attributed the variability on a three weeks time scale to baroclinic TRWs at M1842.
Altogether, the spectral analysis of the velocities showed that the strongest signals are found in the western Flemish Pass. There, bottom intensification of variance occurred. The bottom intensification points to the existence of bottom trapped TRWs in Flemish Pass. To find evidence for this process, the next section compares the signals observed in the Flemish Pass velocity data to expected results from TRW theory. The characteristic time scales of variability as revealed by the spectra are period bands of 20 - 50 days, 10 - 20 days, and 5 - 10 days, in which the occurrence of TRWs in the deep Flemish Pass is anticipated.

6.2.3 The topographic wave signal

A characteristic feature of TRWs is the turning of the principle axis ellipse to a more cross-isobath orientation at higher frequencies, which was observed e.g. by *Thompson and Luyten* (1976). *Pickart and Watts* (1990) explain this behavior with the following mechanism: As a fluid column crosses sloping topography, it is either stretched or squished. This induces a change in potential vorticity, which causes a restoring force that creates the transverse motions of a TRW.

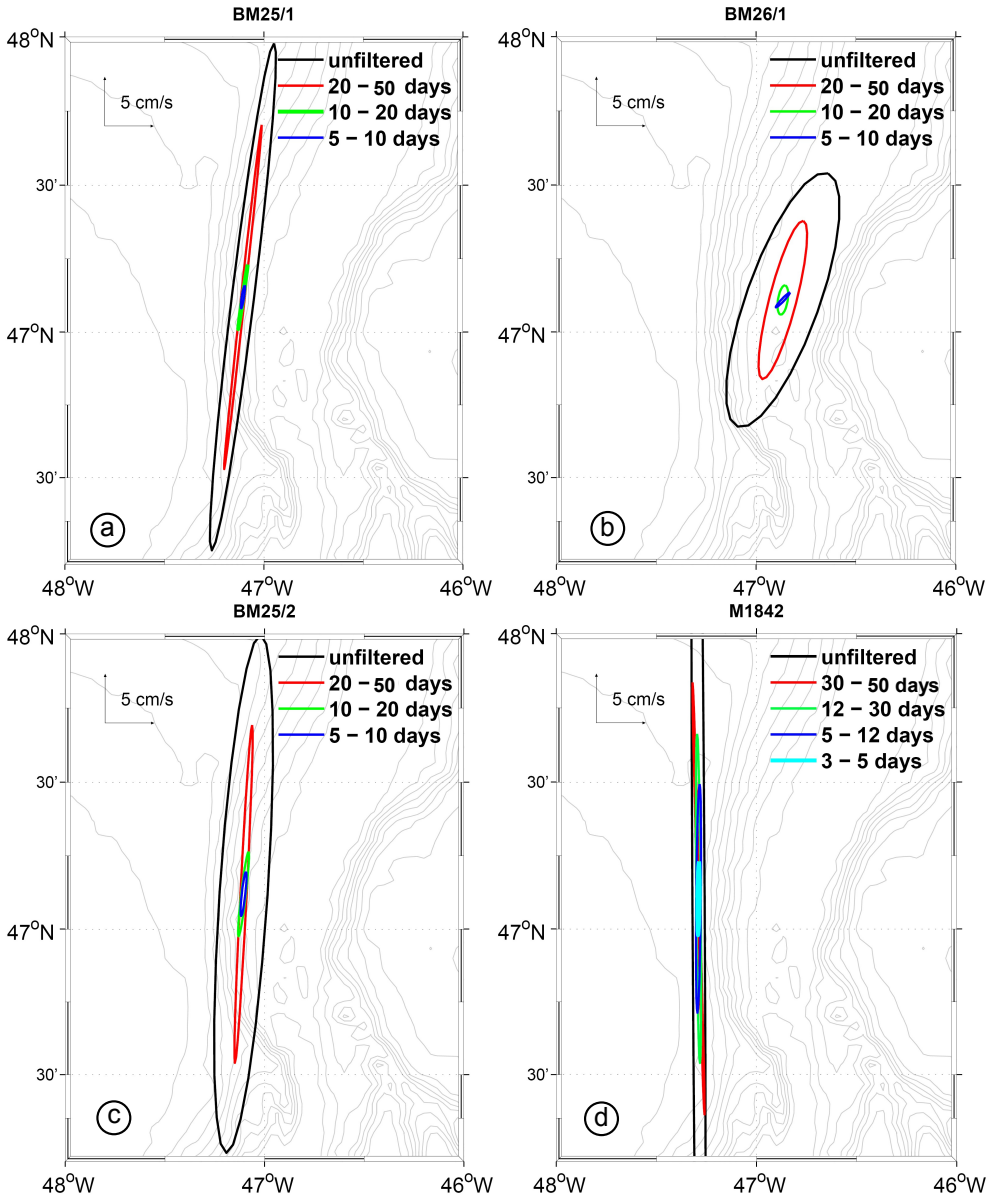

Figure 6.5: Variance ellipses in different period bands from the deepest level of the western slope moorings, a) BM25/1, 2012 - 2013, c) BM25/2, 2013 - 2014, d) M1842, 2013 - 2014, and of the central Flemish Pass, b) BM26/1, 2012 - 2013. Note that the period bands of M1842 differ from those of the deep moorings. The topography is indicated by light gray lines in 100 m depth levels.

In the low frequency range, the restoring force is weak, and the transverse wave motions are nearly along-slope, but the strong restoring force at higher frequencies induces a cross-slope orientation of the wave motions. This observational signature is made use of in the following to verify if the signals found in the spectral analysis

are due to TRWs.
Guided by the spectral analysis (section 6.2.2), variance ellipses were calculated from the bandpass filtered mooring velocity data for the period bands 20 - 50 days, 10 - 20 days, and 5 - 10 days (Figure 6.5). The variance ellipses from the deepest level of the BM25 mooring have very similar shapes for both mooring periods (BM25/1, Figure 6.5a, and BM25/2, Figure 6.5c). As expected from the spectral analysis, the highest variances occurred in the 20 - 50 day period band, the second strongest signal was in the 10 - 20 day period band, and the smallest signal is exhibited in the 5 - 10 day period. Characteristic for the ellipses of all three period bands is that they are of almost linear shape: almost all of the variance is along the major axes of the ellipses, which are in along-slope direction, and barely any variance is in cross-slope direction. This indicates the presence of TRWs [e.g. *Pickart and Watts* (1990), *Kanzow and Zenk* (2014)]. The variance ellipses of the central Flemish Pass (BM26/1, Figure 6.5b) are more circular than at the western slope for the longer period bands 20 - 50 days and 10 - 20 days, which hints to a trapping of the waves at the topography.
As TRWs are transverse waves, the fluid velocity is perpendicular to the wave vector, which means that the wave vector lies perpendicular to the ellipse orientation [*Pickart and Watts* (1990)]. This implies the phase speed orientation angles (relative to downslope) given in Table 6.1. The results shown are exemplary from the deepest level of each mooring as the TRW signal is bottom intensified. Table 6.1 compares the observational results with expected estimates of TRW theory, which were determined using the dispersion relation for TRWs in a stratified ocean as applied by *Pickart and Watts* (1990):

$$\varphi = sin^{-1}\left(\frac{2\pi tanh\left(2\pi ND/\lambda f_0\right)}{N\gamma T}\right) \tag{6.1}$$

where φ is the orientation angle of phase velocity relative to downslope, N is the Brunt-Väisälä frequency, D is the characteristic water depth, λ is the wave length, f_0 is the Coriolis parameter, γ is the bottom slope, and T is the wave period.
These parameters were determined specifically for the Flemish Pass as follows:
A Brunt-Väisälä frequency profile $N = \sqrt{\frac{-g}{\rho}\frac{\partial\rho(z)}{\partial z}}$ was computed from the CTD profiles conducted closest to the mooring position BM25 during the mooring period 2012 - 2014, and compared with an estimate from the World Ocean Atlas 2013 (WOA 2013) annual climatology data, which provides global ocean temperature

Table 6.1: Phase speed orientation angles (relative to downslope) inferred from the variance ellipse analysis of the Flemish Pass ADCP mooring data for specific period bands. Shown are the results for the deepest level of each instrument and the expected theoretical values computed with equation 6.1.

	Phase speed angle (°)			
Instrument	BM25/1	BM25/2	BM26/1	Theory
Period (days)				
20 - 50	6.2	2.9	14.5	1.6 - 4
10 - 20	9.6	6.7	9.0	4 - 8
5 - 10	8.8	6.3	43.7	8 - 20

and salinity data on a 0.25° grid (see Figure 6.6). The WOA 2013 grid point was located about 1.5 km east of the mooring position. Therefore, Brunt-Väisälä frequency profile based on the WOA 2013 data reaches a bit deeper than the CTD based profile, however both profiles agree rather well. The Brunt-Väisälä frequency N in the deep water of the western Flemish Pass is estimated from the profiles at about $0.003\,\mathrm{s}^{-1}$.

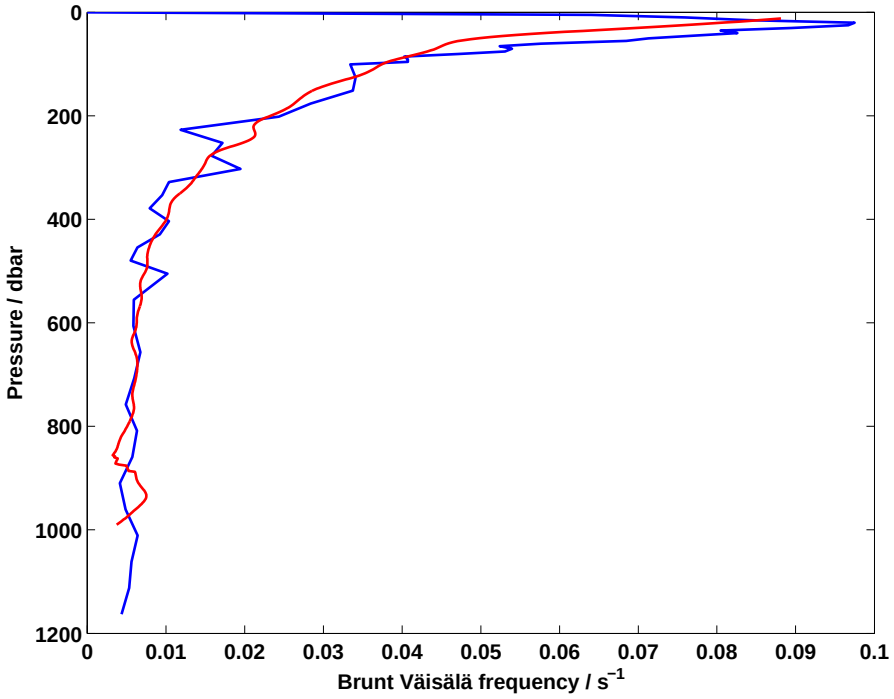

Figure 6.6: Brunt-Väisälä frequency profiles inferred from CTD measurements at the western slope of Flemish Pass during 2012 - 2014 (red), and based on the WOA 2013 data from the grid point closest to the location of the mooring position BM25 (blue).

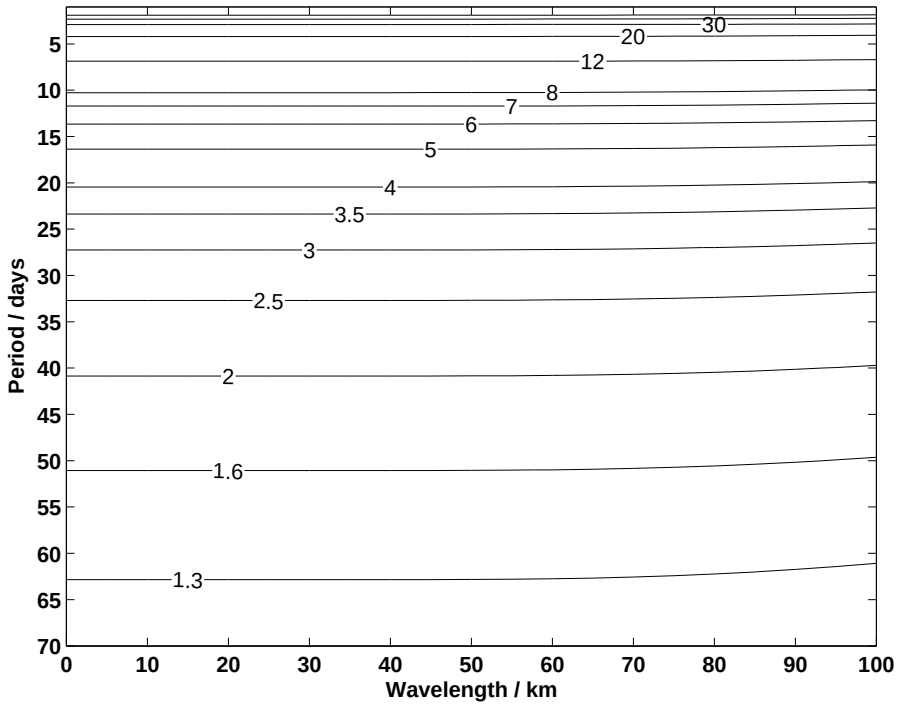

Figure 6.7: Phase speed orientation angles relative to downslope (represented by the contour lines) computed with the dispersion relation of TRWs as applied by *Pickart and Watts* (1990).

The bottom slope γ in the western Flemish Pass was inferred from water depth data, that was typically recorded during the research cruises by the vessel's multi-beam echosounding system. The characteristic water depth D in Flemish Pass is 1200 m. The Coriolis parameter $f_0 = 2\Omega sin(\alpha)$, with the rotation rate of the earth $\Omega = 7.2921 \times 10^{-5} s^{-1}$ and the latitude $\alpha = 47°$N, was calculated to be $1.064 \times 10^{-4} s^{-1}$.

The phase speed orientation angles computed from the TRW dispersion relation (equation 6.1) based on the specific parameters for Flemish Pass are shown in Figure 6.7. The expected theoretical phase speed angle for a wave in the 20 - 50 day period band is 1.6 - 4°. The angle inferred from the variance ellipse analysis of the western slope instrument BM25/2 falls exactly in this range with 2.9°, while it is slightly higher (6.2°) for the data from the first mooring period (BM25/1). The variance ellipse angle from the central mooring (BM26/1) exceeds the theoretical value by more than 10°.

Concerning a wave in the 10 - 20 day period band, the phase speed orientation angles expected from theory are 4 - 8°. The observational estimate of the angle from BM25/2 again falls exactly in this range (6.7°), while the estimates from

both BM25/1 and BM26/1 are slightly higher (9.6° and 9.0°, respectively). The variance ellipse analysis provides a strong indication that the variability observed in the two lower frequency bands 20 - 50 days and 10 - 20 days at mooring BM25/2 is due to bottom trapped TRWs. *Mertens et al.* (2014) observed a 20 - 50 day periodicity from mooring data of the DWBC east of Flemish Cap and related that to baroclinic Rossby waves with a length scale of 25 - 65 km, assuming a typical wave speed c of $1.5\,\mathrm{cm\,s^{-1}}$ [e.g. *Chelton et al.* (2007)]. For the Flemish Pass, this wave speed would translate to a wavelength $\lambda = c/f$ (f: wave frequency) of 26 - 65 km for the 20 - 50 day period band and 13 - 26 km for the 10 - 20 day period band. At about 900 m depth (deepest level of the BM25 ADCP), the Flemish Pass has an approximate width of 36 km, that means only waves with wave lengths smaller than 36 km can be expected in the Flemish Pass. The variance ellipse analysis supports the hypothesis, that the variability in the period bands of 20 - 50 days and 10 - 20 days are induced by TRWs with wave lengths of up to 36 km. The observational phase speed angles of the BM25/1 data are slightly higher than the theoretically expected range for the two lower frequency period bands. However, the almost linear shape of the ellipses (Figure 6.5a) and the strong bottom intensification exhibited in the spectra (Figure 6.4a) still point to the presence of bottom trapped TRWs. The vertical trapping scale H of such a TRW according to theory [e.g. *Gill* (1982)] is $H \approx \frac{f_0 \lambda}{2\pi N} \approx 200\,\mathrm{m}$.

In the higher frequency period band 5 - 10 days, the observational phase speed angle at BM25/1 is within the expected theoretical range (8 - 20°), while at BM25/2, the angle is lower (6.3°), i.e. more along-slope, and at BM26/1, it is higher (43.7°) than the theoretical range. According to *Pickart and Watts* (1990), the observed rotation of the ellipse angles with frequency often does not conform to that predicted by theory, and is in fact the exception rather than the rule.

Another approach to reveal if the higher frequency variability is caused by TRWs was explained by *Thompson and Luyten* (1976). The idea is, that the cross-isobath orientation of the waves at higher frequencies induces up-slope velocity (i.e. in this case a negative zonal velocity component u) near the sloping bottom, which brings denser and therefore colder water up. Equivalently, down-slope flow (positive u) will be followed by higher temperatures θ near the bottom. As a consequence, u and θ should be coherent and in quadrature (i.e. separated in phase by 90°), with u leading. Figure 6.8 shows spectra of magnitude squared coherence and phase between the zonal velocity component (at the deepest level)

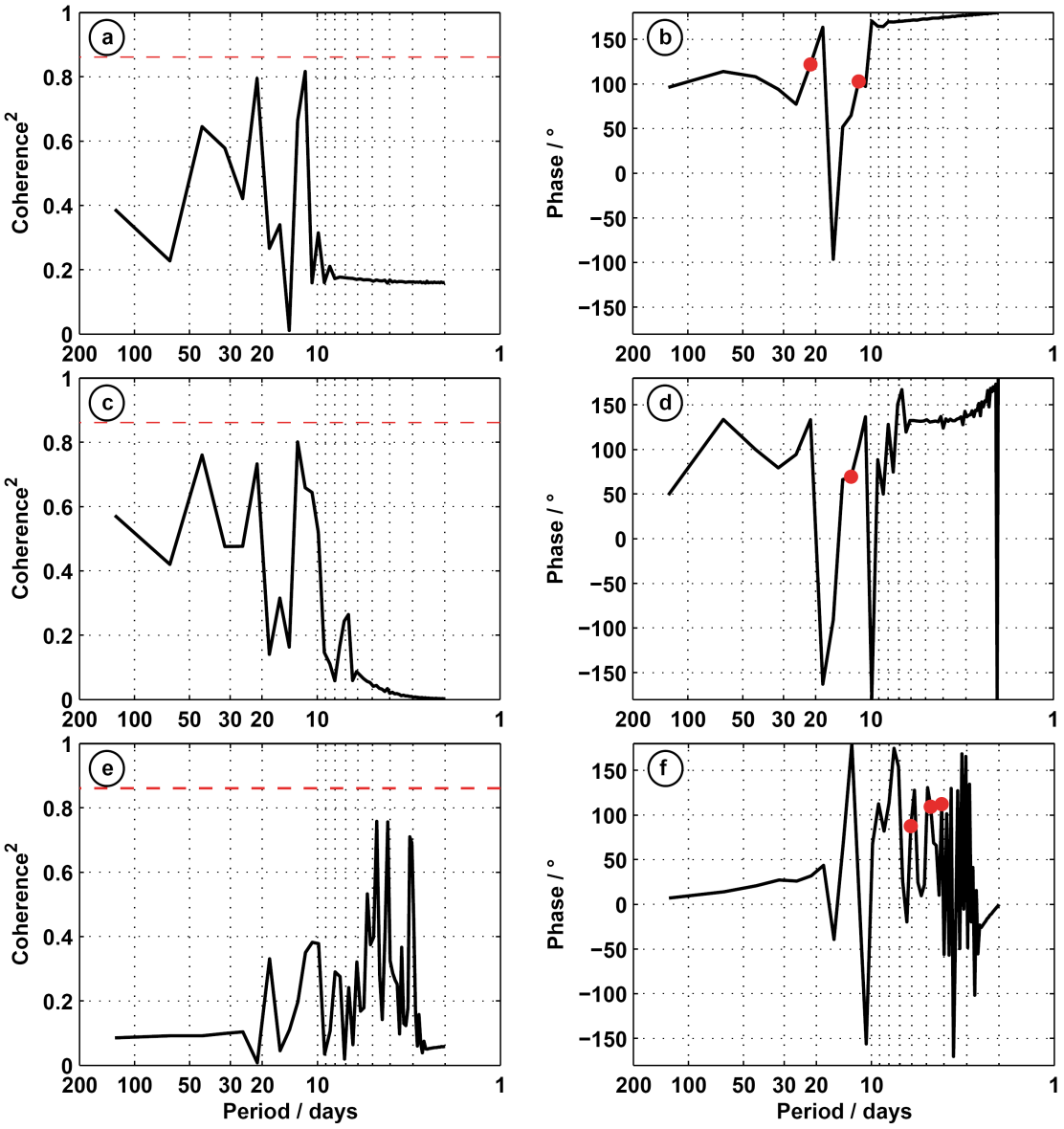

Figure 6.8: Magnitude squared coherence (left column) and phase (right column) between up-slope velocity and temperature for the different period bands: (a, b) 20 - 50 days, (c, d) 10 - 20 days, (e, f) 5 - 10 days. The 95% confidence level is indicated by a red dashed line, the phases of the periods with the highest coherence are marked with red dots.

and temperature at BM25/1 for the period bands 20 - 50 days (Figure 6.8a and b), 10 - 20 days (Figure 6.8c and d), and 5 - 10 days (Figure 6.8e and f). For all three period bands, there is no significant coherence between the up-slope velocity u and temperature θ, no peak in the coherence spectra (Figure 6.8a) exceeds the

95% significance level. In the 20 - 50 days period bands, the phases of the highest coherence peaks are exceeding 100° (Figure 6.8b), while in the 10 - 20 days band, the phase of the highest peak is at 75°. In the 5 - 10 days band, the highest coherence of just under 0.8 occurs at periods of 4 - 5 days. At these periods, u leads θ, and for the 5 day period, the phase difference is fairly close to 90° (87°), while at 4 days, there is a phase difference of 110°. Due to the lack of significance, it is not conclusive that the variability in the high frequency period range (5 - 10 days) at the western slope of Flemish Pass is induced by TRWs or by another process. Further downstream at Cape Hatteras, *Pickart and Watts* (1990) found that the higher frequency fluctuations, which also were oriented more along-slope than expected, were due to variability of the DWBC.
In summary, the lower frequency variability of the LSW flow at the western slope of Flemish Pass is most likely caused by TRWs with periods of 20 - 50 and 10 to 20 days and wavelengths smaller than 36 km. The spectral and variance ellipse analysis for the central Flemish Pass does not indicate an influence of TRWs there. This implies that the TRWs are trapped at the slope of Flemish Pass. A TRW with a wave length of 36 km has a horizontal length scale $L = \lambda/2\pi = 5.7$ km [e.g. *Louis et al.* (1982), *Rhines* (1970)]. The TRW signal measured at mooring BM25/1 therefore does not extend to the location of BM26/1, as they are separated by 18 km. As the central Flemish Pass has a flat bottom, the occurrence of TRWs at the position of BM26/1 is furthermore theoretically not expected as the dispersion relation 6.1 is only defined for a sloping bottom.

A variance ellipse analysis was also performed for the shallow western slope mooring M1842, but different period bands (30 - 70, 12 - 30, 5 - 12, and 3 - 5 days) were examined following the spectral analysis. Even though the variance ellipses are of linear shape pointing in along-slope direction for all period bands,

Table 6.2: Phase speed orientation angles (relative to downslope) inferred from the variance ellipse analysis of the Canadian ADCP mooring M1842 data for specific period bands. Shown are the results for the deepest level and the expected theoretical values computed with equation 6.1.

	Phase speed angle (°)	
Period (days)	M1842	Theory
30 - 70	-0.5	1.2 - 3
12 - 30	0.6	3 - 7
5 - 12	0.7	7 - 20
3 - 5	-1.6	20 - 30

all phase speed orientation angles were smaller than 1°, which does not agree with the theoretical values for these periods (see Table 6.2). In the 12 - 30 days period range however, the observed value of 0.6° is just slightly lower than the range expected from theory ($3° - 7°$), and the spectral analysis (see Figure 6.4d) has shown bottom intensification of the signal. This indicates, that the variability in this period range is caused by bottom trapped TRWs, which confirms results of a study of *Layton* (2016). *Layton* (2016) also analyzed the data of M1842 in comparison with mooring data of the northern entrance of Flemish Pass, and explained the variability on a three weeks time scale with baroclinic bottom trapped TRWs. The shorter and longer term variability might also be induced by TRWs or caused by other processes, which occur in the shallow water or on the continental shelf.

6.3 Summary and discussion

To investigate which processes generate the current reversals in the LSW flow through Flemish Pass, two hypotheses have been examined: 1. The recirculation around Flemish Cap widens and suppresses the southward flow part by extending further into Flemish Pass, and 2. TRWs induce the observed reversals in the LSW flow.

The analysis of the available hydrographic and current velocity time series data of Flemish Pass did not provide any evidence that a westward extension of the recirculation induced the current reversal in Flemish Pass. In contrast, a spatial analysis of the current velocity data revealed that the current reversals were much stronger at the western slope of Flemish Pass and appeared to originate there. A spectral and variance ellipse analysis strongly supported the hypothesis, that TRWs are an important process influencing the variability of the LSW flow in Flemish Pass and inducing the current reversals.

The observation of TRWs in the DWBC have often been reported in the scientific literature from upstream and downstream of Flemish Pass. *Fischer et al.* (2015) for instance found high intra-seasonal variance in the DWBC at 53°N, with a bottom intensified variance maximum at a period of about 10 days, and attributed that to TRWs trapped at the steep topography. At 47°N east of Flemish Cap, *Mertens et al.* (2014) also detected the TRWs at the 10 days period in the DWBC

from moored current meters in the period 2009 - 2011. There, the highest variance occurred in a 20 - 50 days period range though, which *Mertens et al.* (2014) interpreted as incoming baroclinic Rossby waves or eddies from the east. In Flemish Pass, the highest variance was also observed in the 20 - 50 days range, confirming the earlier observations of *Mertens et al.* (2014). However, the signal was confined to the western slope of Flemish Pass, which suggests the influence of a TRW trapped at the topography. Another study of *Layton* (2016), which focused on the current variability at northern entrance of Flemish Pass at 48°N and in the upper water column at 47°N, attributed variability on a time scale of three weeks to baroclinic TRWs. Also further downstream in the DWBC pronounced intra-seasonal variability was found, corresponding in time scales to the variability at 47°N in Flemish Pass and east of Flemish Cap [*Mertens et al.* (2014)]. Time scales of 15 - 60 days were monitored for instance at the tail of the Grand Banks at 42°N [*Schott et al.* (2004), *Schott et al.* (2006)] and at 40°N at the mooring line 'W' [*Peña-Molino et al.* (2012)]. *Peña-Molino et al.* (2012) related the observed variability in the deep flow to TRWs generated by Gulf Stream instabilities. In the Cape Hatteras region (about 36°N), the dominant variability in the DWBC was also explained by bottom trapped TRWs [e.g. *Johns and Watts* (1986), *Pickart and Watts* (1990)].

In regard of the numerous observations of TRWs impacting the variability all along the pathway of the DWBC, the results found for the Flemish Pass fit really well into the bigger picture of the scientific literature. Further processes, which might contribute to the flow variability of LSW in Flemish Pass, are investigated in the next chapter.

7 Remote influence vs. local forcing on the LSW transport variability

In the previous chapter, the influence of TRWs on the transport variability of LSW in Flemish Pass was discussed. Now, the topic of variability driving processes (research question 3, chapter 1) will be further deepened. Firstly, the possibility of a remote connection with upstream processes contributing to the variability in Flemish Pass is addressed. For this purpose, a volume transport time series of the DWBC at 53°N in LSW depth range (400 to 1850 m) was compared with the Flemish Pass transports (Figure 7.1). J. Karstensen [pers. communication] from the Helmholtz Center for Ocean Research (GEOMAR), Kiel, Germany, kindly provided the LSW transport time series inferred from the 53°N mooring array for the analysis.

Secondly, the influence of local wind and sea surface pressure forcing on the Flemish Pass transport variability was examined. The impact of wind forcing has been shown to be non-negligible in modeling studies [e.g. *Han* (2005), *Han et al.* (2008)]. *Han* (2005) attributed one fourth of the Flemish Pass transports to wind forcing. Beyond a local impact, remote wind forcing can furthermore have an influence on current variability by inducing waves, such as Rossby waves or coastal trapped waves [*Brink* (1989)]. A recent modeling study has identified coastal trapped waves to be a variability driving process in Flemish Pass [*Varotsou* (2016)]. This process will be therefore further evaluated in this chapter. The local as well as remote impact of wind forcing is investigated by utilizing observational data from the NCEP/NCAR reanalysis project [*Kalnay et al.* (1996)].

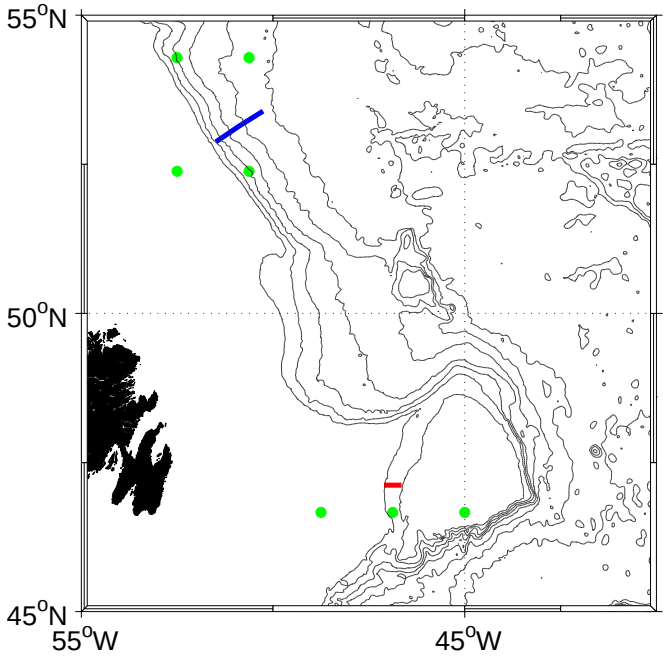

Figure 7.1: Location of the mooring arrays at 53°N (blue, Helmholtz Center for Ocean Research (GEOMAR), Kiel, Germany) and in Flemish Pass at 47°N (red) and grid points of the NCEP/NCAR reanalysis project (green) used to derive time series of wind stress and sea level pressure.

7.1 LSW transports through Flemish Pass in comparison to 53°N

In order to investigate if transport anomalies can be traced from the exit of the Labrador Sea down to the Flemish Pass region, an LSW transport time series from the DWBC at 53°N was compared to the Flemish Pass transports. The mooring array on the 53°N section consisted of three moorings K7, K8, and K9 positioned at 52°51,94'N, 51°28,71'W (K7), 52°56,46'N, 51°18,96'W (K8), and 53°07,84'N, 50°52,53'W (K9) [e.g. *Fischer et al.* (2010), *Fischer et al.* (2015), *Zantopp et al.* (2017)]. No other mooring array is located in closer proximity to the LSW source region. The transport time series is the longest time series available capturing the DWBC and was calculated from current meter data in the LSW depth range 400 to 1850 m of the period January 2011 to July 2014. The time resolution is 5 days. No further processing was applied to the time series. Figure 7.2 exhibits the normalized transport time series of LSW at 53°N and in Flemish Pass, both in a time resolution of 5 days for better comparison. To examine if arrival times of transport

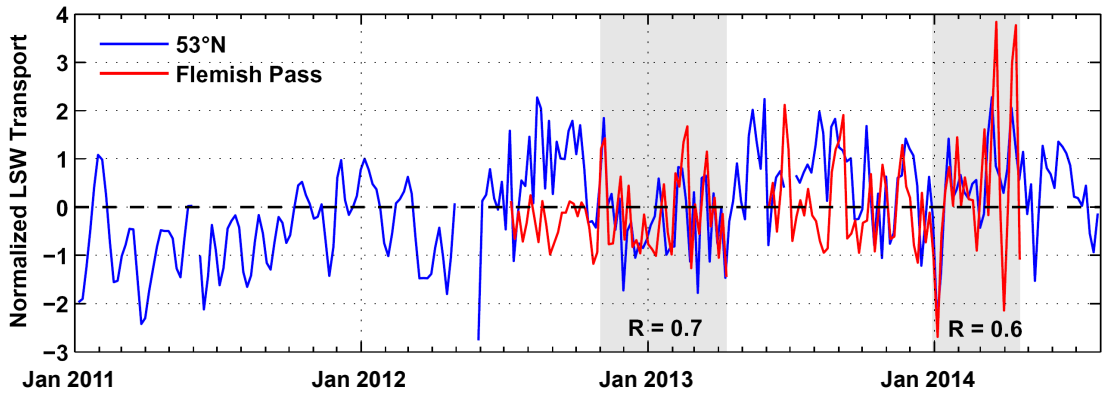

Figure 7.2: Normalized LSW transports in the DWBC at 53°N (blue) and in Flemish Pass at 47°N (red). Time periods of coherent oscillation of the two time series are shaded in gray. The temporal resolution of both time series is 5 days.

anomalies from 53°N can be detected at Flemish Pass, a lag analysis of the two transport time series was performed. From the hydrographic time series presented in chapter 4.2, and also from the scientific literature [e.g. *Stramma et al.* (2004)], a time span of at least a couple of months would be expected for the LSW to spread between the 53°N and the Flemish Pass section. However, the highest significant correlation of R = 0.4 of the two time series resulted for lag 0. Interestingly, during two phases in the winters of 2012/2013 and 2013/2014, coherent oscillations of the transports at 53°N and in Flemish Pass with much higher correlation (R = 0.7 in November to April 2012/2013, and R = 0.6 in January to April 2014, see Figure 7.2) can be observed, while the correlation in the summers and autumns is much lower (R = 0.3 in July to October 2012, and R = 0.1 in June to November 2013). Possible processes which might cause coherent oscillations between 53°N and Flemish Pass could be either local large scale wind or sea surface pressure patterns impacting the barotropic component of the transports along the western boundary [e.g. *Lazier and Wright* (1993)], or remotely generated waves, such as coastal trapped waves or Rossby waves, which also affect current variability [e.g. *Pickart and Watts* (1990), *Mertens et al.* (2014), *Fischer et al.* (2015)]. In the next section, first the local atmospheric forcing at 53°N and in Flemish Pass will be investigated.

7.2 Impact of local atmospheric forcing on the transports at 53°N and in Flemish Pass

The impact of local atmospheric forcing on the transports at 53°N and in Flemish Pass is investigated using NCEP/NCAR Reanalysis 1 data provided by the NOAA/OAR/ESRL PSD, Boulder, Colorado, USA, from their Web site at http://www.esrl.noaa.gov/psd/ [*Kalnay et al.* (1996)]. The data of surface fluxes in the study region is available in daily resolution on a Gaussian grid of about 2° resolution. Time series of wind stress and sea level pressure for the period July 2012 to April 2014 were derived by averaging data from the grid points closest to the 53°N and Flemish Pass mooring arrays (Figure 7.1). The grid points were selected to minimize the standard deviation from the corresponding time series, which was fulfilled by two grid points north and south of the 53°N array (STD $< 0.5\,\mathrm{N\,m^{-2}}$ and STD $< 6\,\mathrm{hPa}$), and three grid points south of the Flemish Pass array (STD $< 0.3\,\mathrm{N\,m^{-2}}$ and STD $< 6\,\mathrm{hPa}$, see Figure 7.1).
The time series of absolute wind stress and sea level pressure from both regions are shown in Figure 7.3, in comparison to the LSW transport time series. To determine if there is a trans-regional impact of the atmospheric forcing which affects both mooring array locations, correlations of the regional time series were calculated for four different phases. The phases were defined from the analysis of correlation of the transports at 53°N and at Flemish Pass (see Figure 7.2): Phase 1 (July - October 2012) and phase 3 (April - December 2013) correspond to the phases in which the LSW transports of both regions do not show any significant correlation, while during phase 2 (November 2012 - April 2013) and phase 4 (January 2014 - April 2014), coherent oscillation oscillation is observed.
Concerning sea level pressure (Figure 7.3c), significant correlation of both regions is found in all four phases, ranging between R = 0.5 to R = 0.8. This shows that sea level pressure patterns have a large scale distribution which is affecting both regions in a similar way at all times. In contrast to that, the wind stress time series (Figure 7.3b) of both regions are only significantly correlated in phases 3 (R = 0.4) and 4 (R = 0.5), while there was no correlation in the first two phases. This indicates that the wind stress pattern in phases 1 and 2 is more localized, while it has a larger scale in phases 3 and 4 which affects both regions.

As a next step, a lag analysis of the wind stress and LSW transport time series was performed to check if there was possibly a delayed influence of the wind

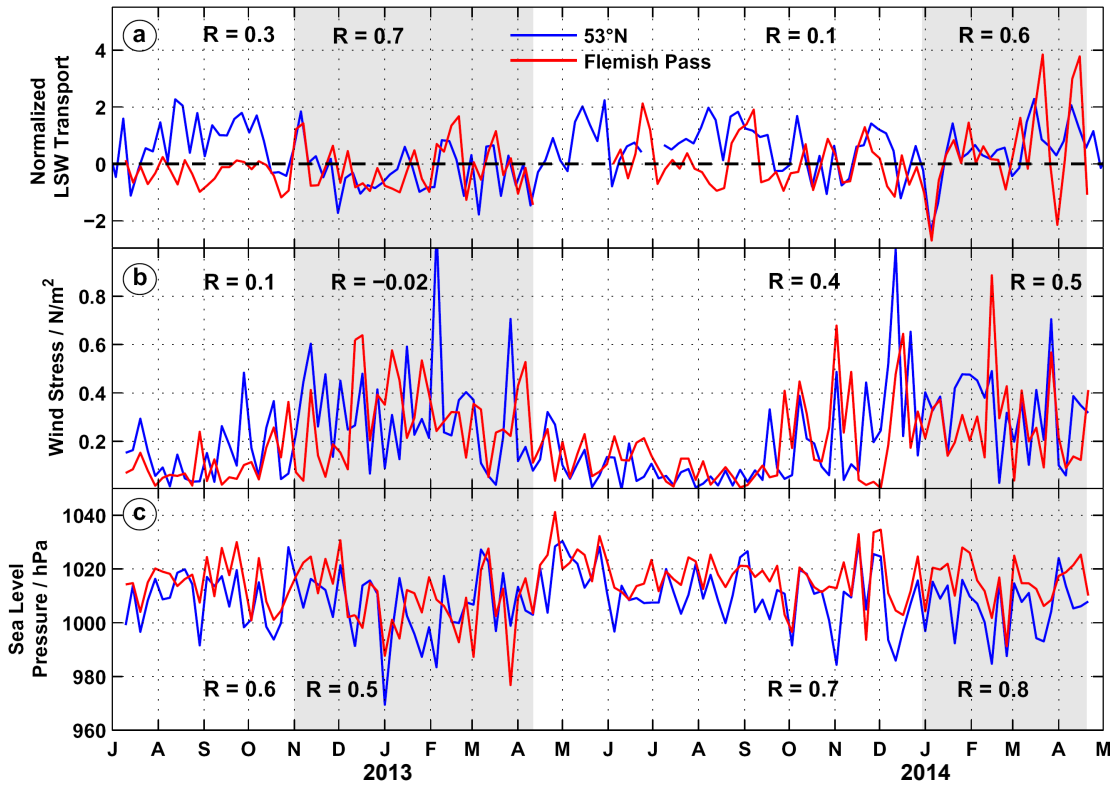

Figure 7.3: Regional time series from the DWBC at 53°N (blue) and Flemish Pass at 47°N (red). (a) Normalized LSW transports (as in Figure 7.2, (b) wind stress ($\mathrm{N\,m^{-2}}$), and (c) sea level pressure (hPa). Time periods of highly correlated LSW transports are shaded in gray. The temporal resolution of the time series is 5 day means.

forcing on the transports. Correlations were determined for both the along-shore and the cross-shore components of wind stress and the LSW transports at 53°N and in Flemish Pass (Figure 7.4). Concerning the along-shore wind stress (Figure 7.4a), the correlations with the LSW transports are generally low. The highest correlation is about 0.3 for both regions at a lag of 0 days. This is hinting to an influence of the local wind stress on the LSW transport variability, but it cannot be considered an evidence, as the correlation is still rather low. At longer lags, the correlations range between -0.27 to 0.16. Similarly low correlations were found for the cross-shore wind stress and LSW transports of both regions, which are distributed between ± 0.24 (Figure 7.4b), providing no clear indication that any lag period is of particular importance.

On the whole, the lag analysis revealed that there is no delayed impact of the

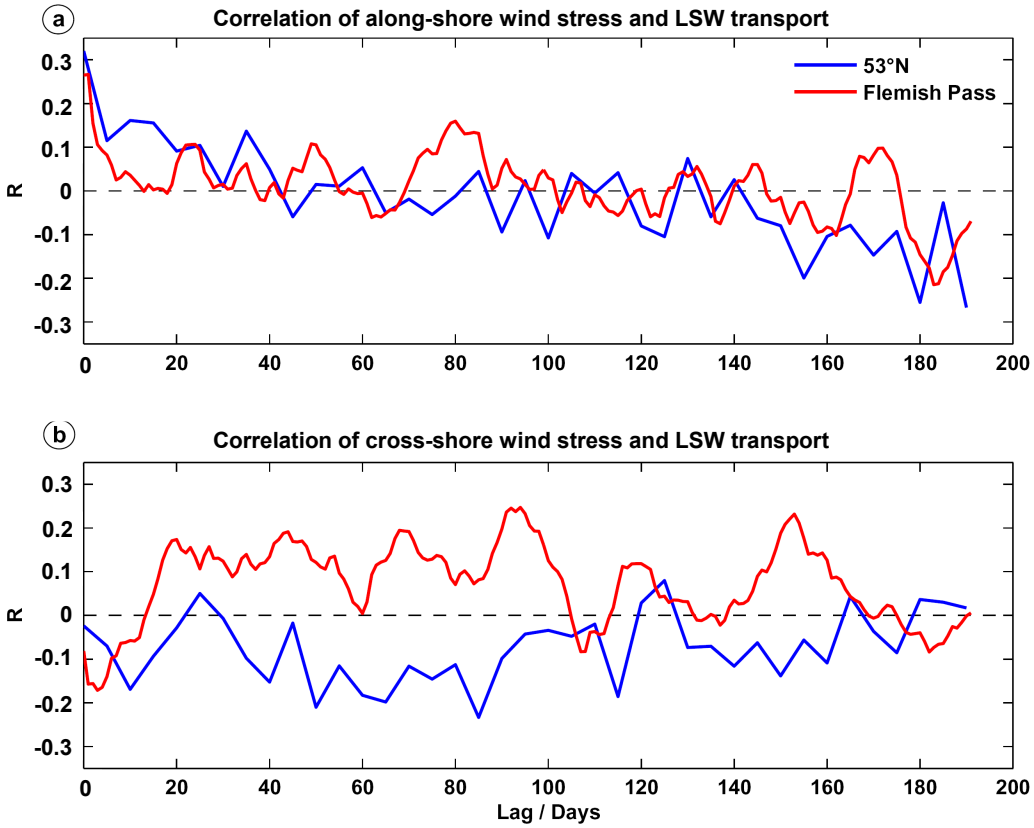

Figure 7.4: Correlation of the LSW transports and (a) along-shore wind stress, and (b) cross-shore wind stress for the 53°N region (blue, 5 day temporal resolution) and the Flemish Pass (red, daily temporal resolution).

local wind stress on the LSW transports at both the 53°N and the Flemish Pass mooring array, but it did not provide an answer to what had caused the coherent oscillations of the transport of both regions.

To get a deeper insight into the wind forcing, a spectral analysis of the wind stress at 53°N and the Flemish Pass was carried out to identify its characteristic time scales. Spectral estimates were calculated by Welch's method [*Welch* (1967)]. A Hamming window length of 128 days and 64 days overlap was chosen for comparability with the LSW transport spectra of Flemish Pass shown in chapter 5.6 (see Figure 5.21). The spectral analysis of wind stress shows that most variance of the along- and cross-shore wind stress occurs on time scales of 6 days and shorter for both the 53°N and the Flemish Pass region (Figure 7.5). The along-shore variance is higher at 53°N (0.02 - 0.025 $N^2\,m^{-4}$) than in Flemish Pass (0.015 $N^2\,m^{-4}$) for periods of less than 6 days. At 53°N, another high peak (0.02 $N^2\,m^{-4}$) is at 11 days.

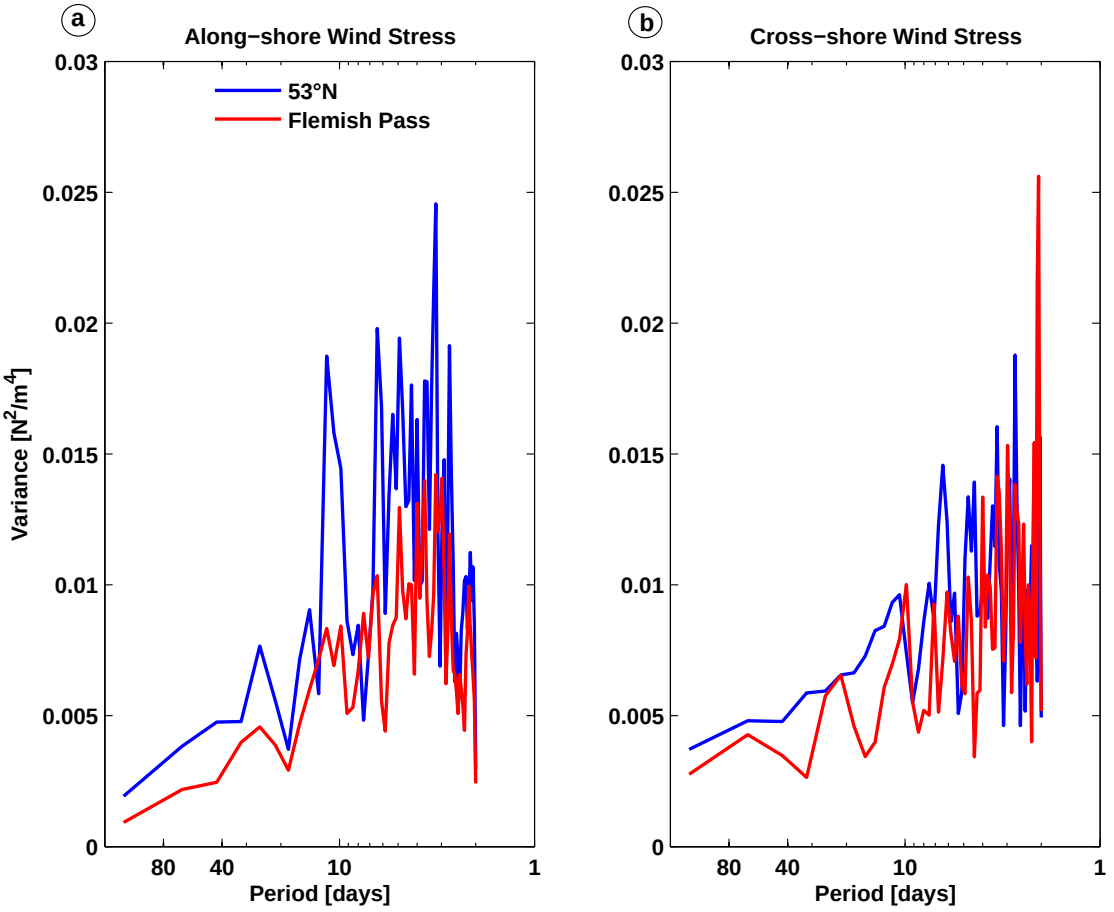

Figure 7.5: Variance-preserving Welch spectra (128 day segments, 64 day overlap) of (a) along-shore wind stress and (b) crosshore wind stress at the mooring arrays in the DWBC at 53°N (blue) and in Flemish Pass, inferred from NCEP/NCAR time series data between July 2012 and April 2014 (which corresponds to the Flemish Pass mooring period).

In both regions, the variance decreases toward longer time scales. The variance of the cross-shore wind stress is comparable for both regions ($< 0.015\,\mathrm{N^2\,m^{-4}}$), with the exception of very short time scales of about two days, at which the Flemish Pass variance is at a maximum ($0.027\,\mathrm{N^2\,m^{-4}}$ as compared to up to $0.016\,\mathrm{N^2\,m^{-4}}$ at 53°N).

The time resolution of the Flemish Pass transport time series is daily, like the wind stress time series. Due to this, a comparison of the transport and wind stress spectra can be performed. The time resolution of the 53°N transport time series is 5 days. The influence of the high frequency variability of wind stress would therefore not be resolved in a the transport spectrum of this time series.

The Flemish Pass spectra of LSW transport (Figure 5.21) of 2012 - 2013 and 2013 - 2014 displayed the highest variance in the 20 to 50 day range, implying that the transport variability is not mainly driven by the high frequency changes of the atmospheric forcing. However, in 2013 - 2014, a smaller variance maximum of about 0.25 Sv occurred in the 5 - 10 day period range, which could be related to the influence of wind stress.
In summary, the results presented in this section indicate that the local wind stress possibly had a weak influence on the LSW transport variability at 53°N and in Flemish Pass, but there is not enough evidence to explain the coherent oscillations between the two regions. To further investigate the occurrences of these oscillations, the next section therefore addresses remote impact of wind forcing on the LSW transports by generation of waves.

7.3 Impact of remotely generated waves on the current velocity in Flemish Pass

A coherent oscillation between 53°N and the Flemish Pass could be generated by different processes. One possible process is a coastal trapped wave (CTW), which is induced by wind stress along the Labrador Shelf and propagates southward along the western boundary [e.g. *Mysak* (1980)], thereby affecting both 53°N and the Flemish Pass. Another mechanism would be an oceanic Rossby wave with a wavelength long enough to affect both regions, excited by wind forcing far offshore and propagating toward the shelf region [e.g. *Mysak* (1980), *Brink* (1989), and *Gill* (1982)].
This section will first provide some information about CTWs. Secondly, a description of the method applied to analyze the remote impact of wind forcing in relation to the available current velocity mooring data will follow. The method was previously used by *Brink* (1989) in the western North Atlantic to analyze the coherence of mooring based current velocity and wind stress curl. *Brink* (1989) found the highest coherence with the curl at remote locations with more than 500 km distance to the moorings, and suggested wind forced Rossby waves as a cause. Subsequently, the results based on the Flemish Pass mooring data and the wind stress provided by NCEP/NCAR will be presented in conjunction with an

interpretation.
CTWs are usually generated by wind stress along the continental shelf causing an input of vorticity and therefore typically have periods of several days [e.g. *Huthnance* (1981), *Maslowski* (1996)]. Their existence is dependent on the presence of a continental slope [*Maslowski* (1996)]. An along-shore current might affect wave modes by advecting the waves or even reverse slower wave modes [*Huthnance* (1981)]. The majority of observations of CTWs are in the coastal sea level [*Huthnance* (1981)]. However, the occurrence of CTWs in a deep current was previously examined by *Pietri et al.* (2014) off the coast of Peru. Using a three dimensional regional model, they related the variability of the Chile-Peru Deep Coastal Current in a depth range of 300 to 1000 m to the influence of a poleward propagating CTW.
TRWs, which were previously described in chapter 6, are sometimes also classified as CTWs [e.g. *Mertens et al.* (2014)], and they are essentially the same wave type [*Maslowski* (1996)]. In contrast to the CTWs, TRWs however can also exist at sloping topography in the deep ocean and do not need the coast to propagate [*LeBlond and Mysak* (1978)]. Here, in the following, the expression CTW will be used without differentiating from TRWs.
To investigate if there is a connection between the current variability in Flemish Pass and remote wind forcing potentially causing a CTW or oceanic Rossby wave, cross spectra and phase spectra of current velocity mooring data and wind stress curl were calculated following the method of *Brink* (1989). Wind stress curl estimates were determined for all NCEP/NCAR grid points in the subpolar North Atlantic between 35° - 65°N and 0° - 70°W. The coherence and phase spectra of wind stress curl and current velocity were derived for each grid point and every depth bin of the ADCP moorings BM25/1, BM26/1, BM25/2, and M1842 in Flemish Pass. The spectra were then averaged into different period bands (20 - 76 days, 10 - 20 days, 6 - 10 days, and 3 - 6 days), which were selected based on the current velocity spectra shown in chapter 6.2.2. Figure 7.6a shows an example of the resulting contours of coherence squared of wind stress curl over the subpolar North Atlantic and the meridional current velocity at the western slope mooring BM25/1 in a depth of 498 m for the period band 6 - 10 days. At this depth, the highest coherence was found. Notice also, that in this period band, the wind driven variability is highest (compare Figure 7.5 for the 53°N and Flemish Pass region). The coherence between the wind stress curl and the meridional

current velocity component (Figure 7.6a) is generally rather low over the entire North Atlantic region. Only a few areas exist where the coherence is significant at the 95% confidence level which corresponds to 0.52. In these areas, the wind stress curl is significantly coherent with the current velocity at BM25/1 in the corresponding deth bin. The areas are located in the eastern Atlantic near to the Iberian Peninsula and at the Mid-Atlantic Ridge, west of Newfoundland, and in the Labrador Sea. The coherent area in the Labrador Sea covers the largest area, it also includes the DWBC region with the location of the 53°N mooring array and further southward toward Flemish Cap.

Figure 7.6b shows the contours of phase between the wind stress curl over the subpolar North Atlantic and the meridional current velocity at mooring BM25/1 in a depth of 498 m for the period band 6 - 10 days. At the location of the 53°N array, the wind stress curl is in phase with the meridional current velocity in Flemish Pass, with a phase difference of less than 20°. This phase difference corresponds to a time delay of about 3 days ($\Delta t = \Delta\varphi \cdot \omega$). A wave, that is excited by the wind stress curl at 53°N and travels about 720 km southward along the continental shelf to Flemish Pass in 3 days would have a propagation speed of $2.8\,\mathrm{m\,s^{-1}}$. For a CTW, a phase speed in this order of magnitude is in the realm of possibility. *Pietri et al.* (2014) for instance estimated a phase speed of $1.2\,\mathrm{m\,s^{-1}}$ for a CTW observed off the coast of Peru.

The analysis of the coherence and phase between the subpolar North Atlantic wind stress curl and the meridional current velocity from all depth bins of mooring BM25/1 has shown that the significantly coherent area in the Labrador Sea including the DWBC at 53°N is a consistent feature in the intermediate depths <550 m. The phase contours within this area are consistent down to a depth of 700 m. For deeper depths, there is a change to negative phases, indicating that the causal relation between the wind stress curl at 53°N and and the current velocity in Flemish Pass does not penetrate the full water column. This hints to a CTW propagating southward along the continental shelf within the intermediate depth range of less than 700 m depth and thereby affecting the LSW flow.

Concerning the other areas of significant coherence in the eastern Atlantic, at the Mid-Atlantic Ridge, and west of Newfoundland (Figure 7.6a), it is rather unlikely that the wind forcing there generates a coherent oscillation at 53°N and Flemish Pass because of their location (shielded by the landmasses of Newfoundland) and distance (Iberian Peninsula) of these areas.

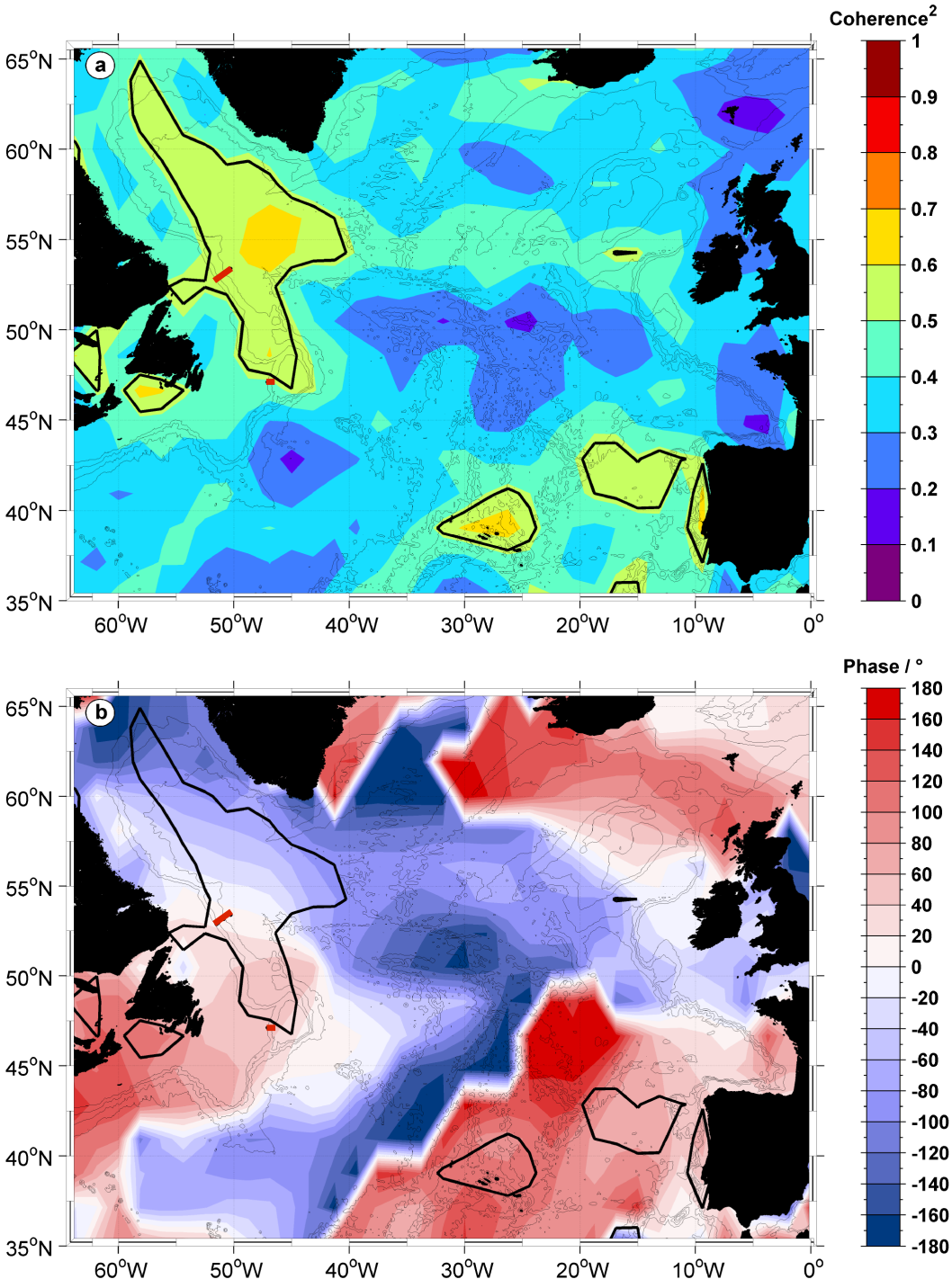

Figure 7.6: Contours of (a) coherence squared and (b) phase between the NCEP/NCAR based wind stress curl and the meridional current velocity at 498 m at mooring BM25/1 for a 6 - 10 day period band. The black contour represents the 95% confidence level. Brown lines indicate the locations of the mooring arrays at 53°N and in Flemish Pass.

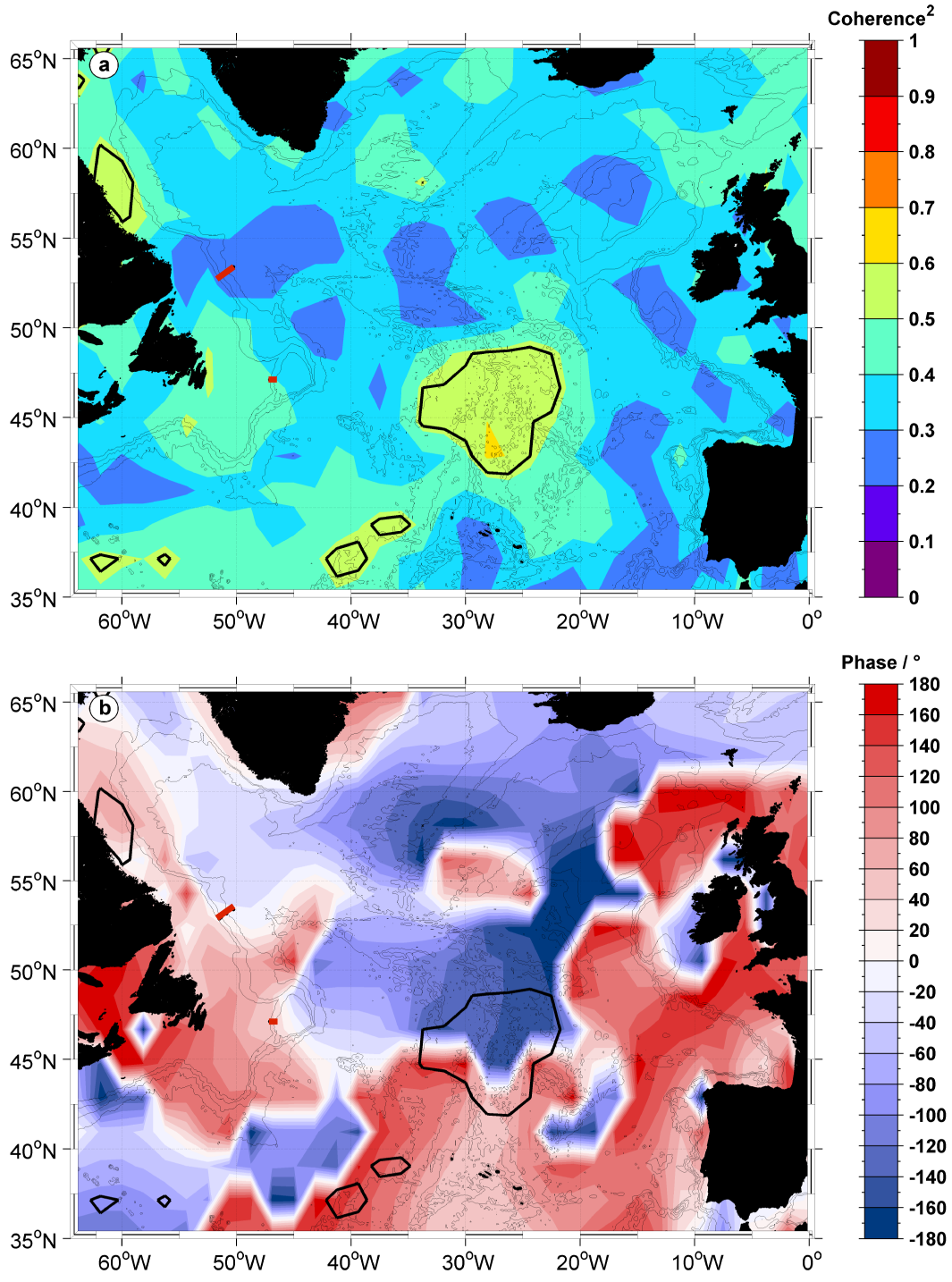

Figure 7.7: Contours of (a) coherence squared and (b) phase between the NCEP/NCAR based wind stress curl and the meridional current velocity at 498 m at mooring BM26/1 for a 6 - 10 day period band. The black contour represents the 95% confidence level. Brown lines indicate the locations of the mooring arrays at 53°N and in Flemish Pass.

The statistical comparison of the North Atlantic wind stress curl and the meridional current velocity at mooring BM26/1 in the central Flemish Pass yielded coherence squared and phase contours (Figure 7.7) of the 6 - 10 days period band, which were fairly different from the ones of BM25/1 (Figure 7.6). At the 53°N array for instance, the coherence is much lower (< 0.3) and not significant, while the phase is slightly similar, but only part of the mooring array is found within a phase difference of less than 20°. Instead, areas of significant coherence are located over the Labrador Shelf north of 55°N, and in the central North Atlantic at the Mid-Atlantic Ridge. In the area at the Mid-Atlantic Ridge, the local wind stress curl is out of phase with the current velocity in Flemish Pass, i.e. changes in the current velocity happened before changes in the wind forcing. The wind stress curl over the Labrador Shelf is in phase with the Flemish Pass current velocity. The phase difference is 80°, which corresponds to a time delay of 11 days. A wave originating from this area and propagating to Flemish Pass within 11 days would have a speed of about $1.7\,\mathrm{m\,s^{-1}}$. A wave of this speed would also cover the distance between 53°N and Flemish Pass within 5 days.
The results based on the data of the central Flemish Pass mooring BM26/1 also hint to the occurrence of a CTW over the Labrador Shelf. However, the estimated area where the wave was generated as well as its propagation speed differ from the results based on the western slope mooring BM25/1. According to *Huthnance* (1981), oceanic currents can affect the modes of CTWs. Therefore, the differences in the current system of Flemish Pass, which has a more baroclinic flow over the western slope and a barotropic flow in the center (see chapter 5.2.1), most likely cause the differences in the results of the statistical analysis for BM25/1 and BM26/1.
CTWs propagating in the DWBC from 53°N to Flemish Pass within 5 days or less and thereby impacting the transport variability of LSW would appear as a coherent oscillation in the transport time series of LSW shown in Figure 7.2, which had a temporal resolution of 5 days. These results support the hypothesis, that the coherent oscillation of the LSW transports in the DWBC at 53°N and in Flemish Pass were induced by wind forced CTWs, generated over the Labrador Shelf. The analysis of the other lower frequency bands unrelated to the wind forcing (20 - 76 days and 10 - 20 days) and of the very high frequency band (3 - 6 days), as well as of the second mooring period (BM25/2, and M1842) did not provide any further insight as to what might have caused the coherent oscillations at 53°N and Flemish

Pass. In the two longer period bands, patches of significant coherence were found in the Labrador Sea, in the Newfoundland basin, in the central North Atlantic over the Mid-Atlantic Ridge, and in the Iceland basin. However, the wind stress curl in these areas was usually out of phase with the meridional current velocity in Flemish Pass. In the shorter period band 3 - 6 days, no significant coherence could be found. The statistical analysis was also performed for the zonal velocity component of the current velocity in Flemish Pass. The results however did not show any stable signal as the areas of significant coherence changed erratically from depth bin to depth bin.
On the whole, the results from the statistical analysis provide a hint, that the coherent oscillations of the LSW transports at 53°N and Flemish Pass might have been caused by CTWs with periods of 6 - 10 days, which were generated by wind stress over the shelf of the Labrador Sea and travel southward along the shelf. Because of their high phase speed of several meters per second, these waves only need about 3 to 5 days from 53°N to reach Flemish Pass.

7.4 Summary and discussion

In this chapter, several processes that potentially influence the transport variability of LSW in Flemish Pass were investigated. The possibility of a remote connection with upstream processes was examined by investigating the coherence of the LSW transport time series of the DWBC at 53°N and Flemish Pass. The analysis revealed coherent oscillations of the LSW transports of both regions occurring during the winter months (November to April 2012/2013, and January to April 2014). As possible drivers of the coherent oscillations, local wind forcing as well as remotely generated waves were considered. A weak correlation of R = 0.3 between the local along-shore wind stress and the LSW transports was found for both regions. Concerning Flemish Pass, this confirms the results of *Han* (2005), who found a non-negligible contribution of wind forcing on the Flemish Pass transports in a model study. However, the coherent oscillations in the LSW transports at 53°N and Flemish Pass could not be explained by the local wind forcing.
The results of a statistical analysis following *Brink* (1989) pointed to wind generated CTWs propagating southward along the Labrador Shelf with a speed of about 2 to 3 $\mathrm{m\,s^{-1}}$ and thereby inducing the coherently oscillating LSW transports

at 53°N and Flemish Pass. These results correspond to the results of *DeTracey et al.* (1996). They suggested that storms in the northern Labrador Sea generate fast CTWs, which propagate southward and influence the current variability at the northeastern Grand Banks. CTWs are mainly observed in coastal sea level records [e.g. *Mysak* (1980)]. A recent study of *Pietri et al.* (2014) however related the variability of the Chile-Peru Deep Coastal Current in a depth range of 300 to 1000 m to the influence of a remotely generated poleward propagating CTW. They estimated a propagation speed of $1.2\,\mathrm{m\,s^{-1}}$, which is of similar magnitude as the results discussed in this chapter. The results presented here also agree with the model study of *Varotsou* (2016), who investigated the transport variability of ULSW in Flemish Pass based on daily current velocity data of the MIT/gcm model in the period 2003 - 2009. *Varotsou* (2016) suggested that the high frequency variability of ULSW volume transports is attributed to CTWs. In contrast to the results presented here, *Varotsou* (2016) estimated lower wave propagation speeds of slightly less than $0.5\,\mathrm{m\,s^{-1}}$.

8 Summary and conclusions

This study focused on the LSW flow through Flemish Pass between the Grand Banks and Flemish Cap at 47°N. One main objective of this study was to investigate if the water flowing through Flemish Pass in the density range of LSW ($\sigma_\theta = 27.68$ - $27.80\,\mathrm{kg\,m^{-3}}$) originated from the central Labrador Sea. LSW formed during deep convection events in the Labrador Sea [e.g. *Lazier* (1973), *Lazier et al.* (2002)] is a main component of the climate modulating AMOC. Flemish Pass is potentially an additional southward export pathway next to the DWBC east of Flemish Cap, which so far had the scientific focus as the major propagation pathway of LSW [e.g. *Fischer and Schott* (2002), *Rhein et al.* (2011), *Mertens et al.* (2014), *Rhein et al.* (2015)]. *Bower et al.* (2011) observed that the southeastern corner of Flemish Cap is a primary location for LSW to leave the DWBC and to be entrained into the interior North Atlantic, and suggested that Flemish Pass protects LSW from being diverted into the interior Newfoundland Basin by meanders of the NAC. Therefore, Flemish Pass is potentially a key region for the southward export of LSW.

The characteristics of the flow and hydrography in Flemish Pass were analyzed from ship based CTD and LADCP measurements along 47°N (chapter 3). The observed flow through Flemish Pass is mainly southward, with a warmer and saltier northward recirculation around Flemish Cap in the east. The elevated temperatures and salinities in the recirculation most likely result from mixing with NAC water south of Flemish Cap (chapter 3.3.2). The long-term hydrographic variability in the deep water of Flemish Pass inferred from CTD sections between 1993 - 2013 was related to the variability found in the formation region of LSW in the central Labrador Sea (chapter 4). The observed trends of warming (0.3°C/decade) and salinification (0.03/decade) in the ULSW density range reflected closely the evolution of the hydrographic properties of ULSW in the Labrador Sea and in the DWBC at 47°N. The increase in temperature and salinity found for the central Labrador Sea confirm the results of *Yashayaev et al.* (2015) and *Kieke and*

Yashayaev (2015). The warming trend observed in Flemish Pass agrees in the order of magnitude with the warming signal of 0.5°C/decade that *Fischer et al.* (2010) found at several locations in the DWBC (55°N, 53°N, 46°N, 43°N) between the Labrador Sea and the tip of the Grand Banks.
By using ULSW time series of hydrographic anomalies of the MIT/gcm model for the period 1960 - 2009, the observed trends in Flemish Pass were identified as part of a multidecadal cycle. Other studies [e.g. *Curry et al.* (1998), *Yashayaev et al.* (2015)] found hydrographic variability of LSW in the Labrador Sea on multi-decadal time scales, and linked it to the variability in the NAO.
The results found for the long-term hydrographic variability of the deep flow in Flemish Pass provide evidence that the water in the LSW density range is indeed LSW from the Labrador Sea. Transport estimates derived from LADCP measurements revealed that the Flemish Pass branch in comparison to the slope part of the DWBC east of Flemish Cap contributes a considerable 15 - 27% to the total southward ULSW transport (chapter 3). DLSW however is mainly transported with the DWBC branch around Flemish Cap (98%). Nevertheless, these results support that the Flemish Pass is an important LSW export pathway besides the DWBC branch, and knowledge of the transport through Flemish Pass is necessary for a complete estimate of the AMOC at 47°N. The transport estimates based on the LADCP measurements only provide snapshots of the strength of the LSW export. The mooring array of the FLEPVAR project for the first time delivered time series data of current velocity measurements in the Flemish Pass LSW layer at 47°N for the period 2012 - 2014. A previous study of *Petrie and Buckley* (1996) derived mooring based transports for the upper water column in Flemish Pass for a period of three month, but did not provide a particular LSW transport. The data of the Flemish Pass mooring array was the basis for the other main objective of this study, to investigate the magnitude and the associated variability of LSW transports through Flemish Pass (chapter 5), as well as the processes that drive the variability (chapter 6 and chapter 7).
The average LSW transport inferred from the data of two moorings deployed in Flemish Pass in the first mooring period 2012 - 2013 was -1.9 ± 0.5 Sv, which agreed well with the average transport derived from ship based LADCP and VmADCP measurements (-2.1 ± 0.5 Sv, chapter 5). In the autumn and winter period, the LSW transports were highly variable, ranging between -3.5 Sv and 0.7 Sv. In the second mooring period 2013 - 214, only one mooring was deployed

on the western slope of Flemish Pass, and the average LSW transport was slightly lower (-1.4 ± 0.5 Sv) than in the previous year. The variability also increased in the winter months, and during extreme events very high southward LSW transports of -5 Sv and northward transports of 3 Sv were reached.
Furthermore, seasonal effects on the LSW transports were investigated based on both, the variability of the density field in Flemish Pass, as well as seasonality in the southward flow through Flemish Pass (chapter 5). *Myers and Kulan* (2012) found that transport estimates of the DWBC at 53°N are quite sensitive to seasonal and interannual variability in the structure of the density field. Concerning Flemish Pass, a seasonal difference in the density field was detected, the effect on the LSW layer transports was less than -0.3 Sv though, and is therefore negligible in the range of the transport uncertainty.
Seasonal effects in the flow of the DWBC were investigated by *Fischer et al.* (2004) and *Fischer et al.* (2015), who observed a pronounced seasonal cycle in the DWBC at 53°N that was confined in the shallow Labrador Current, while they detected a very weak seasonal cycle in the deep flow of the DWBC. Similar results were found for Flemish Pass (chapter 5). Over the western slope of Flemish Pass, the shallow Labrador Current induces a strong shear in the velocity field. There, the seasonal cycle amplitude of the meridional current velocity was almost $\pm10\,\mathrm{cm\,s^{-1}}$ near the surface, and decreased with increasing water depth to only $\pm1\,\mathrm{cm\,s^{-1}}$ near the bottom. In the central Flemish Pass, which has a barotropic velocity structure, the seasonal cycle of the flow was not depth dependent and had a small amplitude of about $\pm2\,\mathrm{cm\,s^{-1}}$ between 540 and 1080 m. As the seasonal cycles of the western slope and the central Flemish Pass had a phase shift causing superposition, the seasonal cycle of the flow had only a very small effect (±0.1 Sv) on the LSW transports of the period 2012 - 2013, which were calculated based on two moorings, one located at the slope and one in the center. In the second mooring period 2013 - 2014, the LSW transports were derived based on only the western slope mooring and therefore the seasonal cycle of the flow through Flemish Pass had a more pronounced effect on the LSW transports (±0.5 Sv).
In addition to the LSW transport time series, a top to bottom transport time series was derived using additional upper water column data from a Canadian mooring located on the western slope of Flemish Pass in the second mooring period 2013 - 2014 (chapter 5). The average top to bottom transport was -6.7 Sv, which agrees with a historical estimate of -6.3 to -9.8 Sv calculated by *Petrie and Buckley*

(1996). The range of the top to bottom transports in 2013 - 2014 was −15 Sv to 1 Sv.

Characteristic time scales of the transport variability in Flemish Pass were determined in a spectral analysis (chapter 5). High intra-seasonal variability with the strongest signal in the 20 - 50 day period range was found. Knowledge about the processes driving the transport variability in Flemish Pass was so far mainly limited to model studies [e.g. *Varotsou et al.* (2015), *Varotsou* (2016), *Han* (2005), *Han et al.* (2008)], or restricted to the upper water column [*Layton* (2016)]. *Han* (2005) for instance attributed one fourth of the Flemish Pass transports to wind forcing based on model data, and *Varotsou et al.* (2015) linked the interannual transport variability of upper LSW in Flemish Pass to changes of the atmospheric forcing and to changes of the NAC's position. Due to the limited duration of the Flemish Pass mooring records (10 months in 2012 - 2013, and 11 months in 2013 - 2014), the focus of this study was to investigate the intra-seasonal variability in Flemish Pass. The analysis of the hydrographic and current velocity time series data of Flemish Pass did not provide any evidence that a spatial extension of the northward recirculation around Flemish Cap influenced the transport variability by inducing current reversals (chapter 6). Results of a spectral and variance ellipse analysis of the Flemish Pass current velocity data strongly supported the hypothesis, that baroclinic TRWs trapped at the western slope with periods of 20 - 50 days are an important process influencing the variability of the LSW flow in Flemish Pass (chapter 6). This agrees with the results of *Layton* (2016), who found baroclinic TRWs in the upper water column at the western slope of Flemish Pass on time scales of three weeks. *Mertens et al.* (2014) observed the highest variance in the DWBC east of Flemish Cap at 47°N in a 20 - 50 days period range as well, and also related it to baroclinic Rossby waves. Downstream of Flemish Pass, several studies [e.g. *Schott et al.* (2006), *Peña-Molino et al.* (2012)] found TRWs impacting the flow of the DWBC at similar time scales as at 47°N, while upstream of Flemish Pass, TRWs with a 10 days period were detected *Fischer et al.* (2015).

Several other processes, like a remote connection to upstream processes, the influence of local wind forcing as well as remotely generated barotropic waves were also investigated as potential drivers of the LSW transport variability (chapter 7). By comparing LSW transport time series of Flemish Pass and the DWBC at 53°N for the period 2012 - 2014, coherent oscillations between both regions were found in

the winter months. These oscillations could not be explained through atmospheric forcing. The results of a statistical analysis following *Brink* (1989) pointed to wind generated CTWs propagating southward along the Labrador Shelf with a speed of about 2 to $3\,\mathrm{m\,s^{-1}}$ and thereby inducing the coherent oscillations in the LSW transports at 53°N and Flemish Pass. These results agree with the model study of *Varotsou* (2016), who attributed high frequency variability of ULSW volume transports to CTWs.

Apart from its importance for the southward export of LSW, the Flemish Pass region is, due to its circulation, a unique area with favorable conditions for marine vertebrates and invertebrates [e.g. *Beazley et al.* (2015)]. It is influenced to a great extent by nutrient and oxygen rich polar waters transported by the Labrador Current [*Stein* (2007)], and the anti-cyclonic gyre around Flemish Cap facilitates the retention of fish larvae (e.g. cod and redfish) [*Kudlo et al.* (1984)]. With ongoing climate change and continuing change of hydrographic conditions, the ecosystem in the Flemish Pass might be impacted. For instance, *Pérez-Rodríguez et al.* (2012) found the recruitment success of certain demersal fish species of the Flemish Cap community varying with temperature changes and assumed this to be a first hint of what to expect as climate change progresses. Therefore, continuing observations of the hydrography and current system in this area are important to understand the diversion and variability of the flow field at Flemish Pass and Flemish Cap as well as the advection and spatial redistribution of water masses, which will lead to an improved understanding of consequences for the local ecosystem. Continuing mooring records would also allow to capture the arrival times of LSW anomalies in the Flemish Pass, and to monitor more accurately how prolonged the warming and salinification trends are and when a turning point is reached. Furthermore, the arrival times of anomalies could be analyzed in more detail in relation to observations upstream and downstream of the Flemish Pass, as it integrates into the large scale monitoring net [*Fischer et al.* (2015)] with moored arrays located in the DWBC at 53°N [e.g. *Fischer et al.* (2010)], 47°N [*Mertens et al.* (2014)], and further south at Line W southeast of Cape Cod. Another question for future research would be to investigate, if there is a linkage between both LSW export pathways at 47°N, through Flemish Pass and east around Flemish Cap. Due to instrument loss, mooring based velocity data of the LSW layer of both pathways was not available yet for overlapping periods of time. Therefore, co-variability of the LSW transports between both pathways could not be investigated so far.

Abbreviations

ADCP	Acoustic Doppler Current Profiler
AMOC	Atlantic Meridional Overturning Circulation
AR	Acoustic releaser
Argo	Global array of temperature/salinity profiling floats
AR7W line	Atlantic Repeat Hydrography Line 7
AVISO	Archiving, Validation and Interpretation of Satellite Oceanographic data
AZMP	Atlantic Zone Monitoring Program
AZOMP	Atlantic Zone Off-Shelf Monitoring Program
BIO	Bedford Institute of Oceanography, Dartmouth, Canada
BSH	Bundesamt für Seeschifffahrt und Hydrographie
CLIVAR	Climate Variability and Predictability
CTD	Conductivity Temperature Depth
CTW	Coastal Trapped Wave
DLSW	Deep Labrador Sea Water
DT-MADT	Delayed Time, Mean Absolute Dynamic Topography
DWBC	Deep Western Boundary Current
FC	Flemish Cap
FFT	Fast Fourier Transformation
FLEPVAR	Transports and variability driving mechanisms in Flemish Pass at the western boundary of the subpolar North Atlantic
FP	Flemish Pass
GEOMAR	Helmholtz Center for Ocean Research, Kiel, Germany
LADCP	Lowered Acoustic Doppler Current Profiler
LC	Labrador Current
LS	Labrador Sea
LSW	Labrador Sea Water
IFM/CEN	Institute of Oceanography at University of Hamburg, Germany
IUP	Institute of Environmental Physics at University of Bremen, Germany
MicroCAT	Temperature/conductivity recorder
MIT/gcm	Massachusetts Institute of Technology General Circulation Model

NAC	North Atlantic Current
NAFO	Northwest Atlantic Fisheries Organization
NAO	North Atlantic Oscillation
NCEP/NCAR	(The United States) National Centers for Environmental Prediction/ National Center for Atmospheric Research
NWAFC	Northwest Atlantic Fisheries Center
PSS	Practical Salinity Scale
RACE	Regional Atlantic Circulation and Global Change
RAFOS	Range and Fixing of Sound floats
RCM	Rotor Current Meter
SBE	Sea Bird Electronics
SFB	Sonderforschungsbereich
STD	Standard deviation
Sv	Sverdrup ($1\,\mathrm{Sv} = 10^6\,\mathrm{m^3\,s^{-1}}$)
TRW	Topographic Rossby Wave
ULSW	Upper Labrador Sea Water
VmADCP	Vessel mounted Acoustic Doppler Current Profiler
WGC	West Greenland Current
WOA	World Ocean Atlas
WOCE	World Ocean Circulation Experiment

Bibliography

Azetsu-Scott, K., E. P. Jones, I. Yashayaev, and R. M. Gershey (2003), Time series study of CFC concentrations in the Labrador Sea during deep and shallow convection regimes (1991–2000), *J. Geophys. Res.*, *108*(C11), 8pp., doi:10.1029/2002JC001317.

Beazley, L., E. Kenchington, I. Yashayaev, and F. J. Murillo (2015), Drivers of epibenthic megafaunal composition in the sponge grounds of the Sackville Spur, northwest Atlantic, *Deep-Sea Res. I*, *98*, 102–114, doi:10.1016/j.dsr.2014.11.016.

Böning, C. W., M. Scheinert, J. Dengg, A. Biastoch, and A. Funk (2006), Decadal variability of subpolar gyre transport and its reverberation in the North Atlantic overturning, *Geoph. Res. Letters*, *33*(L21S01), 5pp., doi:10.1029/2006GL026906.

Bower, A. S., M. S. Lozier, S. F. G.ary, and C. W. Böning (2009), Interior pathways of the North Atlantic meridional overturning circulation, *Nature*, *459*(7244), 243–247, doi:10.1038/nature07979.

Bower, A. S., M. S. Lozier, and S. F. Gary (2011), Export of Labrador Sea Water from the subpolar North Atlantic: a Lagrangian perspective, *Deep-Sea Res. II*, *58*(17), 1798–1818, doi:10.1016/j.dsr2.2010.10.060.

Brink, K. H. (1989), Evidence for wind-driven current fluctuations in the western North Atlantic, *J. Geophys. Res.*, *94*(C2), 2029–2044, doi:10.1016/j.dsr2.2010.10.060.

Broadband Primer (2006), *Acoustic Doppler Current Profiler - Principles of Operation - A Practical Primer*, Teledyne RD Instruments, Poway, CA, 3 ed., P/N 951-6069-00.

Cerviño, S., R. Prego, and M. Gómez-Gesteira (1999), New local-scale hydrographic observation on the Flemish Cap in July 1996, *SCI. Counc. Stud.*, *32*, 17–24.

Chelton, D. B., M. G. Schlax, R. M. Samelson, and R. A. de Szoeke (2007), Global observations of large oceanic eddies, *Geoph. Res. Letters*, *34*(15), 5pp., doi:10.1029/2007GL030812.

Colbourne, E. B., and K. D. Foote (2000), Variability of the stratification and circulation on the Flemish Cap during the decades of the 1950s-1990s, *J. Northw. Atl. Fish. Sci.*, *26*, 103–122.

Curry, R. G., M. S. McCartney, and T. M. Joyce (1998), Oceanic transport of subpolar climate signals to mid-depth subtropical waters, *Nature*, *391*(6667), 575–577, doi:10.1038/35356.

DeTracey, B. M., C. L. Tang, and P. C. Smith (1996), Low-frequency currents at the northern shelf edge of the Grand Banks, *J. Geophys. Res.*, *101*(C6), 14,223–14,235, doi:10.1029/96JC00923.

Dutkiewicz, S., L. Rothstein, and T. Rossby (2001), Pathways of cross-frontal exchange in the North Atlantic Current, *J. Geophys. Res.*, *106*(C11), 26,917–26,928, doi:10.1029/1999JC000089.

Egbert, G. D., and S. Y. Erofeeva (2002), Efficient inverse modeling of barotropic ocean tides, *J. Atmos. Oceanic Technol.*, *19*(2), 183–204, doi:10.1175/1520-0426(2002)019⟨0183:EIMOBO⟩2.0.CO;2.

Emery, W. J., and R. E. Thomson (2001), *Data Analysis Methods in Physical Oceanography*, Pergamon.

Fischer, J., and F. A. Schott (2002), Labrador Sea Water tracked by profiling floats – From the boundary current into the open North Atlantic, *J. Phys. Oceanogr.*, *32*(2), 573–584, doi:10.1175/1520-0485(2002)032⟨0573:LSWTBP⟩2.0.CO;2.

Fischer, J., and M. Visbeck (1993), Deep velocity profiling with self-contained ADCPs, *J. Atmos. Oceanic Technol.*, *10*(5), 764–773, doi:10.1175/1520-0426(1993)010⟨0764:DVPWSC⟩2.0.CO;2.

Fischer, J., F. A. Schott, and M. Dengler (2004), Boundary circulation at the exit of the Labrador Sea, *J. Phys. Oceanogr.*, *34*(7), 1548–1570, doi:10.1175/1520-0485(2004)034⟨1548:BCATEO⟩2.0.CO;2.

Fischer, J., M. Visbeck, R. Zantopp, and N. Nunes (2010), Interannual to decadal variability of outflow from the Labrador Sea, *Geoph. Res. Letters*, *37*(L24610), 5pp., doi:10.1029/2010GL045321.

Fischer, J., et al. (2015), Intra-seasonal variability of the DWBC in the western subpolar North Atlantic, *Prog. Oceanogr.*, *132*, 233–249, doi:10.1016/j.pocean.2014.04.002.

Getzlaff, J., C. W. Böning, C. Eden, and A. Biastoch (2005), Signal propagation related to the North Atlantic overturning, *Geoph. Res. Letters*, *32*(L09602), 4pp., doi:10.1029/2004GL021002.

Gil, J., R. Sánchez, S. Cerviño, and D. Garabana (2004), Geostrophic circulation and heat flux across the Flemish Cap, 1988–2000, *J. Northw. Atl. Fish. Sci.*, *34*, 61–81.

Gill, A. E. (1982), *Atmosphere–Ocean Dynamics*, 662 pp., Academic Press.

Greenberg, D. A., and B. D. Petrie (1988), The mean barotropic circulation on the Newfoundland Shelf and Slope, *J. Geophys. Res.*, *93*(C12), 15,541–15,550, doi:10.1029/JC093iC12p15541.

Hall, M. M., D. J. Torres, and I. Yashayaev (2013), Absolute velocity along the AR7W section in the Labrador Sea, *Deep-Sea Res. I*, *72*, 72–87, doi:10.1016/j.dsr.2012.11.005.

Han, G. (2005), Wind-driven barotropic circulation off Newfoundland and Labrador, *Cont. Shelf Res.*, *25*(17), 2084–2106, doi:10.1016/j.csr.2005.04.015.

Han, G., Z. Lu, Z. Wang, J. Helbig, N. Chen, and B. D. Young (2008), Seasonal variability of the Labrador Current and shelf circulation off Newfoundland, *J. Geophys. Res.*, *113*(C10), doi:10.1080/01431160701271982.

Hayes, R. M., D. G. Mountain, and T. C. Wolford (1977), Physical oceanography and the abiotic influence on cod recruitment in the Flemish Cap region, *ICNAF Res. Doc.*, *77/54*(Serial 5107), 33pp.

Huthnance, J. M. (1981), Waves and currents near the continental shelf edge, *Prog. Oceanogr.*, *10*(4), 193–226, doi:10.1016/0079-6611(81)90004-5.

Johns, W., and D. R. Watts (1986), Time scales and structure of topographic Rossby waves and meanders in the deep Gulf Stream, *J. Mar. Res.*, *44*(2), 267–290, doi:10.1357/002224086788405356.

Kalnay, E., M. Kanamitsu, R. Kistler, W. Collins, D. Deaven, L. Gandin, M. Iredell, S. Saha, G. White, J. Woollen, Y. Zhu, M. Chelliah, W. Ebiszusaki, W. Higgins, J. Janowiak, K. Mo, C. Ropelewski, J. Wang, A. Leetmaa, R. Reynolds, R. Jenne, and J. Joseph (1996), The NCEP/NCAR 40-Year Renanalysis Project, *Bull. Amer. Meteor. Soc.*, *77*, 437–471, doi:10.1175/1520-0477(1996)077⟨0437:TNYRP⟩2.0.CO;2.

Kanzow, T., and W. Zenk (2014), Structure and transport of the Iceland Scotland Overflow plume along the Reykjanes Ridge in the Iceland Basin, *Deep-Sea Res.*, *86*, 82–93, doi:10.1016/j.dsr.2013.11.003.

Keeley, J. R. (1982), Regional differences in water types on the Flemish Cap, *NAFO SCR Doc*, (82/42), 8pp.

Khatiwala, S., and M. Visbeck (2000), An estimate of the eddy-induced circulation in the Labrador Sea, *Geoph. Res. Letters*, *27*(15), 2277–2280, doi:10.1029/1999GL011073.

Kieke, D., and I. Yashayaev (2015), Studies of Labrador Sea Water formation and variability in the subpolar North Atlantic in the light of international partnership and collaboration, *Prog. Oceanogr.*, *132*, 220–232, doi:10.1016/j.pocean.2014.12.010.

Kieke, D., M. Rhein, L. Stramma, W. M. Smethie, D. A. LeBel, and W. Zenk (2006), Changes in the CFC inventories and formation rates of Upper Labrador Sea Water, 1997-2001, *J. Phys. Oceanogr.*, *36*(1), 64–86, doi:10.1175/JPO2814.1.

Kieke, D., M. Rhein, L. Stramma, W. M. Smethie, J. L. Bullister, and D. A. LeBel (2007), Changes in the pool of Labrador Sea Water in the subpolar North Atlantic, *Geoph. Res. Letters*, *34*(L06605), 5pp., doi:10.1029/2006GL028959.

Kieke, D., B. Klein, L. Stramma, M. Rhein, and K. P. Koltermann (2009), Variability and propagation of Labrador Sea Water in the southern subpolar North Atlantic, *Deep-Sea Res. I*, *56*(10), 1656–1674, doi:10.1016/j.dsr.2009.05.010.

Koltermann, K. P., A. V. Sokov, V. P. Tereschenkov, S. A. Dobroliubov, K. Lorbacher, and A. Sy (1999), Decadal changes in the thermohaline circulation of the North Atlantic, *Deep-Sea Res. II*, *46*(1), 109–138, doi:10.1016/S0967-0645(98)00115-5.

Kudlo, B. P., V. A. Borovkov, and N. G. Sapronetskaya (1984), Water circulation patterns on the Flemish Cap from observations in 1977-82, *NAFO Sci. Coun. Studies*, *7*, 27–37.

Layton, C. (2016), Spatial-Temporal Ocean Variability on the northwest slope of Flemish Cap, Master's thesis, Dalhousie Univ., Halifax, Nova Scotia, 96 pp.

Lazier, J. R. N. (1973), The renewal of Labrador Sea Water, *Deep Sea Res. Oceanogr. Abstr.*, *20*(4), 341–353, doi:10.1016/0011-7471(73)90058-2.

Lazier, J. R. N., and D. G. Wright (1993), Annual velocity variations in the Labrador Current, *J. Phys. Oceanogr.*, *23*(4), 659–678, doi:10.1175/1520-0485(1993)023⟨0659:AVVITL⟩2.0.CO;2.

Lazier, J. R. N., R. Hendry, A. Clarke, I. Yashayaev, and P. Rhines (2002), Convection and restratification in the Labrador Sea, 1990–2000, *Deep-Sea Res. I*, *49*(10), 1819–1835, doi:10.1016/S0967-0637(02)00064-X.

LeBlond, P. H., and L. A. Mysak (1978), *Waves in the Ocean*, 602 pp., Elsevier.

Leffler, K. E., and D. A. Jay (2009), Enhancing tidal harmonic analysis: Robust (hybrid L^1/L^2) solutions, *Cont. Shelf Res.*, *29*(1), 78–88, doi:10.1016/j.csr.2008.04.011.

Louis, J. P., B. D. Petrie, and P. C. Smith (1982), Observations of topographic Rossby waves on the continental margin off Nova Scotia, *J. Phys. Oceanogr.*, *12*(1), 47–55, doi:10.1175/1520-0485(1982)012⟨0047:OOTRWO⟩2.0.CO;2.

Lozier, M. S., M. S. McCartney, and W. B. Owens (1995), Anomalous anomalies in averaged hydrographic data, *J. Phys. Oceanogr.*, *24*, 2624–2638, doi:10.1175/1520-0485(1994)024⟨2624:AAIAHD⟩2.0.CO;2.

Marsh, R., B. A. De Cuevas, A. C. Coward, H. L. Bryden, and M. Álvarez (2005), Thermohaline circulation at three key sections in the North Atlantic over 1985–2002, *Geoph. Res. Letters*, *32*(L10604), doi:10.1029/2004GL022281.

Marshall, J., A. Adcroft, C. Hill, L. Perelman, and C. Heisey (1997), A finite-volume, incompressible Navier Stokes model for studies of the ocean on parallel computers, *J. Geophys. Res.*, *102*(C2), 5753–5766, doi:10.1029/96JC02775.

Maslowski, W. (1996), Numerical simulations of topographic Rossby waves along the East Greenland Front, *J. Geophys. Res.*, *101*, 8775–8787, doi:10.1029/95JC03799.

Medhaug, I., H. R. Langehaug, T. Eldevik, T. Furevik, and M. Bentsen (2012), Mechanisms for decadal scale variability in a simulated Atlantic meridional overturning circulation, *Climate Dynamics*, *39*, 77–93, doi:10.1007/s00382-011-1124-z.

Mertens, C., M. Rhein, M. Walter, C. W. Böning, E. Behrens, D. Kieke, R. Steinfeldt, and U. Stöber (2014), Circulation and transports in the Newfoundland Basin, western subpolar North Atlantic, *J. Geophys. Res.*, *119*, 7772–7793, doi:10.1002/2014JC010019.

Myers, P. G., and N. Kulan (2012), Changes in the deep western boundary current at 53°N, *J. Phys. Oceanogr.*, *42*(7), 1207–1216, doi:10.1175/JPO-D-11-090.1.

Mysak, L. A. (1980), Recent advances in shelf wave dynamics, *Rev. Geophys. Space Phys.*, *18*(1), 211–241, doi:10.1029/RG018i001p00211.

National Geophysical Data Center, N. U. D. o. C., NESDIS (2006), ETOPO2, Global 2 Arc-minute Ocean Depth and Land Elevation from the US National Geophysical Data Center (NGDC), doi:10.5065/D6668B75.

Pawlowicz, R., B. Beardsley, and S. Lentz (2002), Classical tidal harmonic analysis including error estimates in MATLAB using T_TIDE, *Comput. Geosci.*, *28*, 929–937, doi:10.1016/S0098-3004(02)00013-4.

Peña-Molino, B., T. M. Joyce, and J. M. Toole (2012), Variability in the Deep Western Boundary Current: Local versus remote forcing, *J. Geophys. Res.*, *117*(C12), 17pp., doi:10.1029/2012JC008369.

Pérez-Rodríguez, A., M. Koen-Alonso, and F. Saborido-Rey (2012), Changes and trends in the demersal fish community of the Flemish Cap, Northwest Atlantic, in the period 1988–2008, *ICES J. Mar. Sci.*, *69*(5), 902–912, doi:10.1093/icesjms/fss019.

Petrie, B., and J. Buckley (1996), Volume and freshwater transport of the Labrador Current in Flemish Pass, *J. Geophys. Res.*, *101*(C12), 28,335–28,342, doi:10.1029/96JC02779.

Pickart, R. S., and D. R. Watts (1990), Deep Western Boundary Current variability at Cape Hatteras, *J. Mar. Res.*, *48*(4), 765–791.

Pietri, A., V. Echevin, P. Testor, A. Chaigneau, L. Mortier, C. Grados, and A. Albert (2014), Impact of a coastal-trapped wave on the near-coastal circulation of the Peru upwelling system from glider data, *J. Geophys. Res.*, *119*(3), 2109–2120, doi:10.1002/2013JC009270.

Rhein, M., J. Fischer, W. M. Smethie, D. Smythe-Wright, R. F. Weiss, C. Mertens, D.-H. Min, U. Fleischmann, and A. Putzka (2002), Labrador Sea Water: Pathways, CFC inventory, and formation rates, *J. Phys. Oceanogr.*, *32*(2), 648–665, doi:10.1175/1520-0485(2002)032⟨0648:LSWPCI⟩2.0.CO;2.

Rhein, M., D. Kieke, S. Hüttl-Kabus, A. Roessler, C. Mertens, R. Meissner, B. Klein, C. W. Böning, and I. Yashayaev (2011), Deep water formation, the subpolar gyre, and the meridional overturning circulation in the subpolar North Atlantic, *Deep-Sea Res. II*, *58*(17), 1819–1832, doi:10.1016/j.dsr2.2010.10.061.

Rhein, M., D. Kieke, and R. Steinfeldt (2015), Advection of North Atlantic Deep Water from the Labrador Sea to the southern hemisphere, *J. Geophys. Res.*, *120*(4), 2471–2487, doi:10.1002/2014JC010605.

Rhines, P. (1970), Edge-, bottom-, and Rossby waves in a rotating stratified fluid, *Geophysical Fluid Dynamics*, *1*(3-4), 273–302, doi:10.1080/03091927009365776.

Roessler, A., M. Rhein, D. Kieke, and C. Mertens (2015), Long-term observations of North atlantic current transport at the gateway between western and eastern Atlantic, *J. Geophys. Res.*, *120*(6), 4003–4027, doi:10.1002/2014JC010662.

Ross, C. K. (1980), Moored current meter data from Flemish Cap, January-July 1979, *NAFO SCR Doc.*, *80/128*(Serial N200), 13pp.

Schneider, L., D. Kieke, K. Jochumsen, E. Colbourne, I. Yashayaev, R. Steinfeldt, E. Varotsou, N. Serra, and M. Rhein (2015), Variability of Labrador Sea Water transported through Flemish Pass during 1993–2013, *J. Geophys. Res.*, *120*(8), 5514–5533, doi:10.1002/2015JC010939.

Schott, F. A., T. N. Lee, and R. Zantopp (1988), Variability of structure and transport of the Florida Current in the period range of days to seasonal, *J. Phys. Oceanogr.*, *18*(9), 1209–1230, doi:10.1175/1520-0485(1988)018⟨1209:VOSATO⟩2.0.CO;2.

Schott, F. A., R. Zantopp, L. Stramma, M. Dengler, J. Fischer, and M. Wibaux (2004), Circulation and deep-water export at the western exit of the subpolar North Atlantic, *J. Phys. Oceanogr.*, *34*(4), 817–843, doi:10.1175/1520-0485(2004)034⟨0817:CADEAT⟩2.0.CO;2.

Schott, F. A., J. Fischer, M. Dengler, and R. Zantopp (2006), Variability of the Deep Western Boundary Current east of the Grand Banks, *Geoph. Res. Letters*, *33*(21), 5pp., doi:10.1029/2006GL026563.

Serra, N., R. H. Kaese, A. Koehl, D. Stammer, and D. Quadfasel (2010), On the low-frequency phase relation between the Denmark Strait and the Faroe-Bank Channel overflows, *Tellus, Ser. A*, *62*(4), 530–550, doi:10.1111/j.1600-0870.2010.00445.x.

Stein, M. (2007), Oceanography of the Flemish Cap and adjacent waters, *J. Northw. Atl. Fish. Sci.*, *37*, 135–146.

Stramma, L., D. Kieke, M. Rhein, F. Schott, I. Yashayaev, and K. P. Koltermann (2004), Deep water changes at the western boundary of the subpolar North Atlantic during 1996 to 2001, *Deep-Sea Res. I*, *51*(8), 1033–1056, doi:10.1016/j.dsr.2004.04.001.

Straneo, F. (2006), Heat and Freshwater Transport through the Central Labrador Sea, *J. Phys. Oceanogr.*, *36*(4), 606–628, doi:10.1175/JPO2875.1.

Sy, A., M. Rhein, J. Lazier, K. P. Koltermann, J. Meincke, A. Putzka, and M. Bersch (1997), Surprisingly rapid spreading of newly formed intermediate waters across the North Atlantic Ocean, *Nature*, *386*, 675–679, doi:10.1038/386675a0.

Talley, L. D., and M. S. McCartney (1982), Distribution and circulation of Labrador Sea Water, *J. Phys. Oceanogr.*, *12*(11), 1189–1205, doi:10.1175/1520-0485(1982)012⟨1189:DACOLS⟩2.0.CO;2.

Therriault, J.-C., B. . Petrie, P. Pepin, J. Gagnon, D. Gregoy, J. Helbig, A. Hermann, D. Lefaivre, M. Mitchell, B. Pelchat, J. Runge, and D. Sameoto (1998), *Proposal for a northwest Atlantic zonal monitoring program*, Ocean Sci. Div. of Fish. and Ocean Can., Dartmouth, Nova Scotia, Canada.

Thompson, R. O. R. Y., and J. R. Luyten (1976), Evidence for bottom-trapped topographic Rossby waves from single moorings, *Deep-Sea Res.*, *23*, 629–635, doi:10.1016/0011-7471(76)90005-X.

van Aken, H. M., M. F. De Jong, and I. Yashayaev (2011), Decadal and multi-decadal variability of Labrador Sea Water in the north-western North Atlantic Ocean derived from tracer distributions: Heat budget, ventilation, and advection, *Deep-Sea Res. I*, *58*(5), 505–523, doi:10.1016/j.dsr.2011.02.008.

Varotsou, E. (2016), Transport variability-driving mechanisms in Flemish Pass at the western boundary of the Subpolar North Atlantic, Ph.D. thesis, Univ. of Hamburg, Hamburg, Germany, 120 pp.

Varotsou, E., K. Jochumsen, N. Serra, D. Kieke, and L. Schneider (2015), Interannual transport variability of Upper Labrador Sea Water at Flemish Cap, *J. Geophys. Res.*, *120*(7), 5074–5089, doi:10.1002/2015JC010705.

Visbeck, M. (2002), Deep velocity profiling using lowered Acoustic Doppler Current Profilers: Bottom track and inverse solutions, *J. Atmos. Oceanic Technol.*, *19*(5), 794–807, doi:10.1175/1520-0426(2002)019⟨0794:DVPULA⟩2.0.CO;2.

Walter, M., and C. Mertens (2013), Mid-depth mixing linked to North Atlantic Current variability, *Geoph. Res. Letters*, *40*(18), 4869–4875, doi:10.1002/grl.50936.

Welch, P. (1967), The use of fast Fourier transform for the estimation of power spectra: A method based on time averaging over short, modified periodograms, *IEEE Transactions on audio and electroacoustics*, *15*(2), 70–73, doi:10.1109/TAU.1967.1161901.

Wong, A., R. Keeley, T. Carval, and A. D. M. Team (2015), Argo Quality Control Manual for CTD and Trajectory Data, doi:10.13155/33951.

Yashayaev, I. (2007), Hydrographic changes in the Labrador Sea, 1960–2005, *Prog. Oceanogr.*, *73*(3), 242–276, doi:10.1016/j.pocean.2007.04.015.

Yashayaev, I., and J. W. Loder (2009), Enhanced production of Labrador Sea Water in 2008, *Geoph. Res. Letters*, *36*(L01606), 7pp., doi:10.1029/2008GL036162.

Yashayaev, I., M. Bersch, and H. M. van Aken (2007), Spreading of the Labrador Sea Water to the Irminger and Iceland basins, *Geoph. Res. Letters*, *34*(L10602), 8pp., doi:10.1029/2006GL028999.

Yashayaev, I., D. Seidov, and E. Demirov (2015), A new collective view of oceanography of the Arctic and North Atlantic basins, *Prog. Oceanogr.*, *132*, 1–21, doi:10.1016/j.pocean.2014.12.012.

Zantopp, R., J. Fischer, M. Visbeck, and J. Karstensen (2017), From interannual to decadal: 17 years of boundary current transports at the exit of the Labrador Sea, *J. Geophys. Res.*, *122*, doi:10.1002/2016JC012271.

Publications

Results of this study were published in the Journal of Geophysical Research:

Schneider, L., D. Kieke, K. Jochumsen, E. Colbourne, I. Yashayaev, R. Steinfeldt, E. Varotsou, N. Serra, and M. Rhein (2015), Variability of Labrador Sea Water transported through Flemish Pass during 1993 - 2013, *J. Geophys. Res., 120* (8), 5514 - 5533, doi:10.1002/2015JC010939.

I am co-author of the following study:

Varotsou, E., K. Jochumsen, N. Serra, D. Kieke, and L. Schneider (2015), Interannual transport variability of Upper Labrador Sea Water at Flemish Cap, *J. Geophys. Res., 120* (7), 5074 - 5089, doi:10.1002/2015JC010705.

I presented preliminary results of this work on the following international conferences as a first author:

Schneider, L., D. Kieke, K. Jochumsen, M. Rhein, E. Varotsou, N. Serra, I. Yashayaev, and E. Colbourne. Variability of Labrador Sea Water exported through Flemish Pass. *Ocean Science Meeting 2014.* Honolulu, HI, USA. February 23 - 28th, 2014. (Talk)

Schneider, L., D. Kieke, K. Jochumsen, M. Rhein, E. Varotsou, N. Serra, I. Yashayaev, and E. Colbourne. Variability of Labrador Sea Water exported through Flemish Pass. *IAHS/IAPSO/IASPEI Joint Assembly 2013.* Gothenburg, Sweden. July 22 - 26th, 2013. (Talk)

Schneider, L., D. Kieke, K. Jochumsen, M. Rhein, D. Quadfasel, E. Varotsou, N. Serra, E. Colbourne, and I. Yashayaev. Export of Labrador Sea Water through Flemish Pass. *EGU General Assembly 2012*. Vienna, Austria. April 22 - 27th, 2012. (Poster)

Acknowledgements

First of all, I want to express my sincere gratitude to Dagmar Kieke, who supervised this work. She was always available for me with helpful scientific advice, feedback in the writing process, and confidence in the success of this project.
I further thank Prof. Torsten Kanzow for his support as a member of my thesis committee and for providing the co-evaluation of this thesis.
Many thanks also to Eirini Varotsou, Kerstin Jochumsen, and Nuno Serra for the excellent cooperation and helpful input during the FLEPVAR project meetings. The model time series used in this study were provided by Nuno Serra and Eirini Varotsou.
I also want to thank Prof. Monika Rhein and the whole Department of Oceanography for providing a nice work environment and open minds for scientific questions. Special thanks to my long term office mates Ilaria Stendardo, Tilia Breckenfelder, and Janna Köhler! I am also thankful for the opportunities to participate in many great ship cruises and being part of the team.
The membership in the Bremen International Graduate School for Marine Sciences (GLOMAR) gave me the opportunity to participate in several international conferences and present my research, and the soft skill as well as scientific courses were of great value to me. The career oriented Fireside Chats organised by Christina Klose are also greatly appreciated.
I would like to extend a special thank you to all who helped me on my way, with your assistance, or by contributing data to this study. The M1842 mooring data were kindly provided by Blair Greenan, BIO, Dartmouth, Canada. Eugene Colbourne, NWAFC, Dartmouth, Canada, provided the AZMP data. Johannes Karstensen, GEOMAR Helmholtz Centre for Ocean Research, Kiel, Germany, made the LSW transport time series from 53°N available to this study, and Igor Yashayaev, BIO, Dartmouth, Canada, contributed the hydrographic time series of LSW of the central Labrador Sea.
Financial support for the FLEPVAR project was provided by the *Deutsche*

Forschungsgemeinschaft (Grants KI-1655 and JO-809).
Argo data were collected and made freely available by the International Argo Program and the national programs that contribute to it (http://www.argo.ucsd.edu, http://argo.jcommops.org). The Argo Program is part of the Global Ocean Observing System. B. Klein, BSH, Hamburg, Germany, kindly provided additional quality control on a subset of the Argo data that were downloaded from the Coriolis data repository on 25 June 2014.
Cruise data of the Bremen group were provided through BMBF granted programs: Nordatlantik, RACE, and FLEPVAR. NCEP/NCAR reanalysis data were made available by the NOAA/OAR/ESRL PSD, Boulder, Colorado, USA, from their web site at http://www.esrl.noaa.gov/psd/. The altimeter products were produced by Ssalto/Duacs and distributed by Aviso with support from CLS-Cnes (https://www.aviso.altimetry.fr/).
Finally, I deeply thank my husband Michael for his continuous support in many different ways, as well as encouragement and understanding. I cannot imagine going through this challenging phase of my life without him on my side.